

**ON HOLOGRAPHIC ENTANGLEMENT ENTROPY AND
SUB-REGION COMPLEXITY OF VARIOUS BLACK
SOLUTIONS IN ADS/CFT**

By

ARANYA BHATTACHARYA

PHYS05201604004

Saha Institute of Nuclear Physics, Kolkata

A thesis submitted to the

Board of Studies in Physical Sciences

In partial fulfillment of requirements

For the Degree of

DOCTOR OF PHILOSOPHY

of

HOMI BHABHA NATIONAL INSTITUTE



June, 2021

Homi Bhabha National Institute

Recommendations of the Viva Voce Committee

As members of the Viva Voce Committee, we certify that we have read the dissertation prepared by **Aranya Bhattacharya** entitled **“On Holographic Entanglement Entropy and Sub-region Complexity of Various Black Solutions in AdS/CFT”** and recommend that it maybe accepted as fulfilling the thesis requirement for the award of Degree of Doctor of Philosophy.

_____ Date: June 2, 2021

Chairman - Prof. Munshi G. Mustafa

Shibaji Roy

_____ Date: June 2, 2021

Guide / Convener - Prof. Shibaji Roy

Harvendra Singh

_____ Date: June 2, 2021

Co-guide - Prof. Harvendra Singh

Aninda Sinha

_____ Date: June 2, 2021

Examiner - Prof. Aninda Sinha

_____ Date: June 2, 2021

Member 1 - Prof. Arnab Kundu

_____ Date: June 2, 2021

Member 2 - Prof. Amit Ghosh

_____ Date: June 2, 2021

Member 3 - Prof. Koushik Ray

Final approval and acceptance of this thesis is contingent upon the candidate's submission of the final copies of the thesis to HBNI.

I/We hereby certify that I/we have read this thesis prepared under my/our direction and recommend that it may be accepted as fulfilling the thesis requirement.

Date: June 2, 2021

Place: Kolkata

Guide: Shibaji Roy

STATEMENT BY AUTHOR

This dissertation has been submitted in partial fulfillment of requirements for an advanced degree at Homi Bhabha National Institute (HBNI) and is deposited in the Library to be made available to borrowers under rules of the HBNI.

Brief quotations from this dissertation are allowable without special permission, provided that accurate acknowledgement of source is made. Requests for permission for extended quotation from or reproduction of this manuscript in whole or in part may be granted by the Competent Authority of HBNI when in his or her judgment the proposed use of the material is in the interests of scholarship. In all other instances, however, permission must be obtained from the author.

Aranya Bhattacharya
Aranya Bhattacharya

Signature of the guide: *Shilpi Roy*

DECLARATION

I, hereby declare that the investigation presented in the thesis has been carried out by me. The work is original and has not been submitted earlier as a whole or in part for a degree / diploma at this or any other Institution / University.

Aranya Bhattacharya
Aranya Bhattacharya

Signature of the guide: Shibaji Roy

LIST OF PUBLICATIONS ARISING FROM THE THESIS

Journal:

1. **Holographic entanglement entropy and entanglement thermodynamics of ‘black’ non-susy D3 brane**

*Aranya Bhattacharya, Shibaji Roy , **Phys. Lett. B** 781 (2018) 232-237, [1712.03470].*

2. **Holographic entanglement entropy, subregion complexity and Fisher information metric of ‘black’ non-susy D3 brane**

*Aranya Bhattacharya, Shibaji Roy , **Phys. Lett. B** 800 (2020) 135032, [1807.06361].*

3. **Entanglement Entropy and Subregion Complexity in Thermal Perturbations around Pure-AdS Spacetime**

*Aranya Bhattacharya, Kevin T Grosvenor and Shibaji Roy , **Phys. Rev. D**100 (2019) 126004, [1905.02220].*

4. **Multipartite purification, multiboundary wormholes, and islands in AdS₃/CFT₂**

*Aranya Bhattacharya , **Phys. Rev. D**102 (2020) 046013, [2003.11870].*

5. Topological shadows and complexity of islands in multiboundary wormholes

Aranya Bhattacharya, Anindya Chanda, Sabyasachi Maulik, Christian Northe and Shibaji Roy , *JHEP 02 (2021) 152*, [2010.04134].

Other publications and preprints (not included in the thesis):

1. HEE and HSC for flavors: Perturbative structure in open string geometries

Avik Banerjee, *Aranya Bhattacharya* and Sabyasachi Maulik, [2008.02705].

2. Islands and complexity of eternal black hole and radiation subsystems for a doubly holographic model

Aranya Bhattacharya, Arpan Bhattacharyya, Pratik Nandi and Ayan K. Patra, , *JHEP 05 (2021) 135*, [2103.15852]

Chapters in Books and Lecture Notes: None

Conferences:

1. Title of Talk: *Holographic entanglement entropy and entanglement thermodynamics of black nonSUSY D3 brane* ,

presented at the Saha Theory Workshop IV (Modern Aspects of String Theory) held at SINP, Kolkata in February, 2018.

2. Title of Talk: *Holographic Entanglement Entropy, Subregion Complexity and Fisher Information metric of black nonSUSY D3 brane* ,

presented at the Julius Maximilians Universitat , Wurzburg, Germany in October, 2018 during academic visit.

3. Title of Talk: *Holographic Entanglement Entropy, Subregion Complexity and Fisher Information metric of black nonSUSY D3 brane* ,
presented at the conference "Current developments in QFT & Gravity" held at SNBNCBS, Kolkata in December, 2018.
4. Title of Talk: *Entanglement and subregion complexity for thermal perturbations over pure AdS* ,
presented in the National Strings Meeting (NSM), 2019, held in IISER Bhopal during 19-24 December, 2019.
5. Title of Talk: *Subregion Complexity version of Page Curve in Multi-boundary Wormholes* ,
presented in the workshop "QI in QFT & AdS/CFT" on 7th August, 2020.
6. Title of Talk: *Island and Complexity in Multiboundary Wormhole Models in AdS₃* ,
presented in the Dual Mystery Channel of Gauge and Gravity channel, a seminar series organized by Theoretical Physics Group, IIT Madras.
7. Title of Talk: *On the Multiboundary Wormhole models of Island* ,
presented in the conference "Strings and Fields, 2020" organized by YITP, Japan during 16-20 November, 2020.

Aranya Bhattacharya
Aranya Bhattacharya

Signature of the guide: Shibaji Roy

To *Baba and Ma.*

ACKNOWLEDGEMENTS

My journey as a PhD student has been nothing out of the ordinary. But, the first person to thank will be my supervisor Prof. Shibaji Roy for always supporting me with my decisions and showing light whenever needed. Whatever research I could do is the result of the freedom to explore newer directions that he provided me with. Particularly his availability, whenever I went through something new and wanted to share, has been great for me. He also inspired me to pursue collaborations and independent thinking. Among other faculties in Theory division, I would particularly like to thank Prof. Asit K. De, Prof. Palash B. Pal, Prof. Arnab Kundu, Prof. Amit Ghosh, Prof. Harvendra Singh and Prof. Munshi G. Mustafa for the illuminating conversations I had with them about Physics and everything else. Especially the lively interactions and fun I had with Prof. Palash Pal and Prof. Munshi G. Mustafa will always be close to my heart. Prof. Asit De's QFT-I, Prof. Arnab Kundu's several courses on AdS/CFT, String Theory and CFT and Prof. Palash Pal's QFT-II had all the techniques and understanding I built upon to have a broader idea about what are the interesting questions one should ask in Physics. Among the non-research staffs of Theory division, it is a pleasure to thank Pradyut da, Dola di, Arun da and Sangita di for their cooperation in administrative matters.

Family always plays a crucial role in any research scholar's career and I am no exception. I have been fortunate that my parents and elder sister have always been like pillars standing by my decisions. At times, them asking questions about my decisions also helped a lot in retrospect. It goes without saying that they played the biggest role in whatever I am today.

It is a pleasure to also thank my brilliant collaborators Kevin, Christian, Sabyasachi,

Avik da, Arpan da, Pratik, Hao and Kausik who helped me in my research. Especially, discussing with Arpanda opened up a new direction in my research. The discussions in the Theory scholar's room about every possible topic starting from Physics to sports have made my stay in SINP memorable. It is therefore a pleasure to thank Aritra da, Chiru da, Kuntal da, Sukannya di, Avik da (choto, boro), Augniva da, Bithika, Supriyo, Ritesh, Ayan, Arunima, Sabyasachi, Udit da, Khursid, Suman, Adil and Sandip for the fun we had together at times during our overlap in worldline.

The three-year stay in MSA-II will always be stored in a memory-counter at the center of my heart and the credit goes to the beautiful camaraderie I shared with Sanjukta di, Chiru da, Aritra da, Kuntal da, Arghya da, Bithika, Supriyo, Ritesh, Rashika, Promita, Saikat and everyone else. Sanjukta di, Aritra da and Chiru da have been more than just seniors for me. I always got extremely valuable suggestions and life lessons from them. At the same time, they allowed me to be more of a friend than a junior and I can't thank them enough for that. Especially Sanjukta di sharing her personal struggles and admiring my efforts regularly have been one of the biggest motivations during my PhD. A special mention would also go to the fun chats I used to have with Bithika and Supriyo in the bus while returning from the institute during our post M.Sc days. I also have Anwesha and Avik to thank for the fun during the Post M.Sc classes. I would then like to give a shout out to the very special one-year overlap and the great time with Rashika (the gel and gem of a friend to cherish forever), Promita, Shubhi, Augniva da, Tanmoy and Chiru da. The food cooked by Biswajit da and Shyamal da in MSA-II made us survive through all the stress put by the brain and heart combined. During my stay in MSA-I for the last couple of years, again I got some nice guys to hang out with (special mention to Astik, Sabyasachi, Gourab da, Tukai, Snehal da, Subhankar, Smruti) and some food to please my palates (Shakti da, Kartik da and Pradip da). Apart from the hostel memories, I interacted with many many

people in the institute and all of them were very nice to me. The JCC programs and musical nights afterwards were probably the best part about it. The time spent with Sukannya di (bondhu-didi as I call her), Shamik da, Rome da, Gourab, Pritam, Suvankar da, Roopamda, Duhita are eternal and we will always keep renewing them with our late-night skyping.

Finally, I would like to mention the two closest people in my life with whom I share the most special connection with. Thanks to Manobina for talking everyday and listening to everything I had to say to myself as well as to you at the end of every single day during last five years and more. Thanks to Soham for staying my closest friend for the last ten years, the long walks and calling me in regular intervals at mid-nights whenever you wrote a new drama, a poem or were going through tough time.

Last but not the least, I would like to thank all the people whom I missed out here. I thank the people of India for paying taxes which fund research in basic sciences. Our country is going through a tough time and I strongly believe that at the end of all these struggle, science and equality will come out victorious over all the stupid religious fanaticism and superstitious belief. This is the greatest thing I have to wish for all the people I want to thank.

Aranya Bhattacharya
Aranya Bhattacharya

CONTENTS

Summary	v
List of Abbreviations	vii
List of Figures	ix
1 Introduction	1
1.1 AdS/CFT and Holography:	2
1.2 Holography and Quantum Information:	4
2 A Brief Review of Entanglement, Complexity and Their Holographic Duals	9
2.1 Entanglement Entropy:	10
2.1.1 Properties of Entanglement Entropy:	11
2.1.2 Entanglement in QFTs:	13
2.2 Entanglement of Purification:	14
2.2.1 Definitions and Properties:	15
2.3 Complexity:	19
2.4 Holographic Proposals:	23

2.4.1	Holographic Entanglement Entropy:	23
2.4.2	Holographic Dual of EoP:	25
2.4.3	Holographic Complexity:	28
2.5	Relative Entropy and Fisher Information:	31
3	Entanglement and Sub-region Complexity for charged and uncharged AdS-Schwarzschild Black holes in General Spacetime Dimensions	35
3.1	The Embedding Function:	39
3.1.1	Uncharged AdS Black Hole:	41
3.1.2	Charged AdS Black Hole:	47
3.2	Holographic Entanglement Entropy:	50
3.2.1	Uncharged AdS Black Hole:	51
3.2.2	Charged AdS Black Hole:	54
3.2.3	Boundary Terms:	56
3.3	Holographic Sub-region Complexity:	61
3.3.1	Uncharged AdS Black Hole:	62
3.3.2	Charged AdS Black Hole:	64
3.4	Entanglement Thermodynamics:	66
4	Entanglement Thermodynamics and Fisher Information Metric for Non-SUSY black D3 brane	73
4.1	D Branes and Relation to Gravity:	75
4.2	Non-supersymmetric ‘black’ D3 branes and decoupling limit:	77
4.3	Entanglement and Thermal Entropy cross over with Strip Sub-region: . . .	83
4.3.1	Holographic entanglement entropy in FG coordinates:	83
4.3.2	Entanglement thermodynamics:	88

4.3.3	Cross-over to thermal entropy:	90
4.4	EE and complexity for (decoupled) ‘black’ non-susy D3 brane in case of spherical subsystem:	92
5	Page Curve and Complexity of Islands in Multiboundary Wormhole Models of Black Hole Evaporation	97
5.1	A Note on recent developments regarding Page curve:	102
5.1.1	Information Paradox and Resolutions (Islands) :	103
5.2	Multiboundary Wormholes and the toy models:	107
5.2.1	Multiboundary Wormhole Models of Black Hole Evaporation:	110
5.3	Connections between EoP and MbW Toy Model:	114
5.3.1	Connections to be drawn:	114
5.3.2	Realization of over-counting:	118
5.4	Sub-region Complexity in AdS_3 and multi-boundary models:	121
5.4.1	Volumes in AdS_3 :	121
5.5	Results	135
6	Conclusion and Outlook	137
6.1	Conclusions from Chapter 3:	138
6.2	Conclusions from Chapter 4:	140
6.2.1	Strip HEE:	140
6.2.2	Spherical sub-region HEE and HSC:	141
6.3	Conclusions from Chapter 5:	142
6.3.1	Entanglement Islands and EoP:	142
6.3.2	Understanding volumes of Islands as CoP:	148
6.4	Outlook and Future Directions:	154

A	Details of Embedding Functions for charged and uncharged AdS BH	157
A.1	Uncharged BH Embedding	157
A.2	Charged BH Embedding	160
A.3	Fourth-Order Change in Entanglement Entropy	162
	Bibliography	165

LIST OF ABBREVIATIONS

1. AdS : Anti-de Sitter
2. CFT : Conformal Field Theory
3. QFT : Quantum Field Theory
4. SYM : Super Yang-Mills
5. QI : Quantum Information
6. BH : Black Hole
7. RT : Ryu- Takayanagi
8. HRT : Hubeny-Rangamani-Takayanagi
9. QM : Quantum Mechanics
10. TFD : Thermo-Field Double
11. QCD : Quantum Chromo Dynamics
12. EE : Entanglement Entropy

13. HEE : Holographic Entanglement Entropy
14. HSC : Holographic Sub-region Complexity
15. EoP : Entanglement of Purification
16. EWCS : Entanglement Wedge Cross Section
17. CV : Complexity = Volume
18. CA : Complexity = Action
19. QES : Quantum Extremal Surface
20. MbW : Multi-boundary Wormhole
21. FG : Fefferman-Graham
22. BTZ : Banados-Teitelboim-Zanelli
23. ADM : Arnowitt-Deser-Misner
24. HQ : Hawking Quanta
25. SI : Shared Interior
26. CoP : Complexity of Purification

LIST OF FIGURES

0.1	RT surface and Volume below RT surface in AdS/CFT	vi
2.1	A schematic diagram of bipartite purification ($AA'BB'$ forms a pure state and EoP is entanglement between AA' and BB')	16
2.2	Representative image for understanding complexity. Let's say, the different shapes with different numbers are the pre-defined gateset that can be used to construct the target state $ \psi_T\rangle$ starting from the reference state $ \psi_R\rangle$. The number of times each of the gates used contributes to the complexity. Also, if we associate different costs with different gates (shapes), the complexity becomes different and the ratios of the costs between different gates are understood as the penalty factors.	21
2.3	Ryu-Takanagi surface in AdS/CFT: The boundary sub-region A is the green circle on the boundary denoted by the blue rectangle. Rest of the region is denoted as B . ϵ is the UV cutoff along z axis. The green curve γ_{RT} along z direction sharing the boundary of A (∂A) is the Ryu-Takayanagi surface.	24

2.4 Entanglement Wedge Cross Section (holographic dual of Bipartite Entanglement of Purification). The boundary sub-regions of the AdS time-slice after removing the top and bottom regions are A and B . The two bulk geodesics (top and bottom) corresponding to the removed grey regions can be thought of as $\tilde{A} \cup \tilde{B}$ which along with $A \cup B$ forms a geometric pure state. Among all possible dotted lines shown in the figure dividing the bulk geodesics into \tilde{A} and \tilde{B} , the minimal is the blue one marked as $\Gamma_{\tilde{A}\tilde{B}}$ (EWCS). 25

2.5 EWCS for tripartite EoP: The combination of A, B, C (boundary regions forming the mixed state) and the the HRT geodesics ($\tilde{A} \cup \tilde{B} \cup \tilde{C}$) of the removed regions are considered to form a tri-partite geometric pure state. $\Gamma_{\tilde{A}\tilde{B}\tilde{C}} = \Gamma_{A\tilde{A}} \cup \Gamma_{B\tilde{B}} \cup \Gamma_{C\tilde{C}}$ becomes the multi-partite EWCS. Contrary to the bipartite case, here the sum of the three orange curves are minimized among all possible choices. 27

2.6 CV and CA conjectures: CV measures the volume of the time-slice where the two sides of the eternal BH are connected by the Einstein-Rosen (ER) bridge. CA measures the action on the causal patch of the ER bridge time-slice. This patch is known as the Wheeler-de-Witt (WdW) patch. (Images are inspired by [11]) 30

3.1 Plots of y_1 , y_2 and y_3 in various dimensions. Note that we do not have y_3 for AdS_{12} 47

3.2 Plots of $\frac{1}{p^2}y_{(0,1)}$ and $\frac{1}{p^2(1+p^2)}y_{(1,1)}$ in various dimensions. 50

3.3 Plots of Δs and Δc to second- and third-order in the uncharged black hole background. The points are explicitly calculated values. The curves are plots of the general formulae. 64

5.1	Penrose diagram of two sided Black Hole with nontrivial island included (red and blue lines represent Hawking partner modes outside and inside the black hole horizon respectively.)	105
5.2	Choice of islands before and after Page time and Page Curve	107
5.3	Two boundary case and Horizon length, equivalent to EWCS for bipartite system.	109
5.4	Change of preferred HRT in 3 boundary model. Left: Before the Page time the HRT surface separates the R_i from the remainder of the pair of pants. Right: After the Page time L_0 has shrunk to L'_0 and the HRT surface has jumped to include the island I	111
5.5	Change of preferred HRT in $n + 1$ -boundary model.	112
5.6	Page curves corresponding to the left: three and right: n boundary models.	112
5.7	The three-boundary Riemann surface as quotients of the two-boundary Riemann surface. The three-boundary surface is obtained by pinching one of the boundaries into two. The island is marked by the closed region spotted by the dotted purple, black, blue, and blackline respectively.	114
5.8	Three and Four Boundary cases : Semicircles to be removed are are marked. Blue-shaded regions represent the shared interiors. These are the choices that minimizes the boundary of the shared interior with respect to the corresponding geometric pure state.	116
5.9	(left) Growth of the multipartite EWCS (for the minimal choice). (right) Comparison between primary (red) and later (green) choice of HRT with the minimal island(blue) growth at different times.	120
5.10	HRT surfaces and entanglement wedges in AdS_3 for one (left) and two intervals. The latter has two phases, (middle) Phase I and (right) Phase II.	124

5.11	Pair of Pants and Polygonal Representation. In the figure, concentric geodesic edges are denoted by C_1 and C_2 , whereas C_a and C_b stand for geodesics that are not concentric. c_1 and c_2 denote the centres of the non-concentric geodesics on the horizontal plane.	125
5.12	Hyperbolic octagon and Causal Shadow in three-boundary wormhole model. . .	131
5.13	Hyperbolic octagon through hyperbolic triangles.	131
5.14	Complexity plots of 3 boundary island model for two solutions of R	133
5.15	Complexity plots of $n + 1$ boundary island model for two choices of R.	134
6.1	A representative figure of islands and purification: Phase I: In the beginning phase, the black hole is the black sphere and there are no Hawking quanta. Phase II: Evaporating black hole is a blue sphere (LHS) and HQ is a blue sphere (RHS). Phase III: (Page time) Red spheres in LHS and RHS are BH and HQ respectively. P (purple spheres) are the purified partner modes on both sides. The information of purification is carried by the island region connecting LHS and RHS.	152

CONCLUSION AND OUTLOOK

In this chapter, we summarize the results obtained in the works included in the thesis to conclude and discuss the prospects of studies along this line of research. We have focused on studying the holographic entanglement entropy and holographic sub-region complexity of various black solutions. After introducing the basic notions and contents of this thesis in chapter 1 and reviewing the very basic definitions of quantum information-theoretic quantities (both quantum-mechanically as well as holographically), we moved on to discussing the works constituting this thesis. Primarily, we studied the perturbative changes of HEE and HSC for the AdS Schwarzschild black holes in general spacetime dimensions in chapter 3. Then we studied QI theoretic quantities for certain non-Susy black solutions in chapter 4. Finally, we discussed the lessons we learn from studying these QI theoretic quantities about the black hole information paradox by studying certain multi-boundary wormhole models in AdS₃ in chapter 5. In the following, we list down the lessons and conclusions from each of those chapters and finally conclude by mentioning certain interesting future directions in section 6.4.

6.1 Conclusions from Chapter 3:

First, we highlight the main findings of chapter 3. Then, the suggestions that these results lead us to make, will follow.

1. We have computed the change in holographic entanglement entropy (HEE), ΔS , and sub-region complexity (HSC), ΔC , for spherical entangling regions of radius R in the background of the uncharged and charged AdS_{d+1} black holes. For the uncharged case, we have performed the calculations perturbatively in the parameter $\lambda = mR^d$, where m is the black hole mass. We find formulae as functions of d for ΔS and ΔC up to the third order and we also provide exact numerical results for $\Delta S^{(4)}$ in spacetime dimensions 3 to 7. For the charged case, the perturbative study has been done with respect to the small parameter $\eta = \frac{R}{z_h}$, where z_h is the charged black hole horizon radius. We compute ΔS and ΔC up to the first four orders and have again found formulae as functions of d .

We observe that the change in entanglement entropy and sub-region complexity at a particular order come with opposite signs relative to one another. This holds to all the orders we have studied for both the uncharged and charged AdS black holes. It also holds to leading order for the case of a scalar perturbation [74, 87]. This exchange in sign is mysterious from the dual field theory perspective and begs an explanation.

2. Another important finding of this work is the proof that the entanglement entropy changes up to some order n depends on the embedding function only up to the highest order less than or equal to $\frac{n}{2}$. This upper bound has not been appreciated previously, to the best of our knowledge. We hope that this allows others to push the calculations

of HEE further. In addition, we note that the change in sub-region complexity up to some order n depends on the embedding function all the way up to that same order. We, therefore, gain a more quantitative sense of the information that is contained in sub-region complexity but not in entanglement entropy.

With these main results and taking inspiration from previous works, largely from [4, 8, 87], we are lead naturally to several suggestions. From an information-theoretic perspective, it appears as though the information is being traded between the entanglement between a boundary sub-region and its complement and the complexity of the CFT state reduced to that sub-region. In particular, [87] in fact inadvertently suggests that the HSC contributes a term to the first law of entanglement that is analogous to work:

$$\Delta E = T_E \Delta S_E + B \Delta C, \quad (6.1)$$

where B is some known d -dependent quantity related to a pressure defined in (3.92). Using the closed-form of the second-order change in HSC, we have been able to fix the d -dependent constant relating this to Fisher information, as proposed previously in [87]. That a first law in the form (6.1) does not hold in general at third-order begs the existence of other information-theoretic quantities at higher orders. We hope that a more complete picture from the perspective of the information geometry will emerge from these investigations.

We note that certain modifications and generalizations to the first law of entanglement have been considered before (e.g., in [8, 140]). Notably, in time-dependent scenarios (e.g., a collapsing black hole), it was found in [140] that the first law is naturally replaced by a certain linear response relation. It would be interesting to study the modifications to the linear response relations that arise in second-order and if they are at all related to complexity

as we have suggested here primarily for the static case.

Recent works have tried to come up with various field-theoretic definitions of complexity from a few different perspectives, for example, geometric and circuit complexity [26–28, 141–144] and path integral complexity [145, 146]. These two perspectives have been very recently bridged in [59, 147]. Using this line of study, it would be interesting to study the fidelity, primarily for free QFTs and then for holographic CFTs. It would be interesting to check whether the third and higher-order expansion terms follow the relations we found in higher orders.

6.2 Conclusions from Chapter 4:

In chapter 4, we have holographically computed the EE and the complexity of the QFT whose gravity dual is given by the decoupled geometry of ‘black’ non-Susy D3 brane of type IIB string theory for spherical subsystems. The field theory, in this case, is non-supersymmetric and non-conformal and we have considered both the strip and spherical entangling regions for computations of HEE. For the HSC study, we have focussed on the spherical subsystems only.

6.2.1 Strip HEE:

For the strip entangling region, we have used Fefferman-Graham coordinates to compute the entanglement entropy. For a small subsystem, we have shown that the total EE can be split into a pure AdS_5 part and an additional part corresponding to the weakly excited state of the field theory. The additional part was then found to match exactly with the earlier result for ordinary black D3 brane when the parameter δ_2 of the non-Susy D3 brane takes a value -2 . In the Fefferman-Graham coordinate, we have obtained the forms of the boundary stress tensor of the non-Susy D3 brane. Using the expressions of the stress tensor and identifying various components with the energy and pressure densities we have shown

that the EE of the excited state satisfies the first law of entanglement thermodynamics proposed earlier. We have also checked that at high temperature the total EE of the decoupled theory of non-Susy D3 brane reduces to the thermal entropy of that of the ordinary black D3 brane and not the ‘black’ non-Susy D3 brane. It is interesting to note that at high temperature the EE of a non-Susy D3 brane prefers to cross over to the thermal entropy of the ordinary black D3 brane, among all possible non-supersymmetric D3 brane configurations (with different values of δ_2).

6.2.2 Spherical sub-region HEE and HSC:

For the spherical entangling region, we have computed the entanglement entropy and sub-region complexity for the decoupled ‘black’ non-Susy D3 brane geometry up to the second-order in perturbation parameter using the prescription of Ryu and Takayanagi. We have extended our calculation of complexity to compute the fidelity and the Fisher information metric using the definition given earlier [87] for both the AdS_5 black hole and the decoupled ‘black’ non-Susy D3 brane geometry for the spherical subsystem. Since the decoupled geometry of ‘black’ non-Susy D3 brane reduces to the standard AdS_5 black hole when its parameter δ_2 takes value -2 , we have observed that both the EE and the complexity for the former geometry indeed reduce to those of the AdS_5 black hole when we put $\delta_2 = -2$, giving a consistency check of our results. We have also checked the entanglement thermodynamics to be consistent for the spherical subsystem and gives the same entanglement temperature as the AdS_5 black hole. We have further observed that although the fidelity and the Fisher information metric of the QFT dual to decoupled ‘black’ non-Susy D3 brane geometry remains the same as those of the AdS_5 black hole when one uses proposal of [87], using a more exact relation [74] without any arbitrary constant gives us a different value of Fisher information in the case of the non-supersymmetric solution,

which is parameter dependent. Putting the right parameter value gives back the AdS_5 black hole result, indicating (4.73) is a more general relation which includes the AdS_5 black hole relation as well.

6.3 Conclusions from Chapter 5:

From chapter 5, we have built a couple of parallel understandings in the context of the multi-boundary wormhole models of island. Firstly we write down the learnings in line of entanglement of purification and lastly, the ideas about complexity of islands as purification complexity.

6.3.1 Entanglement Islands and EoP:

From the connections we made between multipartite entanglement of purification and multi-boundary wormholes in AdS_3 , we can take away the following points.

1. First and foremost, the multipartite entanglement wedge cross-section represents the boundary of the islands described in the toy model of the evaporating black hole. We believe that knowing this would strengthen the possibility of building a concrete understanding of the islands as well as purification in several different ways e.g; quantum error correction, entanglement negativity, and many more. Precisely, in the large n limit, i.e.; where the number of smaller exits is big, multipartite EoP and the shared island match completely. In the multi-boundary wormhole picture, the shared island is the region behind all the horizons present (which is also the case in the original works discussing the actual model) and therefore it falls in the region known as entanglement shadow. Our work suggests that through the multi-boundary wormhole construction, the entanglement shadow can have a description through the multipartite EoP of sub-regions in a vacuum AdS_3 slice.

2. The reproduction of the Page curve helps to describe an evaporating black hole as a unitary system since the Page curve is typically found in systems that evolve unitarily over time. Now, given the appearance of islands, or rather quantum error connection makes sure that the unitarity of the black hole evaporation process is recovered, one would hope that these two things are related. The natural way to somewhat realize the connection is of course the purification of the Hawking quanta after the Page time. This results in the appearance of the nontrivial islands. In our study as well, we use ideas of purification regularly which give rise to the multipartite EWCS, and the area enclosed is understood as the nontrivial island (quantum error correction). In other studies as well, for example, in [133], people have explored connections between entanglement of purification and quantum error correction. But, it would be really interesting to understand such a connection as a triangular relation where the three vertices of the triangle correspond to unitarity, purification, and quantum error correction. Regarding the line connecting unitarity to purification, a realization to start the study is the fact that a reduced density matrix (from which the purification is typically done) is derived by tracing out degrees of freedom from the initial pure state.

$$\rho_{red} = Tr_{(pure-red)}[\rho_{pure}]. \quad (6.2)$$

This tracing out is a non-unitary operation. Therefore the reduced density matrix indeed carries the effect of a non-unitary operation. Hence, it is not beyond expectation that to get back the unitarity completely one needs to apply purification to the reduced mixed state. This is a start that can be pursued in more detail to get a better understanding of the above-mentioned triangle.

3. Although the islands can be intuitively understood as the shared interior, the length associated with the boundary of such a shared interior leads to a problem in overcounting due to which the entropy associated with the shared interior does not follow the Page curve (since the growth of the boundary of the nontrivial island after the Page time persists as it includes the previously chosen HRT surfaces as well). To be precise, in the toy model, it is assumed that the RT surfaces take care of the bulk entropy between the fields that live on different sides of the HRT. But once the new choice of HRT is made, it has both the partner modes in there. The modes for which the partner modes are not yet inside the new HRT, their bulk entanglement with their partners is again taken care of by the new HRT. But if one computes the sum of the length of the shared interior simply considering it to be the boundary of the island, one again counts the bulk entanglement between the modes which have already been purified due to the choice of the new HRT. Let us call the shared interior SI. Then,

$$L(\partial(SI)) = L_{BH} + L_{HQ}. \quad (6.3)$$

SI only comes into the picture after the choice of nontrivial island is minimal. Starting from that point, the boundary of SI also includes L_{HQ} , which have bulk entanglement between partner modes of the two sides of the previous HRT choice, and this is how the overcounting can again come into the picture.

In [110], the authors introduce a second model involving handles and pairs of TFD states of the baby universe and the radiation states to understand the previous overcounting that in the first place led to the information paradox. We see here that even without introducing a new model, one can get the overcounting from the very first model by naively following the formula of the quantum extremal surface to include

the whole length of the boundary of the nontrivial island and get back to the earlier paradox.

This is a warning that taking the intuitive understanding of islands too literally might lead to several problems. In this particular toy model, it is necessary to compute the lengths of the chosen HRTs only at any point in time. It is not only that one does not need to include the bulk entanglement, but it is also wrong to consider the remaining part of the quantum extremal surface formula in terms of the island. This subtlety might also capture important insights in making a connection between islands and QEC more concrete since QEC is well studied in the literature of EoP [133].

4. For the problem of multipartite EoP, one can make simple calculations that show how the multipartite EoP grows over time and how different parts of it contribute to the Page curve in the multi-boundary wormhole model of black hole evaporation in AdS₃. But it brings up another question that needs further understanding and study that whether in multipartite EoP, there is any overcounting taking place that one needs to be careful about. Since we consider the union of smaller black holes as our radiation state, a possible resolution in the purification side is simply considering that in the given limits (one black hole much much larger than all the other ones), the total state behaves as a bipartite state instead of a multipartite state and the entanglement of purification reduces to usual entanglement entropy.

$$\Delta_W(A : B_1 : B_2 : \dots : B_n) \longrightarrow E_P(A : B) = S_A = S_B, \quad (6.4)$$

Where A is the bigger black hole and B is the union of the smaller black holes (B_1, B_2, \dots, B_n) . To specify what is going to be $S_A = S_B$ at different times depends on which part of Δ_W is minimal choice. For example , we can divide Δ_W

into two parts, one coming from the EWCS of two boundary wormhole ($\Delta_{W,1} = \sqrt{L_0^2 - n\ell^2}$) and the other coming from the EWCS of the unions of the smaller boundaries ($\Delta_{W,2} = n\ell$). At all times, we can write,

$$\Delta_W = \Delta_{W,1} + \Delta_{W,2}, \quad (6.5)$$

and at each time (for $n > 2$), in the limit where we consider the multipartite pure state as a bipartite one,

$$E_P(A : B) = S_A = S_B = \min(\Delta_{W,1}, \Delta_{W,2}) = \min(\sqrt{L_0^2 - n\ell^2}, n\ell). \quad (6.6)$$

This is a justifiable assumption since ultimately we are bothered about the entanglement between the radiation state (union of smaller black holes) and the evaporating black hole state. Therefore it is not so unexpected that the initially multipartite situation reduces to a simpler bipartite one. A detailed field-theoretic study similar to [134] in terms of purification would be able to shed more light on the necessity of this consideration. This is an ongoing problem that is in progress. Also, it would be interesting to consider different exits of a multi-boundary case differently and study how would multipartite EoP behaves.

5. At this point, it is also important to note that how a multipartite EoP is reduced to a bipartite case is very similar and pictorially same to choosing just the area of the HRT instead of choosing the area of the nontrivial island in this toy model. In both of the cases, one would encounter the information paradox had the alternate choice been made.

In a recent model introduced in [112], the authors work with end of world branes

and the multi-boundary wormhole appears in the auxiliary system introduced for the purification. They consider something they term as "inception geometry" to propose an extremal surface through which the nontrivial islands can again be marked. They argue that there is some region behind the horizon that can only be found if the Hawking radiation is considered as a union of different subsystems of the radiation. They call such an event quantum/geometric secret sharing. In our discussion through our resolution, we find that it is necessary to finally consider the system of big and smaller black holes as a bipartite pure state to make sense of the Page curve. But nevertheless, it is absolutely necessary to model numerous smaller black holes (subsystem Hawking radiation) to get the analog and intuitive understanding of islands. Had we just considered a bipartite pure state, i.e; a two boundary wormhole, we would never be able to get the shared interior that appears after the Page time. Note that in this case, there is only one choice in choosing the EWCS as well as the HRT. Therefore, our discussion in a way also addresses the necessity of modeling the radiation as a union of subsystems as discussed in [112]. In light of such findings, we prefer to make the following statement,

Although multipartite purification in the multi-boundary wormhole toy model gives back the overcounting once the boundary of the island is computed, it is absolutely necessary to primarily have the multipartite nature in the modeling of the radiation states to have a realization of the islands in the toy model. To resolve the overcounting issue, we nevertheless need to review the model as the bipartite one and choose the minimal one among the two parts of the multipartite EWCS as the entanglement entropy of the bipartite pure state.

6.3.2 Understanding volumes of Islands as CoP:

We have computed the sub-region complexity corresponding to the radiation subsystem in the multi-boundary wormhole models in the second part of this chapter. We have considered two models in which the islands appear, the three-boundary wormhole and the $n+1$ -boundary wormhole. Although the two models are qualitatively similar and the island region in both the models corresponds to the causal shadows, there are some differences as well. In [10], we discussed these causal shadow volumes from three different perspectives, i) Ricci scalar (mentioned in this thesis) ii) kinematic space, and iii) tensor networks and hyperbolic tessellations. In what follows, we explain the understanding built from [10]. As the volume computation using Ricci scalar and topology is what we explained in this thesis, we stress mostly on the same. But we also briefly mention what kinematic space and tensor networks teach us about these volumes.

1. **Sub-region volumes:** This is the central piece of this chapter 5. We computed the volumes corresponding to a bipartite radiation subsystem for the three-boundary wormhole and n -partite one for the $n + 1$ -boundary wormhole. The remaining exit in both cases represents the evaporating black hole. As we have mentioned already the proposals in the literature [4, 71], the volumes dual to the sub-regions capture the complexity of the corresponding state. Therefore, the computation of volumes is aimed at enhancing our understanding of the complexity of the radiation state. Recent findings and especially the implications of Python's lunch [127, 128], suggest that even though quantum extremal surfaces enable us to reproduce the Page curve, it is still exponentially hard to compute the restricted complexity of the radiation state. Therefore, while Hawking was mistaken about entropy, his statements truly apply to complexity. Now, since in these three- and $n + 1$ -boundary wormhole models,

one can reproduce the Page curve consistently, we performed explicit calculations to investigate if the volumes feature precisely such exponential growth. However, it is worth noting that within these multi-boundary models, the volumes can not capture the exponential restricted complexity.

For both models under study, we find two kinds of plots that the volumes dual to the radiation subsystem follow. One is a constantly decaying one whereas the other one is of Gaussian nature. In both cases, at the Page time, a constant volume is added to the otherwise UV divergent volume due to the change of the minimal surface. The universality goes deeper since the overall plots are very similar even though the nature of the Page curves, especially the Page time is quite different in the two models. In the case of the three-boundary model, this volume is simply 2π whereas for the $n + 1$ -boundary analog, it depends on the Page time, here n_{Page} . Therefore, the only difference between the nature of the plots is the jump at Page time being independent or dependent on the Page time. It would be interesting to see if this addition of constant volume at Page time is a consequence of three-dimensional AdS or not. But since the construction of multi-boundary wormholes is only well known for AdS₃, it is hard to check this for general spacetime dimensions.

Now let us come back to the nature of the two kinds of plots (figures 5.14 and 5.15). In both cases, we find that although the minimal lengths increase steadily before the Page time, there is no guarantee that the volumes also increase. For example, for the three-boundary model the HRT length increases until it reaches the Page time, but the Gaussian plot of the volume already starts decreasing *before* the Page time. For the constantly decaying plots, this is even more evident since the volume keeps decreasing irrespective of the nature of the plot that the HRTs follow. Again, the only

effect that the Page transition leaves on the volume is a constant jump. This jump is due to the addition of the causal shadow region and the UV divergent part remains unchanged due to a homology constraint of the boundary spatial lengths. There is nevertheless something universal about the nature of these plots since in both models, we end up with very similar graphs with substantially different considerations only distinguished by the quantity of the constant volume that is added at the Page time. Interestingly, none of our plots feature exponential growth. This begs the question of whether these volumes represent the complexity of the radiation or not. We do not want to make any strong comments regarding that. But what our results show is how the volumes dual to the radiation subsystems evolve with time within the scope of these models. Now, for concluding how exact these models are, one indeed needs to build a better understanding of the actual evaporating black hole rather than a multi-boundary wormhole model. It would be interesting to check if similar calculations can be done in an actual evaporating black hole situation instead of our simplified models. If the results in those cases also mimic what we find, only then can we say that these multi-boundary wormholes can model the evaporating black holes accurately. Otherwise, the conclusion is simply that although within the purview of these models, one can reproduce the Page curves by studying classical HRT surfaces, they are not capable of capturing more complex phenomena like the complexity of the radiation. It might also be interesting to investigate the nature of these volumes if one works with the eternal BH construction using the multi-boundary wormhole geometries. There, we can expect continuing growth of the volume since the BH exit does not shrink (transparent boundary conditions).

2. On the complexity of purification: The volume of the causal shadows for the multi-

boundary wormholes have been discussed before briefly in [138, 139, 148] in the context of purification complexity. The reappearance of these results in our context strengthens the correspondence between the islands and purification. The correspondence between multi-boundary wormholes and entanglement of purification (EoP) was first advocated in [70]. In section 5.3 of this chapter, these similarities were discussed in regards to the multi-boundary wormhole model of islands and multi-partite entanglement of purification. We can therefore argue for a similar but extended version of this correspondence from the understanding of complexity in chapter 5. According to our results, the change of complexity (ΔC) due to the island within these models is simply equivalent to tripartite or multipartite complexity of purification (CoP). The way one talks about purification in the context of the island is that after the Page time, some of the Hawking modes outside the black hole horizon get purified by their partner modes inside the black hole since the radiation subsystem gets access to those partner modes inside the horizon. This happens due to the inclusion of the island regions in the entanglement wedge of the radiation subsystem. In terms of complexity, our results signify that the access to the purifying partner modes also enables the radiation subsystem to access a certain new number of gates which results in the jump at Page time. This jump from no-island to island phase has been also addressed in [149](Section 4) and has been attributed to the mutual complexity, which matches with the multipartite purification complexity as shown in [138, 139]. Within the scope of these models, to the best of our understanding, after the Page time, the access to this new set of gates characterizes the non-trivial nature of the plots of the sub-region complexity (as shown in Figures 5.14 and 5.15). We show a representative figure of the above-mentioned event in Figure 6.1. However, the consistent fact apart from the jump in the two candidate curves is that in both cases

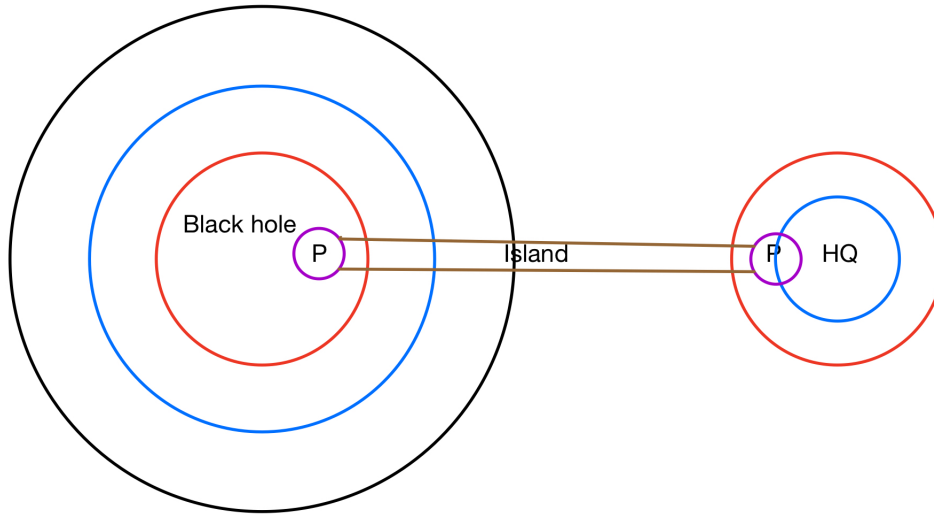


Figure 6.1: A representative figure of islands and purification: Phase I: In the beginning phase, the black hole is the black sphere and there are no Hawking quanta. Phase II: Evaporating black hole is a blue sphere (LHS) and HQ is a blue sphere (RHS). Phase III: (Page time) Red spheres in LHS and RHS are BH and HQ respectively. P (purple spheres) are the purified partner modes on both sides. The information of purification is carried by the island region connecting LHS and RHS.

the mixed state complexity of the final radiation state becomes zero indicating a final pure state. On the other hand, the initial complexity of the two candidate curves shows different features (large value in the decaying one and small or zero value in the other one) indicating that in the very initial phase, the radiation might go through different evolution procedures within these models.

3. **Kinematic Space lessons:** Given the prominent role of bulk regions such as causal shadows and islands in our analysis, we elucidated its properties from a complementary angle in [10]. We have shown how to reconstruct volumes of islands in the CFT through the use of kinematic space. Our analysis displays which quantum information encodes the volume of islands. For a wormhole geometry with $n + 1$ exits, the correlations responsible for the entanglement of each sub-region within a single exit

never contribute to the island's volume. The protagonists are always the correlations arising through the entanglement between the smaller exits. Other contributions to the island's volume arise from geodesics that are anchored in the causal shadow region. They contribute through their chords piercing the island and we have described how these terms can be computed. Moreover, we have combined the expressions for the volume of causal shadows and islands with our general results from pure gravity analyses to derive integral identities for trigonometric integrals, in line with the purpose of integral geometry. These identities might be of interest to the mathematical community, and of course, any physicist working with trigonometric integrals.

4. **Tensor Networks and Volumes:** Finally, through our discussion in [10], we explained how the tensor network approach in multi-boundary wormholes can be used to build a parallel understanding of the throat horizon minimal surfaces and the corresponding volumes. While the number of tensor legs cutting a minimal surface quantifies the length of the throat horizons, the total number of tensor legs within any volume encoded by boundary and bulk surfaces quantifies the volumes. This is a rough way of quantifying volumes inspired by the study in [71]. The limitations of this quantification stem from discretizing hyperbolic space through discrete Coxeter group tessellations.

We have worked with various equivalent definitions of area and volumes within the multi-boundary wormhole models of the island and black hole evaporation. The most quantitative results that we obtain are from the exact volume calculations with the given assumptions of the models in hand. In the other sections, we have partly explained the qualitative lessons and partly turned the qualitative results into quantitative ones.

6.4 Outlook and Future Directions:

The works constituting this thesis explore various properties of HEE and HSC in BH backgrounds. Besides answering a few questions it also leaves open a few interesting directions that can be explored further to understand the holographic and field-theoretic results better. In the following, we briefly mention a few of these directions.

1. **Entanglement Thermodynamics:** As mentioned previously, in [5] we proposed a work-like term using sub-region complexity that fails on its own in the third order. It will therefore be interesting to look into this direction more to figure out what exactly constitutes the full form of the thermodynamics-like relation. These missing pieces are supposed to help us understand the exact QI measures contributing to the change of the overall spacetime extending the *entanglement builds geometry* proposal to *QI builds geometry*.
2. **Non-susy directions:** It would be nice to understand our holographic non-Susy results by introducing a relevant deformation to a supersymmetric CFT and construct a non-Susy field theory. If one can compute EE and complexity even in the simplest possible non-Susy example of field theory, the holographic results can be matched and understood better along the way. Moreover, the fact that our results from [6, 7] show that the version of entanglement thermodynamics remains unchanged gives us hope to propose that even the non-supersymmetric geometries of spacetime can be thought of as being consistently connected to QI theoretic measures.
3. **Purification, Complexity and Quantum Error correction:** Our results from [9, 10] not only indicate that the physics of islands might be related to the purification happening at Page time, but also shows signs of it being related to the holographic quan-

tum error correction [123]. Therefore it would be immensely interesting and worthy to check whether these connections can also be made by a field-theoretic computation. The idea is to try to mimic the island-inclusion using purification in QM or free field theory scenario and check whether one ends up with a Page curve. Also, using recent studies on CoP [60, 61] and quantum error-correcting codes (QECC) in free QFT and pretty basic CFTs [150, 151], one can check whether a connection can be found between purification and QECC.

4. **Complexity for the evolution of Eternal BH-Radiation system:** Apart from this, another interesting holographic problem is to study the complexity of evolution for the eternal BH-radiation system. The motivation is to see if similar signatures of purification can be found at Page time for those models as well. A couple of models that seem interesting from this perspective are [112, 152]. The complexity curve for both BH and radiation states of eternal BH radiation described in [152] has been studied already in [153].

The AdS/CFT and QI remain to be a very active field of research. It has many ramifications that are worthy of being explored and promises to give us a diverse understanding of physical systems. Complexity and entanglement both continue to be critically crucial pieces in these studies and studying more and more quantum mechanical and field theoretical situations are believed to be critical in building a more concrete understanding. On one side, whereas CFT sides are important to understand the results of the holographic studies precisely, the current research also revolves around condensed matter understanding of quantum mechanical phenomena like chaos and quench. The tensor networks also work as a very important piece in these studies, especially in understanding spacetime as quantum circuits where different components of the network represent the entanglement and com-

plexity of the physical systems in the study. We believe the research constituting this thesis in the holographic aspect will play a role in all of these directions once we have a better field-theoretic understanding.

SUMMARY

In this thesis, the detailed computations of holographic entanglement entropy and sub-region complexity have been presented for several black hole solutions. This is done with the larger goal of understanding the connections between quantum gravity and quantum information using the AdS/CFT correspondence [1]. The central notions used in this thesis were introduced in the Ryu-Takayanagi (RT) proposal of holographic entanglement entropy [2, 3] and the sub-region complexity proposal introduced in [4] (see figure 0.1). In the figure, the blue region is the CFT which is divided into two regions A and B . The green surface γ_{RT} , in dual bulk AdS with extra scaling dimension z , is the RT surface. The area of this surface measures the entanglement between the boundary sub-region A and B . The purple volume between γ_{RT} and the region A is proposed to measure the sub-region complexity of the mixed state defined on A . It is proposed to measure the hardness of preparing the mixed quantum state on A . We have done our computations perturbatively for the AdS black holes [5] in general spacetime dimensions. Similar computations and supporting conclusions have been drawn by studying non-supersymmetric D3 brane [6, 7] which hopes to provide us some clue about QCD like theories in the long run. In both of these cases, we have also discussed implications regarding something called entanglement

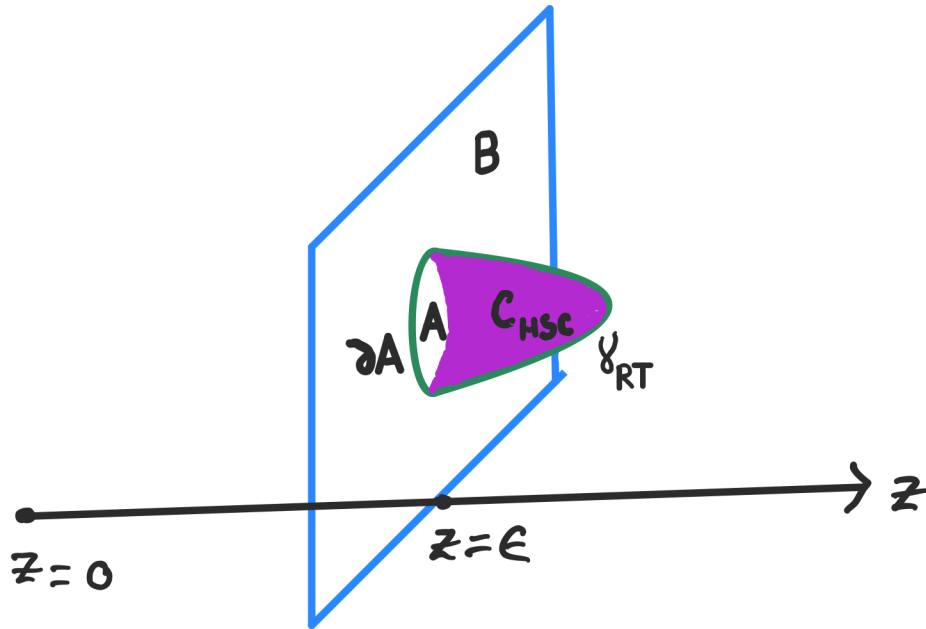


Figure 0.1: RT surface and Volume below RT surface in AdS/CFT

thermodynamics introduced in [8]. In the final part of thesis, we have studied the entanglement and complexity in a model of black hole evaporation [9, 10] in which the apparent version of the black hole information paradox is resolved. Building on our study, we have been able to understand a few connections to this resolution with the physical phenomenon known as purification. After introducing the basic concepts that are necessary for the main part of thesis, we have discussed the research articles constituting this thesis and finally concluded with open future directions.

CHAPTER 1

INTRODUCTION

One of the biggest dreams of theoretical physicists has always been to unify four fundamental forces of nature (electromagnetic, strong-nuclear, weak-nuclear, and gravitational forces). The beautiful framework of quantum field theory successfully incorporated three of these four forces through the standard model of particle physics, leaving out only gravity. The remaining piece of the puzzle, therefore, has been to consistently build an understanding of the quantum nature of gravity. In trying to obtain this, physicists have nevertheless come a long way during the last fifty years. Although the picture is not clear yet, the path towards the ultimate goal has been a beautiful one to date. It has seemed darker at times. The advent of string theory has however taught a lot of things in this regard. The primary success of the theory was to provide us with a consistent theory in higher dimensions that can accommodate all the four forces within its mathematical framework. Eventually, it became clearer that this theory through its many avatars, can also successfully solve not one, but many of the smaller puzzles in the way of the final one. The most exciting one among the derivatives of string theory has undoubtedly been the AdS/CFT (Anti-de Sitter/Conformal

Field Theory) correspondence *a la* Juan Martin Maldacena. This is a duality, like many others present in physics, that is special in itself because it relates the observables of a five-dimensional gravity theory to their respective counterparts in a four-dimensional quantum field theory with some extra symmetries. The correspondence originates from a variant of string theory in ten spacetime dimensions known as the type IIB string theory and is manifest as a strong-weak duality from the perspective of the coupling strengths of the two sides. The gravity side constitutes a theory in five dimensions with constant negative curvature, known as the AdS whereas the exact CFT on the other side is the $\mathcal{N} = 4$ SYM (Supersymmetric Yang-Mills) quantum field theory in four spacetime dimensions. The extra dimension in the gravity side is attributed to the scaling dimension of the bulk theory. Since its birth, the correspondence has been investigated in detail and largely believed to hold in general spacetime dimensions as a co-dimension 1 duality. The symmetry structure of the two sides also goes hand in hand and the observables in the two sides which define the AdS/CFT dictionary mostly agree with each other for almost all the cases where both of the two sides can be computed. Another plus point of the dictionary is that when one intuitively understands what the two observables correspond to in the respective sides, one can compute it in a way that is easier among the two sides by weighing in the difficulties of calculation. In the following, we very briefly discuss the correspondence, which in no way is self-sufficient, but gives a reader some quick exposure to moving forward with.

1.1 AdS/CFT and Holography:

AdS/CFT correspondence [1,12] is also known as the gauge/gravity duality, or at times, holography. The reason behind naming such duality as holography is that it is a crucial realization of something called the *holographic principle*.

In the context of a semi-classical version of quantum gravity, the holographic principle

states that the information stored in a $(d + 1)$ dimensional volume is captured by the d dimensional area measured in units of the Planck area (L_p^d). An important motivation in this respect comes from the Bekenstein bound which asserts that the maximum entropy stored in a volume is given as the area (again, measured in Planck units) divided by $4G_N$, where G_N is the Newton's constant. Hence, the situation is quite similar to the idea of holograms in optics and therefore the name.

In the case of holography, the quantum gravity theory is defined on a manifold $AdS \times Y$, where Y is a compact manifold and the QFT lives on the conformal boundary of the Anti-de Sitter spacetime. As mentioned earlier, the first and most understood version of the duality was worked out in [1] relating $\mathcal{N} = 4$ Super Yang-Mills theory in $3 + 1$ dimensions to type IIB superstring theory on $AdS_5 \times S^5$. The strongest form of this duality states that the four-dimensional SYM theory with gauge group $SU(N)$ and Yang-Mills coupling g_{YM} is equivalent dynamically to the string theory with string length $(l_s =) \sqrt{\alpha'}$ and coupling g_s on the $AdS_5 \times S^5$ with the radius of curvature L (same for both the AdS as well as the compact sphere). The parameters of the two theories are related to each other by the following relation,

$$g_{YM}^2 = 2\pi g_s, \quad 2g_{YM}^2 N = \frac{L^4}{\alpha'^2}. \quad (1.1)$$

Although the above-mentioned exact correspondence is quite interesting, it is extremely hard to do explicit calculations for the exact correspondence. Therefore, most of the time, we deal with a relatively weaker version of the duality. This is done by taking limits on both sides by treating it as a strong-weak duality. Precisely, we work with a strongly coupled version of the field theory ($N \rightarrow \infty, \lambda = g_{YM}^2 N \rightarrow Large$), where the gravity side becomes classical supergravity solutions, which is weakly coupled in terms of the string coupling constant as well as the string length ($g_s, \frac{\alpha'}{L^2} \rightarrow 0$). This is sometimes called the

planar limit, where the strength of the string theory is weakened and the corresponding $SU(N)$ field theory is treated as a large N gauge theory.

The correspondence is sometimes also stated as the equivalence between the partition functions of the bulk and the boundary theories. Apart from this, there is something called the AdS/CFT dictionary [13–15], which is also known as the *Extrapolate Dictionary*. It relates the operators of the field theory to the states(sources) of the gravity theory. The states and operators have the same tensor structure. For example, vector fields A_μ in the bulk is associated with the charges J^μ in the field theory side. Similarly, the metric $g_{\mu\nu}$ is associated with the stress tensor $T^{\mu\nu}$ of the field theory. The variants of the bulk side are associated with an exact quantum state [16] in the boundary theory.

$$\text{Empty AdS} \rightarrow |0\rangle, \text{ Eternal Black Hole in AdS} \rightarrow \text{TFD state.} \quad (1.2)$$

Our treatment in this thesis will be somewhat similar. But we will be following the path of quantum information theory. Given a QI theoretic measure on the field theory side, we will try to compute the same measures by computing something else on the bulk gravity side. We will use proposals that are made primarily on the vacuum state and compute the changes of the QI measures when computed for black hole backgrounds.

1.2 Holography and Quantum Information:

Now that we have briefly talked about the correspondence, the details of which can be found in many beautiful reviews [12, 13, 17, 18], we will concentrate on the things constituting this thesis. We will be assuming the correspondence to hold. That is probably the biggest educated assumption we make throughout the thesis. But we will be concerned about a specific restricted subset of the dictionary which deals with the quantum

information-theoretic quantities. Similar to classical information theory, quantum information theory deals with various ways of information processing and transfer within a quantum mechanical system, in our case the conformal field theory. Entropy plays a major role both in classical and quantum information theory. Classical statistical entropy, which measures the amount of classical information that can be stored in a system, is usually computed by calculating the number of possible microstates in the system. But in quantum information theory, one is usually most concerned about the quantum mechanical state ($|\psi\rangle$) of the theory and how the quantum mechanical degrees of freedom interact with each other. The two important QI theoretic quantities in this context, which we will be studying in the thesis are the entanglement entropy and the complexity. Entanglement typically measures the quantum correlation within a quantum mechanical system whereas complexity is related to the formation of the quantum state $|\psi\rangle$ using a smaller universal set of structural components known as quantum gates. We will discuss more about these quantities in the next chapter.

In this thesis, for the large part, we compute the entanglement entropy and sub-region complexity for various black hole solutions that come within the purview of the AdS/CFT correspondence. The holographic entanglement entropy computations were first discovered in [2, 3] by Shinsei Ryu and Tadashi Takayanagi where they computed the area of the bulk minimal surfaces corresponding to a boundary sub-region. These surfaces are now known as the RT surfaces. This prescription has been subsequently extended further to time-dependent (HRT) [19] and quantum corrected versions [20, 21]. The most recent addition to these corrections has been the discovery of the quantum extremal surfaces (QES) [22]. The computations have matched in most of the cases with the calculations of entanglement entropy in the conformal field theories, although the example of such cases in the CFT side is extremely less in number. Complexity on the other hand is

more of a very recent development [11, 23, 24]. It measures the difficulty of preparing a quantum state. The primary results regarding complexity in AdS/CFT came from certain bulk volume and action computations. However, the definitions in the field theory side of complexity [25–27] is much less understood than the entanglement entropy. But the little that people have been able to work out has already shown promising results and certain matching with the bulk computations. It is expected in general that complexity can teach us something about the system that entanglement can not. For example, one limitation of the entanglement entropy for an evolving quantum system is that it cannot give us much information after the thermalization timescale. On the other hand, complexity is expected to be able to teach us more about that regime since it has more to do with the wave-function of the quantum state in the space of states. The field-theoretic definitions of complexity so far have also been able to probe other physically important phenomenons like quantum quench, chaos [28–30] etc. Therefore, it is indeed worth studying complexity for black holes with the hope of finding interesting signatures of quantum gravity as well.

We focus on computing these QI theoretic quantities for black hole solutions because black holes tend to be the ideal places where the signatures of gravity are at their most extreme. Also one of the central pieces of our final puzzle being the black hole information paradox (described in relevant details in chapter 5), the understanding of black hole solutions as quantum systems is something that is of huge interest to the theoretical high energy physics community. The rest of the thesis is constructed as follows. In chapter 2, we give a brief review of the definitions and computations of entanglement entropy and sub-region complexity for empty AdS spacetimes. In chapter 3, we discuss our perturbative computations of the same for the charged and uncharged AdS Schwarzschild black holes in general spacetime dimensions. We also explain a formulation known as entanglement thermodynamics which will play an important role in most of the thesis. In chapter

4, we discuss similar computations and the entanglement thermodynamics for certain non-supersymmetric black (brane) solutions of type IIB string theory. It is worth mentioning at this point that the gauge-gravity duality has been extended to certain non-conformal examples in reference. But the non-triviality lies in these specific non-supersymmetric solutions where the supersymmetry of the theory is broken explicitly. In chapter 5, we discuss more recent developments in the field involving computations of entanglement entropy between the black hole and the radiations in light of the new tools like quantum extremal surfaces with the long-term goal of solving the black hole information paradox. We discuss our works on this front by studying a couple of simplified models involving ideas of multi-boundary wormholes. We compute both entanglement entropy as well as sub-region complexity in these models and comment upon the physics that we learn from our results. Finally, we conclude in chapter 6 with a summary of the results and interesting future directions.

A BRIEF REVIEW OF ENTANGLEMENT,
COMPLEXITY AND THEIR
HOLOGRAPHIC DUALS

In this chapter, we review the basic definitions and understandings that will be important for the rest of the thesis. Entanglement and complexity are two QI theoretic quantities that are quite relevant in the studies of quantum many-body systems. These quantities act as important probes indicating the structure and the interplay between parts of a quantum system. Here we will review both bipartite as well as the multi-partite structures of entanglement. We will also try to draw a basic sketch of complexity briefly from the perspective of quantum mechanical systems. Finally, we will end the chapter by discussing the holographic proposals for computing various measures of entanglement and complexity in gravity theories dual to quantum field theories due to the holographic duality.

2.1 Entanglement Entropy:

Given a bipartite quantum mechanical system, quantum entanglement measures the quantum correlations between parts of the system. Any quantum state can be of two types (pure and mixed) depending upon the nature of its density matrix. For pure states, one can write the state in the famous Dirac ket representation ($|\psi\rangle$), and the density matrix is written as $\rho_{pure} = |\psi\rangle\langle\psi|$. On the other hand the mixed states, which can be understood as classical probabilistic mixtures of pure states $|\psi_i\rangle$, there is only the density matrix representation $\rho_{mixed} = \sum_i p_i |\psi_i\rangle\langle\psi_i|$, where p_i s are the probabilities of different possible eigenstates $|\psi_i\rangle$ in the mixture.

We will primarily be interested in the situation where the whole state is pure and we wish to measure quantum correlations between two complementary parts of the full pure state. Let us divide pure state degrees of freedom into two regions A and B . In a typical spin chain example, the way to do so is to artificially cut off the chain at some point and divide the lattice points into two groups. Subsequently, the total Hilbert space can be considered as a direct product of two Hilbert spaces corresponding to the two subsystems (A and B), $\mathcal{H}_{tot} = \mathcal{H}_A \otimes \mathcal{H}_B$. The first thing to remember here is that the measure we want to compute should be symmetric under the change of A and B . This ensures that the entanglement between A and B is the same as the entanglement between B and A . The way in which one measures the entanglement between these two regions is by computing something called the reduced density matrix. Given that the total state $A \cup B$ is pure, the reduced density matrix of A is defined by taking partial trace over the degrees of freedom corresponding to B (more precisely, \mathcal{H}_B) which is represented as $\rho_A = Tr_B[\rho_{tot}]$ (similarly, $\rho_B = Tr_A[\rho_{tot}]$). The reduced density matrix ρ_A can be understood as the quantum state of the total system as observed by an observer who has access to the subsystem A only. The entropy

of entanglement is thereafter defined as the von-Neumann entropy of the reduced density matrix

$$S_{EE}(A \sim B) = -Tr[\rho_A \log \rho_A] = -Tr[\rho_B \log \rho_B] \quad (2.1)$$

An important point to remember is again that the entanglement entropy can measure entanglement between parts of a system consistently only when the total state is pure.

For thermal systems also, entanglement entropy can be computed similarly where the total density matrix is given by the thermal density matrix $\rho_{thermal} = \exp -\beta H$ ($\beta = \frac{1}{T}$, T being the temperature and H the Hamiltonian of the system). For thermal systems, the difference between entanglement entropy of two sub-regions approaches the difference between the thermal entropy of the same at a high-temperature limit. Hence entanglement entropy for thermal systems is believed to encode important information about the entropy of the thermal state. This understanding plays a major role in our perturbative calculations in the high-temperature limit presented in chapter 4. Entanglement entropy also follows a few interesting and strong relations that are analogs of the corresponding classical probabilistic definition of entropy. These properties qualify entanglement entropy as a successful quantum information-theoretic quantity and also tell us something about the quantum system under study.

2.1.1 Properties of Entanglement Entropy:

As mentioned earlier, the entanglement entropy satisfies a few properties that are closely related to properties of entropy as defined in classical information theory. We list a few of them below¹.

¹The various sub-additivity relations mentioned here are believed to hold if the quantum system is unitary, which we will assume to hold for all the states we study in this thesis.

1. **Weak Sub-additivity:** For two or more sub-regions, the entanglement entropy follows the following relation,

$$S_{EE}(A \cup B) \leq S_{EE}(A) + S_{EE}(B). \quad (2.2)$$

This inequality is true for classical probability theory as well. However, in the latter, there is something closely related to this inequality known as the theorem of conditional entropy [31]. The conditional entropies in classical probability theory satisfies the following relation,

$$S(\rho_{A \cup B} | \rho_A) = S(\rho_{A \cup B}) - S(\rho_A) \geq 0, \quad S(\rho_{A \cup B} | \rho_B) = S(\rho_{A \cup B}) - S(\rho_B) \geq 0. \quad (2.3)$$

However, it is easy to check that if $A \cup B$ is an entangled pure state, this relation is not satisfied by the entanglement entropies (since $S_{EE}(A \cup B) = 0$, whereas $S_{EE}(A, B) > 0$). Hence the entanglement entropy can not be understood simply as a straight-forward quantum analog of the conditional entropy defined by classical probabilities. The sub-additivity relation allows one to define another interesting quantity known as the mutual information (I) that follows $I(A, B) = S_{EE}(A) + S_{EE}(B) - S_{EE}(A \cup B)$.

2. **Araki-Lieb inequality:** The closest inequality to the conditional entropy theorem that S_{EE} follows is known as the Araki-Lieb inequality. It holds for two or more sub-regions.

$$S_{EE}(A \cup B) \geq |S_{EE}(A) - S_{EE}(B)|. \quad (2.4)$$

The Araki-Lieb inequality can be derived from the weak sub-additivity most gener-

ally by a mathematical formulation known as purification [31].

3. **Strong Sub-additivity:** For three or more sub-regions, the following relation always holds and is known as the strong form of the sub-additivity [32].

$$S_{EE}(A \cup B) + S_{EE}(B \cup C) \geq S_{EE}(B) + S_{EE}(A \cup B \cup C). \quad (2.5)$$

Again, the strong sub-additivity relation is also followed by the conditional entropies [33, 34] in classical information theory and can be recast as $S(A|BC) \leq S(A|B)$. It looks very similar to the strong sub-additivity if we write the latter in terms of the mutual information $I(A, BC) \leq I(A, B)$. From the perspective of quantum systems, the validity of strong sub-additivity also qualifies the complete system as a unitary one [35].

4. **2nd form of Strong Sub-additivity:** The strong sub-additivity has another version which is the following

$$S_{EE}(A \cup B) + S_{EE}(B \cup C) \geq S_{EE}(A) + S_{EE}(C). \quad (2.6)$$

All these inequalities written above are relations that have been proved and strengthened the understanding of EE as a valid QI quantity.

2.1.2 Entanglement in QFTs:

Now let us shift to QFTs from QM and mention very briefly the behavior of entanglement as studied in QFTs. For $d + 1$ dimensional continuum QFTs (d space dimensions), the entanglement entropy between two regions A and $B = \text{Complement}(A)$ is typically divergent where the divergence is regularised by the introduction of a UV cutoff a and the

coefficient of the divergent term is proportional to the area of the boundary ∂A of A that distinguishes A and B . This is known as the area law of entanglement [36–42] and plays a major role in understanding the probable relation between entanglement and black hole entropies.

$$S_{EE}(A) = c_1 \frac{Area(\partial A)}{a^{d-1}} + \dots(\text{subleading terms}). \quad (2.7)$$

The area law indicates that the entanglement between A and B is strongest at the boundary separating them from one another. The computations are done using the replica trick where instead of computing the $tr_A(\rho_A \log \rho_A)$ directly, which is immensely hard to do even in case of simplest situations, one takes n -copies of the Riemann surface to compute $tr_A(\rho_A^n)$. This supposedly gives the so-called Renyi entropy and one can get the entanglement entropy by analytically continuing to $n \rightarrow 1$.

In the following section, we discuss the situation when the complete state of interest is mixed and we want to measure entanglement between parts of the mixed state. There are a few measures of mixed state entanglement available in the literature, [43] e.g; entanglement of purification, squashed entanglement, the entanglement of formation, logarithmic negativity, etc. However, we concentrate only on the entanglement of purification in this thesis. This is because of the simple reason that compared to the other mixed state measures, EoP has a clearer and better holographic proposal which can be applied readily and can provide us with insightful information regarding the mixed state. In the case of a mixed state, one needs to carry out a process called purification to define an entanglement measure.

2.2 Entanglement of Purification:

Purification is the process of making a mixed state pure. Although there are numerous measures in quantum information theory, most of them are sensitive to the state at hand

being a pure one. However, the mixed states behave quite differently than a pure one. A mixed state density matrix ($\rho_{mixed} = \sum_i p_i |\psi_i\rangle\langle\psi_i|$)² follows the following property

$$Tr[\rho_{mixed}] = 1, Tr[\rho_{mixed}^2] < 1. \quad (2.8)$$

The standard way to purify a mixed state is to add an auxiliary system with the mixed state where the total state after adding the auxiliary system becomes a pure state. Hence, the mixed state becomes a particular reduced state after tracing out a few degrees of freedom from the purified state. But, for a single mixed state, there might exist more than one way of purification. Given all possible purifications, a particular one is chosen concerning the information-theoretic measure one wants to calculate in a given scenario. Here, we will be concerned with the entanglement of purification which is a candidate measure for entanglement in mixed states and is argued to be related to other measures, e.g; entanglement negativity, squashed entanglement, etc. EoP has been recently computed for free scalar field theories [44] and also in the context of quantum many-body systems in [45]³.

2.2.1 Definitions and Properties:

The entanglement of purification (EoP) [46, 47], as the very name suggests, is related to the purification of a mixed quantum state. The precise definition of entanglement of purification between A and B for a bipartite mixed state AB ($= A \cup B$) is the minimal

²Thermal states are also considered to be mixed states. Remember that we mentioned previously that the entanglement entropy for thermal density matrix at high temperatures is found to match with thermal entropy. Hence, one might run into an apparent contradiction that how is that possible if entanglement entropy is not a good measure of entanglement for mixed states. But in fact, there is no contradiction. It is indeed right that entanglement entropy does not measure quantum correlations between parts of a mixed state. However, it does indeed measure classical correlations and hence can match with the thermal entropy of the thermal system at high temperatures. This is because the thermal entropy in that limit behaves like the classical statistical entropy and captures the same classical correlations as the entanglement entropy.

³In [45], although many-body systems have been studied, the mixed states under study were bipartite (not multi-partite).

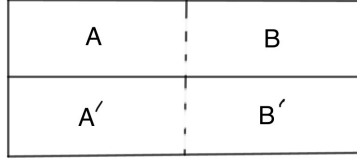


Figure 2.1: A schematic diagram of bipartite purification ($AA'BB'$ forms a pure state and EoP is entanglement between AA' and BB')

entanglement entropy between AA' and BB' , where A' and B' are auxiliary systems added to make the whole state $AA'BB'$ pure. It is important to remember the fact here that there can be infinitely many ways to choose A' and B' such that the total state is pure. Among all those possible purifications, the preferred choice for EoP is dictated by the minimum of entanglement entropy between AA' and BB' . Hence, one starts from a mixed density matrix ρ_{AB} and extends the Hilbert space from $\mathcal{H}_A \otimes \mathcal{H}_B$ to a pure state Hilbert space $\mathcal{H}_A \otimes \mathcal{H}_B \otimes \mathcal{H}_{A'} \otimes \mathcal{H}_{B'}$. The EoP ($E_P(\rho_{AB})$) is then defined as the following quantity,

$$E_P(\rho_{AB}) = \min_{|\psi\rangle_{AA'BB'}} S_{AA'}. \quad (2.9)$$

We will not discuss the properties of the bipartite EoP, which can be found in [44]. However, we will discuss the properties of multi(n)-partite EoP below. Properties of bipartite EoP are consistent with the properties of n -partite EoP when and if one takes $n = 2$.

Multi-partite states and entanglement:As mentioned earlier, since the QI theoretic quantities are important in the context of quantum many-body systems, the other quantities which are also of interest to physicists are the multi-partite entanglement measures. To compute such quantities, one divides the quantum system into more than 2 parts. Now, a multi-partite pure state can be fully separable, partially separable, or fully entangled and

identification of such states involve many criteria. By separability, one means whether the pure state can be written as a product between the states on different parts of the system. It is worth pointing out that a bipartite system cannot be partially separable. It can either be fully separable or fully entangled. For a multi-partite pure state [48], the entanglement is calculated by the sum of all possible bipartite entanglement entropies that can be computed within the system. By all possible bipartite entanglement, we mean that if we divide the state into n parts and take one of them, we first compute the entanglement between that part and its complement. The same is done for all other parts. Finally, the n partite entanglement entropy is given by the sum of n such bipartite entanglement entropies. Let's say we begin with a n -partite pure state $A_1 A_2 \dots A_n$, then the multi-partite entanglement entropy is given by the sum of the entanglement entropies S_{A_i} with their respective complements in the whole state. So S_{A_1} is the entanglement between A_1 and $A_1^c = A_2 \cup A_3 \dots \cup A_n$.

$$S_{n-EE}(\text{multi}) = \sum_{i=1}^n S_{A_i}. \quad (2.10)$$

We will however be concerned about multi-partite mixed states. The simplest way to grasp the idea of such a state is, to begin with, a mixed state and divide the mixed state degrees of freedom into more than two regions.

Similar to multi-partite entanglement for pure state, multi-partite entanglement of purification [49–51] for a mixed state is where instead of a bipartite mixed state AB, we start with a multi-partite mixed state $A_1 A_2 \dots A_n$ and add auxillary systems A'_1, A'_2, \dots, A'_n to make it pure. Then we compute the minimum of $\sum_i S_{A_i A'_i}$ for $i = 1, \dots, n$.

The mathematical expression through which it is denoted is the following

Definition:

For a n -partite mixed state, with density matrix $\rho_{A_1 A_2 \dots A_n}$, the multipartite entangle-

ment of purification is defined as,

$$\Delta_{n(P)}(\rho_{A_1 A_2 \dots A_n}) = \min_{|\psi\rangle_{A_1 A'_1 A_2 A'_2 \dots A_n A'_n}} \sum_{i=1}^n S_{A_i A'_i}. \quad (2.11)$$

This boils down to the definition of bipartite entanglement of purification once n is taken to be 2 with appropriate normalization ($\frac{1}{n}$ factor in the above definition). Let us call the bipartite EoP as $E_P (= \Delta_{2(P)})$.

Properties:

1. If one of the systems gets decoupled, $\rho_{A_1 \dots A_n} = \rho_{A_1 \dots A_{n-1}} \otimes \rho_{A_n}$, then

$$\Delta_P(A_1 : \dots : A_n) = \Delta_P(A_1 : \dots : A_{n-1}). \quad (2.12)$$

This is natural as if one of the systems is decoupled, the n -partite state is not mixed anymore. Then again, the mixed state to be considered becomes the $(n - 1)$ -partite.

2. For a n -partite pure state $|\psi\rangle_{A_1 \dots A_n}$,

$$\Delta_P(A_1 : \dots : A_n) = \sum_{i=1}^n S_{A_i}. \quad (2.13)$$

This relation ensures that once the system becomes pure, the EoP definition boils down to the usual entanglement measure of pure states. Therefore, the multi-partite EoP provides results of multi-partite entanglement entropy if the state of interest is pure.

3. For a n -partite product state ($\rho_{A_1 \dots A_n} = \rho_{A_1} \otimes \rho_{A_2} \otimes \dots \otimes \rho_{A_n}$),

$$\Delta_P(A_1 : \dots : A_n) = 0. \quad (2.14)$$

This is in relation to the last property of pure states. This simply ensures the fact that if the state is a product state, the multi-partite EoP gives a zero which is again consistent to the fact there is zero entanglement for product states.

4. Δ_p is bounded from above as follows,

$$\Delta_P(A_1 : \dots : A_n) \leq \min_i (S_{A_1} + \dots + S_{A_1 \dots A_{i-1} A_{i+1} \dots A_n} + \dots S_{A_n}). \quad (2.15)$$

5. Δ_p is bounded from below as follows,

$$\Delta_P(A_1 : \dots : A_n) \geq I(A_1 : \dots : A_n), \quad (2.16)$$

where $I(A_1 : \dots : A_n)$ is the n-partite mutual information.⁴ The last two properties can be treated as the mixed state analogues of the sub-additivity relations.

All of these are followed by bipartite EoP as well once one takes $n = 2$. Now that we have defined the entanglement measures and discussed their properties, let us now discuss the basics of complexity in the following section.

2.3 Complexity:

Complexity is a QI theoretic measure that should be of more concern to an experimental physicist than a theoretical one. It measures the practical difficulty in preparing a quantum state. In this preparation, the building components are of paramount importance and the measure of course depends mostly on the predefined set of elementary quantum gates one is allowed to use while preparing the quantum state in hand. One consequence of using these pre-defined set of quantum gates is that one can only construct a complicated quantum

⁴Mutual information is another QI theoretic quantity which we will not be discussing in this thesis. The definition and various properties of mutual information can be found in [32].

state up to some tolerance ϵ . By the pre-defined universal gate set specific to a problem (/dimension of the state), one generally means the minimum number of operators (/gates) without the identity operator that is needed to span the space of all possible states on the space of states starting from a typical initial state.

Complexity has been studied previously in detail in the QI literature mostly for qubit systems to understand quantum circuits and to propose several different bounds on the number on the gates needed [25, 52, 53]. In qubit systems, one can work with the Pauli matrices to form the simplest elementary quantum gates, and therefore the whole circuit of an n-qubit state can be represented in terms of higher dimensional Pauli matrices. However, for most of the literature, the systems that have been studied are unitary ones which is also the case for most of the QM systems. But this also limits the study to the finite-dimensional pure states. For mixed states and infinite-dimensional field-theoretic states, there remains the question of whether unitary gates are the most optimal choices or not [27]. The basic idea is nevertheless quite easy to grasp. Given a reference state $|\psi_R\rangle$ and a target state $|\psi_T\rangle$, one has to find the optimal unitary U that takes the reference state to some final state $|\psi_{T-\epsilon}\rangle$, where the final state is same as the target state up to certain tolerance ϵ . There are other minute details one can consider while constructing such a circuit like assigning a different cost to different gates (penalty factors) to build a circuit with non-uniform cost functional. By the non-uniform cost functional, one simply means to assign different weights to different gates within the pre-defined gate set. This enables to model a scenario where one gate involves more cost (/hard work) than the other. This breaks the symmetry of cost between the gates. But we will not be bothered about these details in our study since we will be mostly concerned about the holographic (sub-region) proposal of complexity in this thesis.

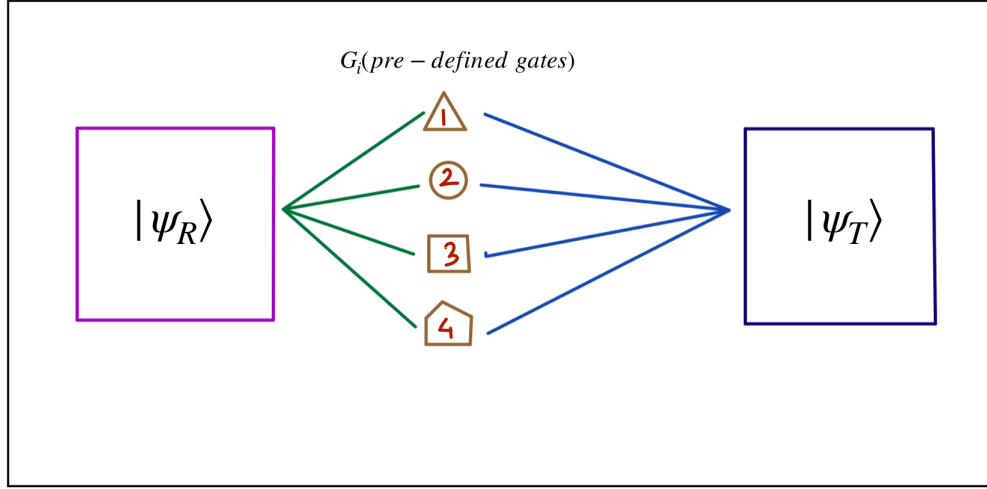


Figure 2.2: Representative image for understanding complexity. Let's say, the different shapes with different numbers are the pre-defined gateset that can be used to construct the target state $|\psi_T\rangle$ starting from the reference state $|\psi_R\rangle$. The number of times each of the gates used contributes to the complexity. Also, if we associate different costs with different gates (shapes), the complexity becomes different and the ratios of the costs between different gates are understood as the penalty factors.

$$|\psi_{T-\epsilon}\rangle = U_T|\psi_R\rangle, \quad |\langle\psi_T|\psi_{T-\epsilon}\rangle|^2 \leq \epsilon. \quad (2.17)$$

The job is therefore to construct the above unitary U_T by using set of the elementary quantum gates $\{G_i\}$. In doing so, Nielsen [25, 53] compared this situation as an optimal Hamiltonian control problem which is constructed out of the universal gate set.

$$|\psi_T\rangle = e^{-i\int_0^1 H(t)dt}|\psi_R\rangle. \quad (2.18)$$

where time is normalized to 1 and the Hamiltonian ($H(t)$) is written as follows,

$$H(t) = \sum_i (\gamma^\sigma)^i(t)\sigma_i, \quad (2.19)$$

where $\gamma^\sigma(t)$ are control functions notifying whether at a particular t , a gate was on or off [25,52]. σ_i are generalized Pauli matrices. These are the set of n -fold tensor products of the single qubit Pauli matrices. Once this Hamiltonian is optimized, the problem eventually becomes a problem of minimizing a cost function constructed of the control functions. Usually, a cost function $f(\gamma(t))$ is integrated in the t coordinate where one assumes that at $t = 1$, the circuit-construction is complete. This integration of the chosen cost function is known as the cost functional ($C_f(\gamma)$) and is minimized to derive the complexity($C_f(U_T)$). As shown in [25], this eventually becomes a geometric problem of finding geodesic in a class of geometries known as *Finsler* geometry.

$$C_f(\gamma) = \int_0^1 dt f(\gamma(t)) , C_f(U_T) = \inf_{\gamma} [C_f(\gamma)] . \quad (2.20)$$

Following the same basic set up, the complexity of free field theories (bosonic and fermionic) was computed in [26,27,54,55], where different norms can be used as the cost function choices and the unitary can be thought of as the path ordered exponential of the Hamiltonian to be optimized. In the case of discrete free QFT on a lattice with harmonic oscillators playing the role of the degrees of freedom, the minimization procedure leads to finding the minimal geodesic in a many-parameter family of geodesics in the space of unitaries ($GL(N, R)$).

Very recently some very constrained states in CFT [56–59] have also been calculated. There have also been some cases where complexity for mixed states has been studied in such setups by starting with a mixed state and then adding purifying degrees of freedom [60,61]. The complexity of the mixed states is then quantified as the minimum complexity of the pure state among all possible purifications of the mixed state.

2.4 Holographic Proposals:

2.4.1 Holographic Entanglement Entropy:

In this subsection, we discuss the holographic proposals of the computation of entanglement entropy. In recent times, the AdS/CFT correspondence has been used to decode secrets of a quantum theory of gravity through an elegant geometrization of concepts from quantum information theory. This quest started by the Ryu-Takayanagi (RT) conjecture [2, 3] and its covariant generalization [19] for computing entanglement between boundary subsystems through bulk calculations. The conjecture was later derived as an instance of generalized entropy for Euclidean gravity solutions in [20]. In its original incarnation, the RT formula seeks to evaluate the entanglement entropy S_A of any subsystem A in the d -dimensional dual QFT by computing the area of a codimension-2 minimal surface γ_{RT} homologous to A in the bulk space-time following

$$S_{HEE} = \frac{\text{Area}(\gamma_{RT})}{4G_N^{(d+1)}}, \quad (2.21)$$

which remains true as long as we consider pure classical gravity.

For the AdS₃/CFT₂, this formula matches exactly with the CFT result and it is in general believed to hold in general space-time dimensions. Infinite strip and spherical sub-regions are the two typical entangling regions chosen in the boundary to compute the holographic entanglement entropy. For 2d CFTs with central charge c , a sub-region of length ℓ , the entanglement entropy can be computed using the replica trick [37, 38]. The entanglement in such a case with the rest of the subsystem is

$$S_{CFT_2} = \frac{c}{3} \ln\left(\frac{\ell}{\epsilon}\right), \quad (2.22)$$

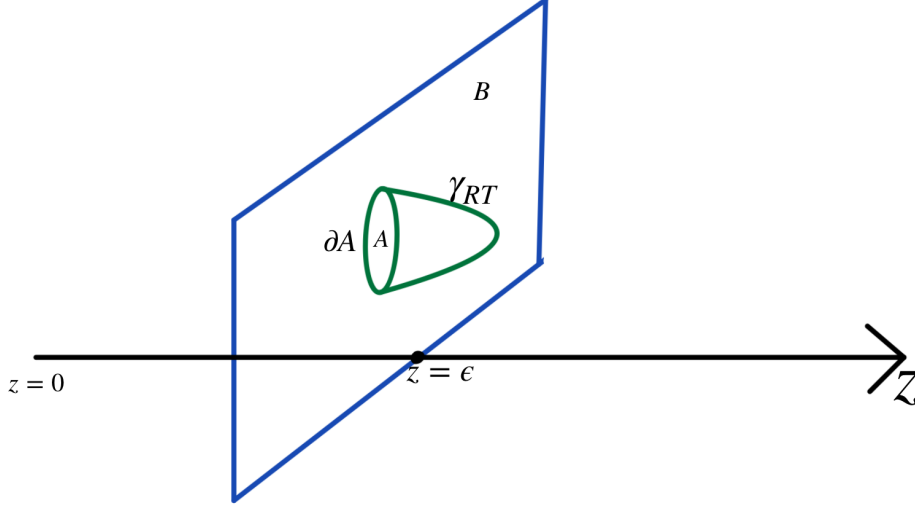


Figure 2.3: Ryu-Takayanagi surface in AdS/CFT: The boundary sub-region A is the green circle on the boundary denoted by the blue rectangle. Rest of the region is denoted as B . ϵ is the UV cutoff along z axis. The green curve γ_{RT} along z direction sharing the boundary of A (∂A) is the Ryu-Takayanagi surface.

where ϵ is a UV regulator near the boundary. This result is reproduced exactly when the Ryu-Takayanagi proposal is applied to empty AdS_3 where one uses the relation between the central charge and the AdS length scale $c = \frac{3R}{2G_N}$. It is also worth noting that the various sub-additivity inequalities have also been proved [62] directly from the holographic RT proposal for three and higher space-time dimensions.

It is worth mentioning though that it is very hard to compute entanglement entropy between sub-regions in higher dimensional CFTs. Therefore the holographic proposal acts as the simple tool for computation in such scenarios. In the following, we now discuss the holographic proposal for computing EoP for bulk mixed states based on the RT prescription.

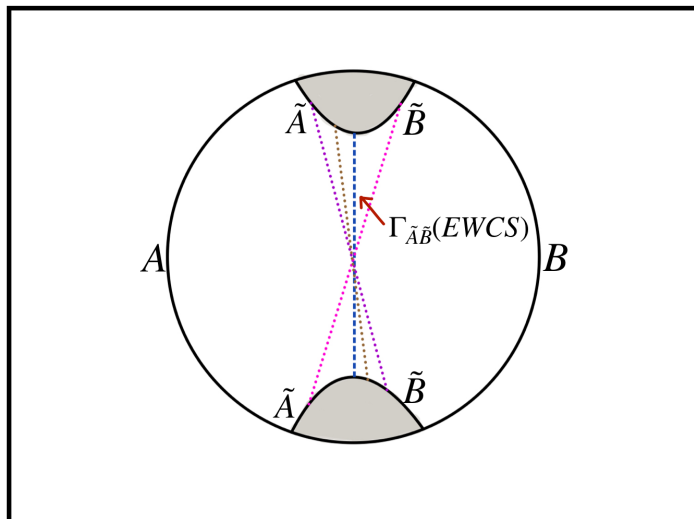


Figure 2.4: Entanglement Wedge Cross Section (holographic dual of Bipartite Entanglement of Purification). The boundary sub-regions of the AdS time-slice after removing the top and bottom regions are A and B . The two bulk geodesics (top and bottom) corresponding to the removed grey regions can be thought of as $\tilde{A} \cup \tilde{B}$ which along with $A \cup B$ forms a geometric pure state. Among all possible dotted lines shown in the figure dividing the bulk geodesics into \tilde{A} and \tilde{B} , the minimal is the blue one marked as $\Gamma_{\tilde{A}\tilde{B}}$ (EWCS).

2.4.2 Holographic Dual of EoP:

The holographic duals of various purification measures have been proposed in various articles [63–66]. Here we firstly discuss the holographic dual (E_W) of the bipartite EoP (E_P) and then the n -partite case. For holographic states, it was conjectured that the holographic dual of E_P is the minimum entanglement wedge cross-section which is the dotted line in figure 2.4. The mathematical definition of entanglement wedge cross-section is the following,

$$E_W(A : B) = \min\{Area(\Gamma); \Gamma \subset M_{AB} - M_{A \cap B}\} \text{ separates } A \setminus B \text{ and } B \setminus A,$$

where M denotes the entanglement wedge of some specified interval in the boundary CFT. $A \setminus B = (A - A \cap B)$ and $B \setminus A = (B - B \cap A)$. In Figure 2.4, the boundary

sub-regions A and B do not have any overlap. Hence $A \cap B = 0$. Also, it is important to note that the grey regions are eliminated and therefore the boundary state on $A \cup B$ or the dual bulk state is mixed. In the given scenario, the bulk eliminated regions are marked through the grey regions below the geodesics on the top and bottom parts of Figure 2.4. Γ is the bulk geodesic which is minimal among all possible geodesics dividing bulk states corresponding to A and B . This is also known as the entanglement wedge cross-section (EWCS). [63, 64, 67]

Typically for understanding purposes, it is easier to compare with the usual definition of purification (by adding additional degrees of freedom) if one considers that the geodesics connecting the boundary points of the removed (grey) sub-regions while constructing the mixed state ⁵ in consideration (the geodesics marked as the combination of \tilde{A} and \tilde{B} in Figure 2.4) play the role of the purifying degrees of freedom in a way in the bulk proposals. But, one does not know a priori what separates \tilde{A} and \tilde{B} , which is expected to be crucial for computation of EoP as stated before in the definition of EoP. The minimal surface $\Gamma_{\tilde{A}\tilde{B}}$ plays the role of this separating surface. It divides both the top and the bottom geodesics into \tilde{A} and \tilde{B} . Now, there can be infinitely many bulk geodesics connecting points between the top and the bottom geodesic and all of them could be candidate purifying surfaces. However, the minimal among all of those geodesics (in terms of area of the geodesics in general space-time dimensions) is the preferred $\Gamma_{\tilde{A}\tilde{B}}$. This minimization is the bulk dual to the minimization operation in the quantum mechanical definition of EoP. An arguably more canonical bulk proposal of EoP (named as reflected entropy) was given later in [68]. We will however stick to the definition of [63] for this thesis. If the two subsystems A and B are taken disjointly and symmetrically in an AdS_3 Poincare disk (as in figure 2.4) such

⁵After removing the grey regions from the boundary and the bulk of the full Poincare disk, the state dual to the rest of the system is a mixed state in general.

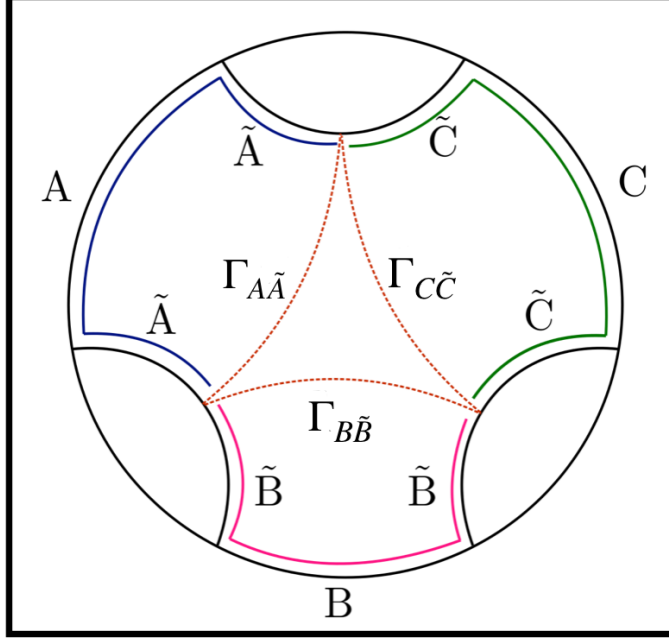


Figure 2.5: EWCS for tripartite EoP: The combination of A, B, C (boundary regions forming the mixed state) and the the HRT geodesics ($\tilde{A} \cup \tilde{B} \cup \tilde{C}$) of the removed regions are considered to form a tri-partite geometric pure state. $\Gamma_{\tilde{A}\tilde{B}\tilde{C}} = \Gamma_{A\tilde{A}} \cup \Gamma_{B\tilde{B}} \cup \Gamma_{C\tilde{C}}$ becomes the multi-partite EWCS. Contrary to the bipartite case, here the sum of the three orange curves are minimized among all possible choices.

that their length is ℓ and distance is d , the holographic EoP (denoted as E_W) is found to be

$$E_W(A : B) = \begin{cases} \frac{c}{6} \log[1 + \frac{2\ell}{d}] & \text{if } d < (\sqrt{2} - 1)\ell \\ 0 & \text{if } d > (\sqrt{2} - 1)\ell \end{cases} \quad (2.23)$$

This phase transition (negative jump) of EoP at $d = (\sqrt{2} - 1)\ell$ is somewhat similar to the behaviour of mutual information $I(A : B)$.⁶

Multi-partite EWCS: For multi-partite states, one needs to consider sub-regions involving boundary and bulk sub-regions (similar to the bipartite case as shown in figure

⁶The holographic mutual information have also been investigated in great details in [69].

2.4) $A, B, C, \tilde{A}, \tilde{B}, \tilde{C}$ (for a tri-partite case) and then compute the multi-partite minimal entanglement wedge cross-section $\Gamma_{\tilde{A}\tilde{B}\tilde{C}}$, where $A \cup \tilde{A} \cup B \cup \tilde{B} \cup C \cup \tilde{C}$ is a geometric pure state. This is pictorially described in figure 2.5 [64, 70]. Actually in case of bipartite entanglement of purification as well, the boundary sub-regions $A \cup B$ is typically a mixed state, but $(A \cup B \cup \tilde{A} \cup \tilde{B})$ is considered to be a geometric pure state and the minimal length dividing the whole system into two is considered to be the bipartite entanglement of purification. The HRTs $(\tilde{A} \cup \tilde{B}, \tilde{B} \cup \tilde{C}$ and $\tilde{C} \cup \tilde{A})$ serve as the ancilla systems (A'_i parts mentioned in subsection 2.2.1) added to make the geometric state a pure one. One important point to remember for the multi-partite EWCS however is that one needs to minimize the length of the sum of $\Gamma_{A\tilde{A}}, \Gamma_{B\tilde{B}}$ and $\Gamma_{C\tilde{C}}$, which is different from minimizing the individual contributions. As argued in [64], for the tri-partite case, this minimized sum is found when $\Gamma_{A\tilde{A}}, \Gamma_{B\tilde{B}}$ and $\Gamma_{C\tilde{C}}$ by themselves form a closed curve $\Gamma_{\tilde{A}\tilde{B}\tilde{C}}$ by sharing the boundary points with each other as shown in figure 2.5.

In [63], it has been checked that E_W follows the same set of properties as E_P , whereas, in [64], $\Delta_{n(W)}$ and $\Delta_{n(P)}$ have been found to share the same set of properties. [64] deals with this property-matching in a quite detailed way. It is also worth noting that although [64] has been successful in finding the correct curve that satisfies all the properties of tripartite EoP, finding analytical results for the length of such a curve, in a spirit similar to equation (2.23) for bipartite EoP, is a hard job in general. We will discuss a holographic scenario where the multi-partite EWCS can be computed approximately, later in chapter 5 of this thesis.

2.4.3 Holographic Complexity:

Holographic complexity came into the picture much later. Motivated primarily by the area and the holographic dictionary, Susskind and collaborators suggested [23] that just like

the extremal (minimal) area, extremal (maximal) volume slices in AdS should also mean something physical for the boundary CFT. This statement was also inspired by the growth of this maximal volume slice (where the time coordinates asymptote to boundary time) that was found while studying two-sided AdS eternal BH, which is believed to be dual to the thermo-field double state of the CFT. However, in this case, there was no sub-region a priori, to begin with, and therefore whatever the volume corresponds to was expected to tell us something about the whole boundary state. By looking at the growth of the volume, which in terms of the thermalization timescale of the BH persists much longer than the growth of entanglement between the two sides of the TFD state, Susskind et al argued that this volume is dual to the complexity of the TFD state. They also vouched for another property of complexity looking at the growth, which is that it can provide us with more information about the evolution of the system than entanglement entropy can. This conjecture is known as the CV conjecture. It has been studied in detail for diverse situations.

Another proposal for the complexity was given later in [11, 24], which computes the action of the causal domain of dependence of the maximal slice (Wheeler-de-Witt patch) and is known as the CA proposal. It is also a candidate for holographic complexity. The CV and CA proposals differ in some cases. But to understand which one is the more suited dual of the CFT state complexity, the definition and properties on the CFT side have to be investigated in far more details that have been done till now. Since it is still a work in progress, we won't be commenting upon these things in this thesis. The respective formulas for the CV and CA are given below.

$$C_V = \left(\frac{V(\gamma)}{R G_N} \right), \quad C_A = \frac{I_{WDW}}{\pi \hbar} \quad (2.24)$$

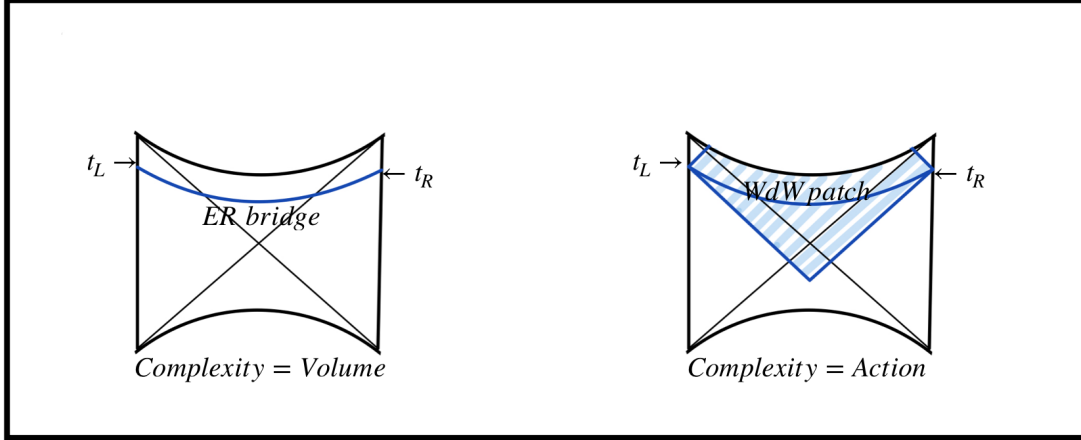


Figure 2.6: CV and CA conjectures: CV measures the volume of the time-slice where the two sides of the eternal BH are connected by the Einstein-Rosen (ER) bridge. CA measures the action on the causal patch of the ER bridge time-slice. This patch is known as the Wheeler-de-Witt (WdW) patch. (Images are inspired by [11])

where R is the AdS radius, $V(\gamma)$ is the maximum volume of the co-dimension one bulk surface (time-sliced) bounded by the two boundaries of the black hole and I_{WdW} is the action of the Wheeler-de-Witt patch.

Holographic Sub-region Complexity: We will take the CV conjecture as our starting point and expand upon this to understand how can one calculate the complexity of a sub-region (a mixed state in general) inspired by the CV proposal. This was what Alishahiha did exactly in [4]. The corresponding volume proposal for a sub-region is simple. Given a boundary sub-region, the RT surface divides the bulk into two regions which can be associated as the entanglement wedges of the subsystem A and B respectively. Alishahiha proposed that given a boundary sub-region, we simply need to specify the RT surface and then compute the volume between the RT surface and the boundary subsystem to come up with a volume that is specific to a sub-region. This is known as the holographic sub-region complexity (HSC). We show this volume in

$$C_{HSC} = \frac{V(\gamma_{RT})}{8\pi R G_N}. \quad (2.25)$$

This volume is argued to quantify the complexity of preparing the reduced density matrix corresponding to the boundary state. Therefore, it should be associated with the idea of the complexity of purification. This volume has been computed for a few different settings in [71, 72]. But the overall idea remains the same. In [71], the authors find that this volume in AdS_3 can be written completely in terms of the length of the boundary sub-region and the topology of the bulk region. Therefore, the sub-region complexity in AdS_3 is termed as *Topological complexity*, which will play a crucial role in our considerations in Chapter 5. The details of the computations of sub-region complexity done in [4] will be clear through our discussions in Chapter 3.

2.5 Relative Entropy and Fisher Information:

In this section, we finally discuss a couple of important and insightful QI distance measures that will be put in use in the following chapters. Relative entropy [73, 74] is a QI measure that indicates distinguishability between two density matrices ρ and σ . It is defined as

$$S(\rho|\sigma) = Tr(\rho \text{Log}(\rho)) - Tr(\rho \text{Log}(\sigma)). \quad (2.26)$$

Two most important properties followed by relative entropy are the following,

- 1. Non-negativity:** $S(\rho|\sigma) \geq 0$, with $S(\rho|\sigma) = 0$ when $\rho = \sigma$.
- 2. Monotonicity:** It means that given two density matrices if we trace over the same number of degrees of freedom, the relative entropy between the new reduced density ma-

trices are always less than the relative entropy of the full density matrices.

$$S(\rho_1|\sigma_1) \leq S(\rho_{12}|\sigma_{12}), \text{ where } \rho_1 = \text{Tr}_2(\rho_{12}) \text{ and } \sigma_1 = \text{Tr}_2(\sigma_{12}). \quad (2.27)$$

First Law of Entanglement:

Relative entropy can be used to define a relation similar to thermodynamic entropy and energy between the entanglement entropy and the modular Hamiltonian [35]. For this thesis, let us define the modular Hamiltonian as the following. Given a reference density matrix σ , the *modular Hamiltonian* is defined as $\mathcal{H}_\sigma = -\log(\sigma)$. One can also define something called modular free energy as the following

$$F_1(\rho) = \text{Tr}(\rho\mathcal{H}_\sigma) - S_{EE}(\rho). \quad (2.28)$$

Now, it is easy to write the relative entropy as

$$S(\rho|\sigma) = F_1(\rho) - F_1(\sigma) = \Delta\langle\mathcal{H}_\sigma\rangle - \Delta\langle S_{EE}\rangle. \quad (2.29)$$

The monotonicity then implies the following relation between the expectation value of the modular hamiltonian and the entanglement entropy.

$$\Delta\langle\mathcal{H}_\sigma\rangle \geq \Delta\langle S_{EE}\rangle. \quad (2.30)$$

This inequality (2.30) is known as the ***First Law of Entanglement*** and will be one of the crucial points of the following chapter.

Quantum Fisher Information:

If we start from the reference density matrix σ and write ρ as a perturbed density matrix $\rho = \sigma + \varepsilon\sigma_1 + \varepsilon^2\sigma_2 + \dots$, the relative entropy is found to be a function of this perturbative parameter ε and begins at least quadratic in the parameter, $S(\rho|\sigma) = \mathcal{O}(\varepsilon^2) + \dots$. This implies that upto first order in the parameter [74], the first law can be written as

$$\delta\langle\mathcal{H}_\sigma\rangle = \delta S_{EE}. \quad (2.31)$$

Now that we know that the perturbatively relative entropy begins only from the second order, we define the *quantum Fisher information* [32, 35, 75] as the coefficient of ε^2 . In the expression below, the $\varepsilon\sigma_1$ part in Log is needed (although there is an ε^2 multiplied after the trace operation) because otherwise, the derivative operation inside the trace would always give zero results.

$$S(\sigma + \varepsilon\sigma_1|\sigma) = \frac{1}{2}\varepsilon^2 \text{Tr} \left(\sigma_1 \frac{\partial}{\partial \varepsilon} \text{Log}(\sigma + \varepsilon\sigma_1) \right). \quad (2.32)$$

In the next chapter, we will explicitly use the ideas introduced in this chapter. We will explain such a perturbative situation from a holographic perspective and discuss proposals regarding Fisher Information from the area and volume calculations.

ENTANGLEMENT AND SUB-REGION
COMPLEXITY FOR CHARGED AND
UNCHARGED ADS-SCHWARZSCHILD
BLACK HOLES IN GENERAL SPACETIME
DIMENSIONS

This chapter is based on [5].

Corrections to the RT formula arising from bulk entanglement entropy of the RT surface were first proposed at leading order in the bulk Planck constant in [21], extended to all orders in [22] (see [76] as well) and fully justified in [77]. These corrections have been checked in several cases [78], although it is difficult to do this for general perturbations away from pure AdS due to complications in determining the modular Hamiltonian for

generally excited states. On the other hand, there has also been some work in finding higher-order corrections in the RT term itself (these are higher-order in a small parameter measuring the perturbation away from pure AdS, e.g. the AdS black hole mass) [74, 79, 80]. These corrections are also expected to be related to the change of energy density and pressure density of the gravity theory in the same way as the normal thermodynamic entropy is related to the change of energy and other thermodynamic variables.

In the business of calculating the HEE, typically two types of subsystems are considered, namely the infinite strip and the ball subsystem. These cases were studied in detail in the AdS black hole background to first order in the black hole mass [81]. This was followed by a detailed analysis up to second order in a small perturbation away from pure AdS (e.g., as a pure metric perturbation, one produced by a bulk scalar, or one produced by a boundary current) [74].

Some recent works endeavor to capture important physics with these second-order effects. The leading-order change in HSC for a spherical sub-region comes at second order, which has led to connections with fidelity susceptibility [4] and Fisher information [75, 82–87].

Complexity is a notoriously difficult concept to define in quantum field theory in a way that does not appear to hinge on various arbitrary choices. Ordinarily, the measure of complexity involves minimizing the number of unitary transformations (within some choice of such transformations) required to transform the state of a system from some choice of reference state to the desired target state. In the context of the AdS/CFT correspondence, the cleanest aspect of this definition of complexity is the target state: we are interested in CFT states which have known AdS duals. We hope that we can gain some insight into complexity by studying it perturbatively around holographic states.

In a sense, what we do is a sub-region-reduced version of the idea explored in [88]. This

latter work tries to extract data about the so-called “cost function” [32, 53, 89], which was introduced to describe “minimal paths” between reference and target states in state space, by studying the behavior of complexity under small variations in the target state. Keeping the reference state fixed, the variation in complexity is controlled just by the endpoint of the optimal path in state space. This result has been dubbed the “first law of complexity” [88]. More concretely, a set of coordinates x^a is introduced on the space of unitary transformations $U(x^a)$ from some reference state $|\psi_R\rangle$, which can also be interpreted as a set of coordinates on the space of states $U(x^a)|\psi_R\rangle$. The path from the reference state $|\psi_R\rangle$ to the target state $|\psi_T\rangle = U_T|\psi_R\rangle$ minimizes the cost $\int_0^1 ds F(x^a(s), \dot{x}^a(s))$ of paths between the reference and target state, where F is some “cost function”. Under a small variation δx^a of the target state, the leading-order change in complexity is

$$\delta C = p_a \delta x^a \Big|_{s=1} \quad \text{with} \quad p_a = \frac{\partial F}{\partial \dot{x}^a}. \quad (3.1)$$

Geometrically, then, δC is related to the angle between the tangent to the optimal path at the target state and the displacement vector describing the variation away from the target. If $\delta C = 0$ at leading order, as is typically found to be the case for the spherical sub-region (shown in section 3.3), then the tangent to the optimal path and the displacement of the target state are orthogonal at this order. The next-to-leading term is related to second derivatives of F (for details, see [88]). This keeps going, of course, with higher-order corrections to (sub-region) complexity being related to higher derivatives of the cost function. Thus, the side-aim is to gain some insight into what the cost function might look like by studying small changes in holographic states.

In [88] the starting target state was the ground state of the CFT, dual to pure AdS, and the perturbation was introduced by a bulk scalar field excitation corresponding to a co-

herent state. The complexity was that of the entire state, not a sub-region reduced state. Furthermore, that calculation was done within the “complexity equals action” framework. In our present discussion, however, we focus on thermal perturbations around pure AdS, our states will be reduced to a spherical boundary sub-region, and we will be working within the “complexity equals volume” (sub-region) framework. Nevertheless, we share the same goal of studying the behavior of (sub-region) complexity in the vicinity of holographic states to gain some insight into what paths from some reference state to a target state might look like.

In this chapter, we consider the changes in HEE and HSC for a spherical sub-region in the uncharged and charged black hole background. The leading-order (LO) result for the HEE is what is often referred to as the “first law of entanglement” [74] (mentioned in (2.30)). At next-to-leading-order (NLO) for the HEE comes Fisher information, which has been related holographically to canonical energy [75] and bulk entanglement [87]. For the HSC, the only thing known is that it vanishes identically for a spherical sub-region in the AdS₃ black hole background, the first-order term vanishes identically, and the second-order result is known only in the AdS₄ black hole background [4, 87]. So far, the second-order result is not known in any other dimension and nothing is known at higher orders. Our goal is to fill in some of these gaps by computing second- and third-order corrections to the HSC in closed-form as functions of d . We provide closed-form formulae for the HEE up to third order as well as exact numerical expressions in fourth-order. We also do these calculations for the case of a charged AdS black hole, which is an example in which the current perturbation also plays a role in addition to the metric perturbation.

We also consider the first law of entanglement thermodynamics proposed in [8] and which was shown therein to hold at first order. Combining previous work on holographic complexity [4] and Fisher information [87], we propose a refinement of the first law of

entanglement thermodynamics to include a general work term done on the system: $\Delta E = T\Delta S + W$. This work term is different from the $V\Delta P$ term discussed in [8]. This latter term appears at first order already and can be absorbed in the ΔE term by the equation of state with a suitable redefinition of the entanglement temperature. These previous works naturally suggest that this work term be related to the change in HSC. However, now we find that the relation, which now holds at second order, does not hold at third order. This leads us to speculate that other information-theoretic quantities of interest might also play a role in a putative first law.

In the rest of the chapter, we firstly discuss the details of the embedding function in section 3.1. Then we discuss the perturbative computations of HEE for uncharged and charged BH in section 3.2. We also propose a general way of understanding which order embedding contributes to which order change of HEE building upon our study for the charged and uncharged BH in general dimensions. In section 3.3, we discuss similar study for the volumes (HSC). Finally, we explain the entanglement thermodynamics and the study of Fisher information from areas and volumes in section 3.4.

3.1 The Embedding Function:

First, we will discuss the case of the uncharged AdS_{d+1} -Schwarzschild black hole (BH) of mass m as a model example of a purely metric perturbation away from pure AdS (or, in the language of the dual field theory, a stress tensor perturbation). Then, we will discuss the case of a charged BH as well as a model example of a perturbation involving a current. The latter is not a pure current perturbation but is a mix of current and stress tensor perturbations. Generically, non-metric perturbations will inevitably be accompanied by metric perturbations via backreaction. Since we are interested in higher-order corrections to entanglement entropy and sub-region complexity, we cannot in general ignore backreaction.

Thankfully, the charged AdS black hole furnishes us with a fully back-reacted solution involving a current perturbation. We will expand the embedding function of the RT surface associated with a spherical boundary sub-region of radius R in the limit when R is much smaller than the black hole radius of the background. For the uncharged black hole, this is equivalent to a “small mass” or “low temperature” expansion. For the charged case, the horizon radius depends on both the mass and charge of the black hole. However, the charge does not have to be small in our perturbative analysis, and so, even for the charged case, one may think of the perturbation as being in the smallness of the mass of the black hole.

For the uncharged black hole, the first-order embedding function is known. We provide an analytic expression as a function of d for the second-order result, which was not known before this work. While we have not been able to find a closed-form analytic expression for the third-order embedding function, we do supply explicit expressions for it in the cases of AdS₃ to AdS₇ to cover the cases of immediate import to AdS/CFT applications.

For the charged black hole, there are orders which arise between the orders that are present in the uncharged case. What is called the n -th order in the uncharged case corresponds to what is more appropriately called the nd -th order in the charged case. It turns out that there are simple relationships between the nd -th order embedding functions in the charged case and the n -th order embedding functions in the uncharged case. The first in-between order is $2d - 2$ with all others being sums of multiples of d and $2d - 2$. Already at order $2d - 2$, we are unable to give closed-form analytic expressions for the corresponding embedding function. However, we provide the details of the derived embedding functions in the appendix A. We give details of two kinds of embedding functions one can choose, for both of which the final results (changes of HEE and HSC) remain the same.

3.1.1 Uncharged AdS Black Hole:

We will work with the metric of a $(d+1)$ -dimensional planar AdS-Schwarzschild black hole of mass m . The action that one starts with is simply the Einstein-Hilbert action in $(d+1)$ dimensions.

$$S_{bulk} = \frac{1}{16\pi G_N^{(d+1)}} \int d^d x \sqrt{-g} \left[\mathcal{R} + \frac{d(d-1)}{L^2} \right], \quad (3.2)$$

where \mathcal{R} is the Ricci scalar and L is the AdS radius. Here, the second term in the action is specific to AdS spacetime introduced due to the following relation between cosmological constant Λ and AdS radius in $(d+1)$ spacetime dimensions,

$$\Lambda = -\frac{d(d-1)}{2L^2}. \quad (3.3)$$

The form of the metric, derived as a solution of the vacuum Einstein's equation following the above action, is¹

$$ds^2 = \frac{L^2}{z^2} \left[-f(z) dt^2 + \frac{dz^2}{f(z)} + dr^2 + r^2 d\Omega_{d-2}^2 \right], \quad (3.4)$$

where $t \in (-\infty, \infty)$ is the time coordinate, $z \in (0, z_h)$ is the bulk radial coordinate with the boundary at $z = 0$ and black hole horizon at z_h given by $mz_h^d = 1$, r is the boundary radial coordinate, Ω_{d-2} is the collection of boundary angular coordinates, and $f(z)$ is the blackening function

$$f(z) = 1 - mz^d. \quad (3.5)$$

¹A different metric is used in [81], which is equivalent to this one up to first order in m in the region $mz^d \ll 1$.

We work with the entangling region B , which is a ball of radius R (i.e., $0 \leq r \leq R$). The corresponding RT surface is described by a spherically symmetric embedding function $z = z(r)$, such that

$$z(R) = 0. \quad (3.6)$$

The surface is often parametrized by $r = r(z)$ instead, which is well-adapted to the computation of counterterms [90] and the HSC [4]. However, there is a technical issue in that the domain of z itself receives corrections in m . As a consistency check, we have performed the second-order calculations using the $r(z)$ parametrization as well, yielding identical results. Higher-order computations were done purely in the $z(r)$ parametrization. One drawback of the $z(r)$ parametrization is that it obscures the need for a cut-off at a small value $z = \epsilon$. Nevertheless, since we are computing only the difference relative to the pure AdS background, no such cut-off will be required. The area of the RT surface as a function of $z(r)$ is

$$A = \Omega_{d-2} L^{d-1} \int_0^R dr \frac{r^{d-2}}{z(r)^{d-1}} \sqrt{1 + \frac{z'(r)^2}{f(z(r))}}, \quad (3.7)$$

where $z'(r) = \frac{dz(r)}{dr}$ and $\Omega_{d-2} = \frac{2\pi^{\frac{d-1}{2}}}{\Gamma(\frac{d-1}{2})}$ is the volume of the $(d-2)$ -sphere with unit radius. This area functional is extremized by solving the Euler-Lagrange equation. The embedding function is expanded as

$$z(r) = z_0(r) + \lambda z_1(r) + \lambda^2 z_2(r) + \lambda^3 z_3(r) + \dots, \quad (3.8)$$

where the small expansion parameter is

$$\lambda = mR^d = \left(\frac{R}{z_h}\right)^d, \quad (3.9)$$

and the Euler-Lagrange equation likewise expanded up to third order in λ to derive the equations satisfied by z_0, z_1, z_2 and z_3 . It is convenient to measure lengths in units of R and pass to the dimensionless variables (in the relation below, $0 \leq x \leq 1$, since $0 \leq r \leq R$ was chosen previously)

$$x \equiv \frac{r}{R}, \quad y(x) \equiv \frac{z(r)}{R}. \quad (3.10)$$

The boundary condition (3.6) becomes

$$y(1) = 0. \quad (3.11)$$

The function $y_0(x)$ is the pure AdS embedding

$$y_0(x) = \sqrt{1 - x^2}. \quad (3.12)$$

The equation for $y_n(x)$ for $n \geq 1$ can be written as a Riemann-Papperitz equation [91]

$$y_n'' + p(x)y_n' + q(x)y_n = \sigma_n(x), \quad (3.13)$$

where

$$p(x) = \frac{d - 2 - 2x^2}{x(1 - x^2)}, \quad (3.14)$$

$$q(x) = -\frac{d - 1}{(1 - x^2)^2}, \quad (3.15)$$

and $\sigma_n(x)$ is a driving function.

The homogeneous part of this Riemann-Papperitz equation is identical for all orders, including the in-between orders that arise in the charged black hole case. This is the case because the homogeneous part of the equation for y_n comes from expanding just the pure-AdS part of the area functional to quadratic order in y_n and then taking the variation of the result concerning y_n . The genuinely difficult part of this equation is the driving function $\sigma_n(x)$ which depends on a complicated nested hierarchy of second-order differential operators acting on each previous term, each operator itself depending on even earlier terms. Needless to say, this problem increases in difficulty extremely quickly. The first-order embedding is relatively easy to solve in general d , taking on a rather simple closed-form (3.17). Already at second order, the result (3.19) is fantastically more complicated. In the third order, we are unable to find a closed-form for the solution as a function of d .

The problem is made simpler if we relax the requirement of finding a formula as a function of d and instead compute the result for specific values of d . Of course, the computation increases in difficulty as d increases, especially when d is odd. In fact, we are able to determine the third-order embedding for $d = 12$, but not for $d = 11$. Nevertheless, we provide the third-order results for AdS₃ to AdS₇, thereby covering the cases most commonly considered in the context of applications of the AdS/CFT correspondence.

For $n = 1$, the driving function is given by

$$\sigma_1(x) = \frac{1}{2}(1 - x^2)^{\frac{d-3}{2}} [2(d-1) - (d+2)x^2]. \quad (3.16)$$

The first-order solution with boundary condition (3.11) is

$$y_1(x) = -\frac{(1 - x^2)^{\frac{d-1}{2}}(2 - x^2)}{2(d+1)}. \quad (3.17)$$

The Fefferman-Graham version of this result is in [74]. The $r(z)$ parametrization result is in [4, 81]. We have verified that our $y_1(x)$ above is consistent with both of the aforementioned results.

The second-order embedding function $y_2(x)$ does not contribute to the second-order change in HEE and is therefore not computed in [74, 81]. It is needed for the second-order change in HSC, which is studied in [4]. This latter work gives the result without explicit computation for the second-order change in HSC for $d = 2$ and $d = 3$ and the second-order embedding function is not mentioned there either, presumably having been taken for granted. In fact, we know that the change in HSC for $d = 2$ should vanish identically at all orders since the BTZ black hole is locally equivalent to AdS_3 , the distinction being purely a topological one. Therefore, the relevant data point of genuine interest in [4] is the change in HSC in $d = 3$. An explicit expression for the second-order embedding for AdS_4 , in the form $r_2(z)$ is given in [87]. However, the result for the change in HSC therein is in conflict with that in [4]. Therefore, we will give the expression for $y_2(x)$ for general dimension. To the best of our knowledge, this has not been done previously.

For $n = 2$,

$$\sigma_2(x) = -(1-x^2)^{d-\frac{7}{2}} \left(\frac{d^2(d-1)}{(d+1)^2} - \frac{5d^3-3d^2+d-1}{2(d+1)^2} x^2 + \frac{5d^3+6d^2-6d-1}{4(d+1)^2} x^4 - \frac{d-1}{4} x^6 \right). \quad (3.18)$$

The solution is

$$y_2(x) = \frac{1}{16\sqrt{w}} \left(\frac{\sqrt{\pi} d(d-1) \Gamma(d+1)}{2^d d+1 \Gamma(d+\frac{3}{2})} P + \frac{(d-1)(2d-1)(d-2)}{(d+1)^2} P_0 - \frac{3d^3-15d^2+11d-3}{(d+1)^2} P_1 - \frac{2d^3+3d^2-3d+2}{(d+1)^2} P_2 - (d-1)P_3 \right), \quad (3.19)$$

where $w = 1 - x^2$, and

$$P = B\left(w; \frac{d}{2}, \frac{3-d}{2}\right), \quad (3.20)$$

$$P_n = PB\left(w; \frac{d}{2} - 1 + n, \frac{d-1}{2}\right) - \frac{2w^{d-1+n}}{d(d-1+n)} {}_3F_2\left(1, \frac{3}{2}, d-1+n; \frac{d}{2} + 1, d+n; w\right), \quad (3.21)$$

where $B(w; a, b)$ is the incomplete beta function and range of w is same as range of x .

In the third order, we do not have a general formula for the embedding function, but we give expressions for these in spacetime dimensions 3 to 7. Again, this covers all the usual cases of interest within the AdS/CFT context. In the third order, we do not provide the forms of the embedding functions in the $r(z)$ parametrization as we perform our calculations exclusively in the $z(r)$ parametrization, as in [74]. To get a sense of the behavior of these higher-order embedding functions, we plot them in Figure 3.1. Notice that the behavior of the embedding function near $x = 1$ for the case of AdS_3 is very different compared to the higher-dimensional cases. This will turn out to be crucial in the analysis of boundary

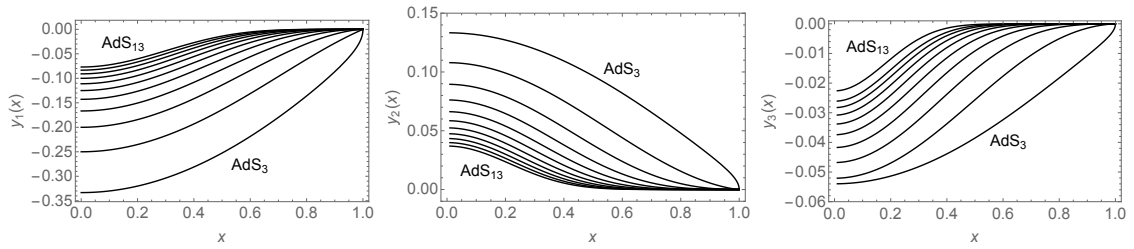


Figure 3.1: Plots of y_1 , y_2 and y_3 in various dimensions. Note that we do not have y_3 for AdS_{12} .

terms in subsection 3.2.3.

The general expression for $y_2(x)$ as a function of d is very useful since we can use it to generate y_2 for any value of d without having to solve its defining differential equation each time. However, we are not actually able to perform the integrals needed to calculate the higher-order changes in HEE and HSC using the general form of $y_2(x)$. This complication will actually only be relevant to the second- and third-order changes in HSC. Therefore, we must infer formulae for these quantities from results at specific values of d .

3.1.2 Charged AdS Black Hole:

We will now consider the charged AdS_{d+1} black hole, which represents a class of perturbation away from pure AdS that also involves a boundary current in addition to a boundary stress tensor. The metric for the charged AdS BH takes on the same form as for the uncharged case (3.4) with the blackening function (3.5) replaced with

$$f(z) = 1 - \left(1 + q^2 z_h^2\right) \frac{z^d}{z_h^d} + q^2 z_h^2 \frac{z^{2d-2}}{z_h^{2d-2}}. \quad (3.22)$$

Here the introduction of the new parameter q is due to the presence of a current.² The gauge potential corresponding to this current has a single nonzero component,

$$A_0(z) = \sqrt{\frac{2(d-1)}{d-2}} q \left(1 + \frac{z^{d-2}}{z_h^{d-2}} \right). \quad (3.23)$$

This is the same form of metric and gauge field used in [74]. Note that there is no charged AdS₃ black hole solution since the metric simply reduces to the uncharged case when $d = 2$. For convenience, we define the dimensionless parameter

$$p \equiv qz_h, \quad (3.24)$$

which is treated as an $\mathcal{O}(1)$ constant.

Unlike the previous case (uncharged AdS BH), for which we defined $\lambda = \frac{R^d}{z_h^d} = mR^d$, in this case, we define our dimensionless variables in the following way,

$$x \equiv \frac{r}{R}, \quad y(x) \equiv \frac{z(r)}{R}, \quad \eta \equiv \frac{R}{z_h}. \quad (3.25)$$

Here, η is our perturbation parameter, which corresponds to the condition $\frac{R}{z_h} \ll 1$. Note that in the charged case, the orders in the expansion are controlled by two non-negative integers n_1 , contributing $n_1 d$, and n_2 , contributing $2n_2(d-1)$. Thus, let us define the two-component vector \vec{n} and its “size” $|\vec{n}|$ as the order at which it contributes:

$$\vec{n} = \begin{pmatrix} n_1 \\ n_2 \end{pmatrix}, \quad |\vec{n}| = n_1 d + 2n_2(d-1). \quad (3.26)$$

²This term is related to the charge density carried by the horizon at $z = z_h$.

Then, we expand the embedding function as

$$\begin{aligned}
y(x) &= \sum_{\vec{n}=\vec{0}}^{\infty} \eta^{|\vec{n}|} y_{\vec{n}}(x) \\
&= y_{(0,0)}(x) + \eta^d y_{(1,0)}(x) + \eta^{2d-2} y_{(0,1)}(x) + \eta^{2d} y_{(2,0)}(x) + \eta^{3d-2} y_{(1,1)}(x) + \cdots,
\end{aligned} \tag{3.27}$$

with $y_{(0,0)}(x)$ being the pure AdS embedding function,

$$y_{(0,0)}(x) = \sqrt{1 - x^2}. \tag{3.28}$$

An important comparison between the expansion parameters of the uncharged and charged black holes is due here. As functions of their respective horizon radius z_h , one can see that $\lambda = \eta^d$. Thus, the orders which are integer multiples of d in the charged case correspond to the orders present in the uncharged case and must reduce to the latter when $q = 0$. On the other hand, the orders which are not simple integer multiples of d (e.g., $(2d - 2)$, $(3d - 2)$, etc.) are not present in the uncharged AdS BH.

With this in mind, we solve the embedding in the same way as we did in the uncharged case. The orders at integer multiples of d can be written simply in terms of the uncharged black hole embeddings in the following way,

$$y_{(n,0)}(x) = (1 + p^2)^n y_n(x), \tag{3.29}$$

where n is a non-negative integer.

For the newly appearing orders, however, it is difficult to come up with general expressions. Instead, we have to compute the embedding functions on a case by case basis for d

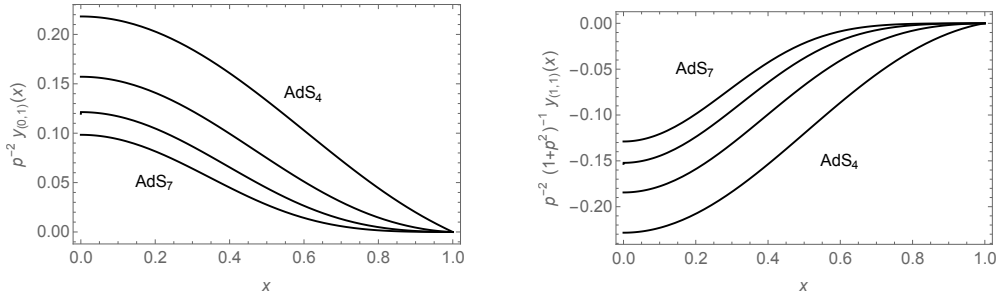


Figure 3.2: Plots of $\frac{1}{p^2}y_{(0,1)}$ and $\frac{1}{p^2(1+p^2)}y_{(1,1)}$ in various dimensions.

values starting from 3 to 6. In this chapter, we have considered up to order $(3d - 2)$ for the charged black hole case. Again, to get a qualitative sense of the embedding functions, we plot different order embedding functions in Figure 3.2.

3.2 Holographic Entanglement Entropy:

It is convenient to define the reduced HEE

$$s \equiv \frac{S}{2\pi\Omega_{d-2}\left(\frac{L}{\ell_P}\right)^{d-1}}. \quad (3.30)$$

In terms of the dimensionless variables,

$$s = \int_0^1 dx \frac{x^{d-2}}{y(x)^{d-1}} \sqrt{1 + \frac{y'(x)^2}{f(y)}}, \quad (3.31)$$

where

$$f(y) = 1 - \lambda y(x)^d \quad (3.32)$$

for the uncharged black hole and

$$f(y) = 1 - (1 + p^2)\eta^d y(x)^d + p^2\eta^{2d-2}y(x)^{2d-2} \quad (3.33)$$

for the charged black hole.

3.2.1 Uncharged AdS Black Hole:

The explicit appearance of λ in (3.31) is due to its appearance in the metric. When this factor of λ is expanded out, we refer to this as the “metric contribution” to the higher-order HEE. We introduce the notation s_n to denote the metric contribution at order λ^n .

There is also the “embedding contribution”, which comes from expanding the embedding function as

$$y(x) = y_0(x) + \lambda y_1(x) + \lambda^2 y_2(x) + \lambda^3 y_3(x) + \dots . \quad (3.34)$$

We pick out the term in s_n of the form $y_{n_1}(x) \cdots y_{n_k}(x)$ where $n_1 \leq \cdots \leq n_k$ and where some number of derivatives may act on the embedding functions. This term is denoted

$$s_{n,n_1 \cdots n_k}, \quad (3.35)$$

and is a term in s of order $\lambda^{n+n_1+\cdots+n_k}$. We make two exceptions in the above notation regarding $y_0(x)$. The indices n_i are taken to be nonzero as long as at least one of them is nonzero. In other words, as far as the indices n_i are concerned, we ignore factors of $y_0(x)$ as long as we are extracting a term that contains at least one higher-order correction to the embedding function. Otherwise, we write only one 0 after the comma in the subscript. For example, $s_{0,0}$ is the pure AdS result, while $s_{1,11}$ is a term in s that is of order λ^3 and consists of first expanding the metric to first order and then expanding the embedding function and picking out the terms that are quadratic in $y_1(x)$ and its derivatives. Since we are only

interested in the difference from pure AdS, we define³

$$\Delta s = s - s_{0,0}. \quad (3.36)$$

We expand this out in powers of λ ,

$$\Delta s = \lambda \Delta s^{(1)} + \lambda^2 \Delta s^{(2)} + \lambda^3 \Delta s^{(3)} + \dots. \quad (3.37)$$

As argued in [74], to calculate the first-order change in HEE, one needs only the zeroth-order embedding function. In fact,

$$\Delta s^{(1)} = s_{1,0} = \frac{1}{2} \int_0^1 dx x^{d-2} \frac{y_0 y_0'^2}{\sqrt{1 + y_0'^2}} = \frac{1}{2} \int_0^1 dx x^d = \frac{1}{2(d+1)}. \quad (3.38)$$

The reason why y_1 does not contribute to $\Delta s^{(1)}$ is that, after integration by parts, its contribution vanishes by the equation of motion for y_0 . However, a boundary term is generated in the course of integrating by parts. In fact, this boundary term does not vanish and must instead be subtracted out so that the variational principle for y_0 be well-defined. Furthermore, in principle, there is an infinite hierarchy of such subtractions at higher and higher order. We will discuss these boundary terms for both the uncharged and charged cases in subsection 3.2.3.

For the same reason as above, to compute the second-order change in HEE, one needs the embedding only up to the first order.⁴ In the course of our analysis of boundary terms in

³Note that counterterms must be subtracted from the pure AdS result if one wants to calculate that term by itself (see [90]). This must also be done for the AdS black hole background separately. One considers differences in HEE partly in order to avoid these complications.

⁴The nontrivial relationship between the depth of the RT surface in the bulk and the radius R of the entangling region complicates the disentangling of second-order contributions when using the $r(z)$ parametrization. Nevertheless, using this method we get results consistent with the $z(r)$ parametrization if we use the full embedding function to second order.

Section 3.2.3, we will derive the useful relations (3.54) and (3.65). Using these relations, we find

$$\Delta s^{(2)} = s_{0,2} + s_{0,11} + s_{1,1} + s_{2,0} = \frac{1}{2}s_{1,1} + s_{2,0}. \quad (3.39)$$

Using (3.65) to solve for $s_{0,11}$ in terms of $s_{1,1}$ is a substantial simplification since the latter is operationally much easier to compute than is the former. Nevertheless, we still verified this relation explicitly in this case. The final result is

$$\Delta s^{(2)} = -\frac{\sqrt{\pi}}{2^{d+4}} \frac{(d-1)\Gamma(d+1)}{(d+1)\Gamma(d+\frac{3}{2})}. \quad (3.40)$$

For the third-order change, one finds

$$\begin{aligned} \Delta s^{(3)} &= s_{0,3} + s_{0,12} + s_{1,2} + s_{0,111} + s_{1,11} + s_{2,1} + s_{3,0} \\ &= s_{0,111} + s_{1,11} + s_{2,1} + s_{3,0}. \end{aligned} \quad (3.41)$$

Indeed, the central result of Section 3.2.3 states that the embedding function up to the first order is sufficient to compute Δs up to the third order. The final result is

$$\Delta s^{(3)} = \frac{(9d^2 - 19d + 6)}{192(d+1)^2} \frac{\Gamma(d+1)\Gamma(\frac{d+1}{2})}{\Gamma(\frac{3(d+1)}{2})}. \quad (3.42)$$

With y_2 , we ought to be able to compute $\Delta s^{(4)}$. However, as previously stated, we are unable to evaluate the necessary integrals using the general form of y_2 in (3.19). Already at this point, the results for specific values of d are sufficiently complicated that we are unable to infer a general formula as a function of d .

To summarize,

$$\Delta s^{(1)} = \frac{1}{2(d+1)}, \quad (3.43)$$

$$\Delta s^{(2)} = -\frac{\sqrt{\pi}}{2^{d+4}} \frac{(d-1)\Gamma(d+1)}{(d+1)\Gamma(d+\frac{3}{2})}, \quad (3.44)$$

$$\Delta s^{(3)} = \frac{(9d^2 - 19d + 6)}{192(d+1)^2} \frac{\Gamma(d+1)\Gamma(\frac{d+1}{2})}{\Gamma(\frac{3(d+1)}{2})}. \quad (3.45)$$

The first- and second-order terms agree with [74]. The third-order term is a genuinely new result. Note that $\Delta s^{(2)} \leq 0$, as required by the first law of entanglement [74]. Interestingly, $\Delta s^{(3)}$ is positive and the $\Delta s^{(4)}$ results are all negative. It appears that Δs is positive in odd orders and negative in even orders.

3.2.2 Charged AdS Black Hole:

For the charged AdS BH, the perturbation parameter is η . Thus, the change of entanglement entropy with respect to pure AdS can be written as the following expansion,

$$\Delta s = \eta^d \Delta s^{(1,0)} + \eta^{2d-2} \Delta s^{(0,1)} + \eta^{2d} \Delta s^{(2,0)} + \eta^{3d-2} \Delta s^{(1,1)} + \dots, \quad (3.46)$$

where we extend the notation for the expansion of the embedding function introduced in (3.27) to the change in HEE: $\Delta s^{(\vec{n})}$ is the term in Δs of order $|\vec{n}|$, where $|\vec{n}|$ was defined in (3.26).

Our goal, in this case, is to compute the change in HEE for the charged BH up to order $(3d - 2)$. As shown in [74], to compute the HEE up to order $(2d - 2)$, it is enough to

take only $y_{(0,0)}(x)$. As in the uncharged case, this fact is actually just one of a hierarchy of such facts, which is the central result of our analysis of boundary terms in Section 3.2.3. For example, to compute the change in HEE to order $(3d - 2)$, it is enough to use the embedding up to order d , which is $y_{(1,0)}(x)$. This is due to the fact that the contribution of $y_{(0,1)}(x)$ to $\Delta s^{(1,1)}$ vanishes by virtue of the Euler-Lagrange equation defining $y_{(1,0)}(x)$.

We have already mentioned how to get $y_{(1,0)}(x)$ from the uncharged BH results in (3.29). Using this, we can determine the change of HEE up to our desired order. The following are the results up to order $(3d - 2)$,

$$\Delta s^{(1,0)} = \frac{(1 + p^2)}{2(d + 1)} = (1 + p^2)\Delta s^{(1)}, \quad (3.47)$$

$$\Delta s^{(0,1)} = -p^2 \frac{d - 1}{2} \pi^{\frac{d+1}{2}} \frac{\Gamma(\frac{d}{2})}{\Gamma(d + \frac{1}{2})}, \quad (3.48)$$

$$\Delta s^{(2,0)} = -(1 + p^2)^2 \frac{\pi^{\frac{1}{2}}}{2^{d+4}} \frac{(d - 1)\Gamma(d + 1)}{(d + 1)\Gamma(d + \frac{3}{2})} = (1 + p^2)^2 \Delta s^{(2)}, \quad (3.49)$$

$$\Delta s^{(1,1)} = p^2 (1 + p^2) \frac{(3d - 5)\Gamma(d)\Gamma(\frac{d+1}{2})}{8(d + 1)\Gamma(\frac{3d}{2} + \frac{1}{2})}. \quad (3.50)$$

We observe that for the charged BH, $\Delta s^{(1,0)}$ and $\Delta s^{(1,1)}$ are positive definite whereas $\Delta s^{(0,1)}$ and $\Delta s^{(2,0)}$ are negative definite. Another fact that we can observe from (3.47) and (3.49) is the relation between changes of HEE for uncharged and charged black holes. This

can be generalized in the following way,

$$\Delta s^{(n,0)} = (1 + p^2)^n \Delta s^{(n)}, \quad (3.51)$$

where n is an integer. This is an expected observation analogous to (3.29). These results will be important again after we compute the change of sub-region complexity.

3.2.3 Boundary Terms:

As in [74], we implicitly subtract off some boundary terms in the change in HEE. This is justified as long as we take care to do this consistently. We give two cautionary examples which demonstrate that consistency requires certain integral boundary terms to be subtracted out. It should then be clear how to formalize these examples into proof of the central results of this subsection:

1. Uncharged BH: $\Delta s^{(n)}$ is determined by the embedding function up to and including $y_{\lfloor \frac{n}{2} \rfloor}$;
2. Charged BH: $\Delta s^{(\vec{n})}$ is determined by the embedding function up to and including $y_{\vec{m}}$, where \vec{m} is the highest possible order such that $|\vec{m}| \leq \frac{|\vec{n}|}{2}$.

The relationship (3.29) between the embedding function for the uncharged case and the charged case implies that the first point above is a special case of the second point. In other words, the second point reduces to the first when $q = 0$.

As a generalization of the fact discussed earlier that y_1 does not contribute to $\Delta s^{(1)}$, consider the contribution of y_n to $\Delta s^{(n)}$ for $n \geq 1$, which is just

$$s_{0,n} = \int_0^1 dx \left(\frac{\delta s_0}{\delta y} \Big|_0 y_n + \frac{\delta s_0}{\delta y'} \Big|_0 y'_n \right), \quad (3.52)$$

where the symbol $|_0$ means “set $y = y_0$ ”. Integrating by parts and ignoring boundary terms gives

$$s_{0,n} = \int_0^1 dx \left[\frac{\delta s_0}{\delta y} - \left(\frac{\delta s_0}{\delta y'} \right)' \right] \Big|_0 y_n. \quad (3.53)$$

The expression in the square brackets is precisely the Euler-Lagrange equation defining y_0 , which therefore vanishes when evaluated on $y = y_0$. Thus,

$$n \geq 1 : \quad s_{0,n} = 0. \quad (3.54)$$

Of course, a boundary term was ignored in the process, which is given by

$$s_{0,n}^{\text{bdy}} = \left(\frac{\delta s_0}{\delta y'} \Big|_0 y_n \right) \Big|_{x=1} - \left(\frac{\delta s_0}{\delta y'} \Big|_0 y_n \right) \Big|_{x=0}. \quad (3.55)$$

Note that $\frac{\delta s_0}{\delta y}$ vanishes at $x = 0$ for the full function y and not just y_0 . Since y_n is finite at $x = 0$, the boundary contribution at $x = 0$ vanishes. However, even though $y_n(1) = 0$, the boundary contribution at $x = 1$ does not necessarily vanish because $\frac{\delta s_0}{\delta y'}$ contains a factor of y^{1-d} , which diverges as $x \rightarrow 1$. Indeed, for $n = 1$, one sees from (3.17) that y_1 is y_0^{d-1} multiplied by a function which is finite at $x = 1$. The resulting boundary term is

$$s_{0,1}^{\text{bdy}} = \frac{1}{2(d+1)}, \quad (3.56)$$

which happens to be exactly equal to $\Delta s^{(1)} = s_{1,0}$. If one were to include $s_{0,1}^{\text{bdy}}$, then one would overestimate $\Delta s^{(1)}$ by a factor of 2.

For $n = 2$, one can show that the behavior of y_2 in (3.19) near $x = 1$ is $(1 - x^2)^{d-\frac{3}{2}}$, whereas $y_0^{1-d} \sim (1 - x^2)^{\frac{1-d}{2}}$. Thus, the boundary function behaves like $(1 - x^2)^{\frac{d}{2}-1}$ near $x = 1$ and thus the boundary term vanishes identically except for $d = 2$ or AdS₃. Since

we do not have y_3 or higher in closed analytic form as a function of d , we cannot prove that this holds in general, but we have verified up to AdS_{13} (not included AdS_{12}) that the boundary term also vanishes when $n = 3$ except for AdS_3 . As was hinted at earlier, that AdS_3 is a special case can be seen quite clearly in the plots of the higher-order embedding functions in Figure 3.1. The intuition here is that the boundary term $s_{0,n}$ arises because y_n is not “flat enough” at $x = 1$. Evidently, y_1 is never flat enough, regardless of the value of d . On the other hand, for $n \geq 2$, y_n is flat enough except for AdS_3 , which is not flat at all. Nevertheless, the boundary term must be subtracted out anyway.

It should be clear why the boundary term must be subtracted out of the final result, or simply ignored in the first place. If this is not done, then the variational principle used to determine $y_0(x)$ is not well-defined. As in the case of the Gibbons-Hawking-York boundary term in General Relativity, the appropriate boundary term must be added (or, indeed subtracted) to provide a well-defined and consistent variational principle.

For our second example highlighting the technicalities of boundary terms, consider the contribution of y_n to $\Delta s^{(n+1)}$ for $n \geq 1$. Firstly, let us discuss how one derives the Euler-Lagrange equation for y_1 . The leading term quadratic in y_1 is $s_{0,11}$, which is of order 2. We add to $s_{0,11}$ all the terms which are of order 2 and linear in y_1 , namely $s_{1,1}$. Finally, we take a variation of the sum $s_{0,11} + s_{1,1}$ with respect to y_1 . Let us first write this sum out:

$$s_{0,11} + s_{1,1} = \int_0^1 dx \left(\frac{\delta^2 s_0}{\delta y^2} \Big|_0 y_1^2 + \frac{\delta^2 s_0}{\delta y \delta y'} \Big|_0 y_1 y_1' + \frac{\delta^2 s_0}{\delta y'^2} \Big|_0 y_1'^2 + \frac{\delta s_1}{\delta y} \Big|_0 y_1 + \frac{\delta s_1}{\delta y'} \Big|_0 y_1' \right). \quad (3.57)$$

The variation with respect to y_1 gives

$$\frac{\delta(s_{0,11} + s_{1,1})}{\delta y_1} = 2 \frac{\delta^2 s_0}{\delta y^2} \Big|_0 y_1 - \left(\frac{\delta^2 s_0}{\delta y \delta y'} \Big|_0 \right)' y_1 - 2 \left(\frac{\delta^2 s_0}{\delta y'^2} \Big|_0 y_1' \right)' + \frac{\delta s_1}{\delta y} \Big|_0 - \left(\frac{\delta s_1}{\delta y'} \Big|_0 \right)' \quad (3.58)$$

The vanishing of the above variation is the Euler-Lagrange equation for y_1 . Note that the homogeneous part of the equation comes from $s_{0,11}$. In general, the homogeneous part of the equation for y_n when $n \geq 1$ comes from $s_{0,nn}$. It is therefore not surprising that the homogeneous part of the Riemann-Papperitz equation (3.13) defining y_n is the same for all $n \geq 1$.

Now, note that the contribution of y_n to $\Delta s^{(n+1)}$ for $n \geq 1$ comes from $s_{0,1n}$ and $s_{1,n}$. The first of these contains a relative factor of 2 when $n = 1$ versus when $n \geq 2$:

$$n = 1 : \quad s_{0,11} = \int_0^1 dx \left(\frac{\delta^2 s_0}{\delta y^2} \Big|_0 y_1^2 + \frac{\delta^2 s_0}{\delta y \delta y'} \Big|_0 y_1 y_1' + \frac{\delta^2 s_0}{\delta y'^2} \Big|_0 y_1'^2 \right), \quad (3.59)$$

$$n \geq 2 : \quad s_{0,1n} = \int_0^1 dx \left(2 \frac{\delta^2 s_0}{\delta y^2} \Big|_0 y_1 y_n + \frac{\delta^2 s_0}{\delta y \delta y'} \Big|_0 (y_1 y_n' + y_n y_1') + 2 \frac{\delta^2 s_0}{\delta y'^2} \Big|_0 y_1' y_n' \right). \quad (3.60)$$

The other contribution, $s_{1,n}$, is given for $n \geq 1$ by

$$n \geq 1 : \quad s_{1,n} = \int_0^1 dx \left(\frac{\delta s_1}{\delta y} \Big|_0 y_n + \frac{\delta s_1}{\delta y'} \Big|_0 y_n' \right). \quad (3.61)$$

Integrating by parts and ignoring boundary terms gives

$$n = 1 : \quad s_{0,11} = \int_0^1 dx \left[\frac{\delta^2 s_0}{\delta y^2} \Big|_0 y_1 - \frac{1}{2} \left(\frac{\delta^2 s_0}{\delta y \delta y'} \Big|_0 \right)' y_1 - \left(\frac{\delta^2 s_0}{\delta y'^2} \Big|_0 y_1' \right)' \right] y_1, \quad (3.62)$$

$$n \geq 2 : \quad s_{0,1n} = \int_0^1 dx \left[2 \frac{\delta^2 s_0}{\delta y^2} \Big|_0 y_1 - \left(\frac{\delta^2 s_0}{\delta y \delta y'} \Big|_0 \right)' y_1 - 2 \left(\frac{\delta^2 s_0}{\delta y'^2} \Big|_0 y_1' \right)' \right] y_n, \quad (3.63)$$

$$n \geq 1 : \quad s_{1,n} = \int_0^1 dx \left[\frac{\delta s_1}{\delta y} \Big|_0 - \left(\frac{\delta s_1}{\delta y'} \Big|_0 \right)' \right] y_n. \quad (3.64)$$

When $s_{0,1n}$ and $s_{1,n}$ are summed together, then, for $n \geq 2$, the expression multiplying y_n is precisely the Euler-Lagrange equation defining $y_1(x)$ and therefore the sum vanishes. For $n = 1$ one has to multiply $s_{0,11}$ by 2 to get the same result. Therefore,

$$n = 1 : \quad 2s_{0,11} + s_{1,1} = 0, \quad (3.65)$$

$$n \geq 2 : \quad s_{0,1n} + s_{1,n} = 0. \quad (3.66)$$

Of course, boundary terms were ignored to get the above result. These boundary terms should actually appear on the right-hand side of the above equations, instead of 0. Nevertheless, these boundary terms have to be subtracted out anyway to yield a well-defined and consistent variational principle for $y_1(x)$.⁵ In fact, we have an even more immediate sign that these boundary terms must be subtracted out: if not, then the result for $\Delta s^{(2)}$ for the AdS₃ black hole would be $\frac{1}{120}$ instead of $-\frac{1}{180}$. This is a positive number, which violates the first law of entanglement stated in [74].

This argument generalizes completely to the following statement: the contribution of y_n to $\Delta s^{(n+m)}$ for $n \geq 1$ and $m < n$ vanishes. Also, for $m = n$, the contribution is just equal

⁵Again, at least in the case of $n = 2$ and $n = 3$, which is as far as we have expanded the embedding function in this work, it turns out that the boundary terms that have been ignored above actually vanish identically except for AdS₃. So, the process of subtracting out these boundary terms is only nontrivial for the case of AdS₃.

to $-s_{0,nn}$. The procedure is exactly the same as with $m = 1$. The desired contribution is

$$\sum_{q=0}^m \sum_{P(m-q)} s_{q,P(m-q)n}, \quad (3.67)$$

where $P(m - q)$ stands for all partitions of $m - q$ into a list of integers which are non-decreasing read left to right. Meanwhile, the Euler-Lagrange equation for y_m is derived by taking the variation with respect to y_m of the exact same sum, but with y_n replaced with y_m . The same analysis as for $m = 1$ shows that

$$\sum_{q=0}^m \sum_{P(m-q)} s_{q,P(m-q)n} = \begin{cases} 0, & n \geq 1 \text{ and } m < n, \\ -s_{0,nn}, & n \geq 1 \text{ and } m = n. \end{cases} \quad (3.68)$$

The sum does not simplify in general for $m > n$ and is generally nonzero.

This argument generalizes with only cosmetic changes to the charged case: the contribution of $y_{\vec{n}}$ to $\Delta s^{(\vec{n}+\vec{m})}$ vanishes when $|\vec{m}| < |\vec{n}|$ and is equal to $-s_{0,\vec{n}\vec{n}}$ when $|\vec{m}| = |\vec{n}|$.

These statements are equivalent to the central result stated at the beginning of this subsection.

3.3 Holographic Sub-region Complexity:

We now compute the change in HSC. The volume is given by

$$V = \Omega_{d-2} L^d \int_0^R dr r^{d-2} \int_{\epsilon R}^{z(r)} \frac{dz}{z^d \sqrt{f(z)}}, \quad (3.69)$$

where we have introduced a cut-off ϵR near $z = 0$. The HSC is related to this by (2.25).

We define the reduced HSC c as the HSC measured in units of $\frac{\Omega_{d-2}}{d-1} \left(\frac{L}{\ell_P}\right)^{d-1}$:

$$c \equiv \frac{C}{\frac{\Omega_{d-2}}{d-1} \left(\frac{L}{\ell_P}\right)^{d-1}}. \quad (3.70)$$

In terms of the dimensionless variables,

$$c = (d-1) \int_0^1 dx x^{d-2} \int_\epsilon^{y(x)} \frac{dy}{y^d \sqrt{f(y)}}. \quad (3.71)$$

The subscript notation we defined for s carries through for c . The blackening functions $f(y)$ for uncharged and charged black holes are as mentioned in Section 3.2. An important point to remember here is that, in contrast to the HEE case, to calculate the HSC to some order, we require the embedding function up to that same order. The simplifications that arose in the HEE case were due to the fact that the embedding function is derived by minimizing the area integral. No such simplification will occur in general for the volume integral. Now we jump into specific results for the uncharged and charged BH in the following subsections.

3.3.1 Uncharged AdS Black Hole:

The quantity of interest here is the change in going from the pure AdS case to the uncharged AdS black hole case,

$$\Delta c = c - c_{0,0}. \quad (3.72)$$

which is finite as $\epsilon \rightarrow 0$ and is at least first order in λ :

$$\Delta c = \lambda \Delta c^{(1)} + \lambda^2 \Delta c^{(2)} + \lambda^3 \Delta c^{(3)} + \dots. \quad (3.73)$$

In fact, we find that the first-order term vanishes. This result was stated in [4, 92] and demonstrated explicitly in [87]. Therefore, the change in HSC is at least second order. Again, since we are unable to compute the requisite integrals using the general formula for y_2 in (3.19), nor do we have a general formula for y_3 , we must infer the general formulae for $\Delta c^{(2)}$ and $\Delta c^{(3)}$ from the results at specific values of d . This might seem rather hopeless at first. However, we do have some amount of guidance from the pieces in $\Delta c^{(2)}$ and $\Delta c^{(3)}$ that depends only on y_0 and y_1 , which we can compute exactly. This guidance is enough for us to determine the formulae in general. We use the results for AdS₃ to AdS₇, the cases of greatest interest in the AdS/CFT context, to come up with general formulae as functions of d . We then test these formulae in the cases of AdS₈ to AdS₁₃, excluding AdS₁₂ for $\Delta c^{(3)}$ since y_3 for AdS₁₂ is too lengthy and complicated to compute the requisite integrals. The results as functions of d are

$$\Delta c^{(1)} = 0, \tag{3.74}$$

$$\Delta c^{(2)} = \frac{\sqrt{\pi}}{2^{d+2}(d+1)} \frac{\Gamma\left(\frac{d+1}{2}\right)}{\Gamma\left(\frac{d}{2}-1\right)}, \tag{3.75}$$

$$\Delta c^{(3)} = -\frac{d(9d-4)(2d-3)(d-1)(d-2)}{192(d+1)^2} \frac{\Gamma\left(d-\frac{3}{2}\right)\Gamma\left(\frac{d+1}{2}\right)}{\Gamma\left(\frac{3d}{2}+1\right)}. \tag{3.76}$$

The AdS₃ and AdS₄ results for $\Delta c^{(2)}$ agree with [4], namely 0 and $\frac{1}{128}$, respectively. Now, we have a formula for general d , not only for $\Delta c^{(2)}$, but for $\Delta c^{(3)}$ as well.

We observe some interesting behavior in Δs and Δc up to third order in uncharged

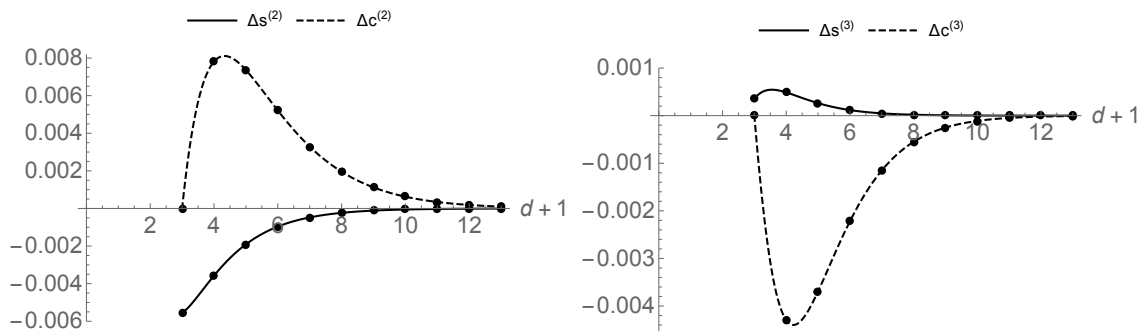


Figure 3.3: Plots of Δs and Δc to second- and third-order in the uncharged black hole background. The points are explicitly calculated values. The curves are plots of the general formulae.

black holes. Note that $\Delta s^{(2)}$ is negative whereas $\Delta c^{(2)}$ is positive (or 0 for AdS_3). In the third order, the signs flip and $\Delta s^{(3)}$ is now positive whereas $\Delta c^{(3)}$ is negative (or 0 for AdS_3). Only the sign of $\Delta s^{(2)}$ is constrained to be negative by the first law of entanglement [74]. It is tantalizing that, Δc appears to be of opposite sign as compared with Δs at each order (see Figure 3.3). We will find that this behavior continues to hold for the charged black hole. It would be interesting to see if this behavior persists in other scenarios and to higher orders and if it can be proven in general.

3.3.2 Charged AdS Black Hole:

In the charged AdS black hole case, we expand Δc up to the first four orders for general d :

$$\Delta c = \eta^d \Delta c^{(1,0)} + \eta^{2d-2} \Delta c^{(0,1)} + \eta^{2d} \Delta c^{(2,0)} + \eta^{3d-2} \Delta c^{(1,1)} + \dots \quad (3.77)$$

Again, as in the case of entanglement entropy, we find

$$\Delta c^{(1,0)} = (1 + p^2)\Delta c^{(1)}, \quad (3.78)$$

$$\Delta c^{(2,0)} = (1 + p^2)^2\Delta c^{(2)}, \quad (3.79)$$

similar to (3.29) and (3.51). For the newly appearing orders $(2d - 2)$ and $(3d - 2)$ in the charged BH case, we use embedding functions $y_{(0,1)}(x)$ and $y_{(1,1)}(x)$ derived for $d = 3, 4, 5$ and 6 , presented in Appendix B of [5]. Using these embedding functions, we compute the sub-region complexity changes at orders $(2d - 2)$ and $(3d - 2)$ for the aforementioned d values. As in the uncharged case, we can separate out the dependence of these results on $y_{(1,0)}$, which we do know for general d values. Using this piece as guidance, we can deduce the changes of sub-region complexity at order $(2d - 2)$ and $(3d - 2)$ for general d . We then checked our formula against results calculated for d values higher than 6 (up to 10). Indeed, our formula reproduces correct results in those cases as well. The following are our expressions of $\Delta c^{(0,1)}$ and $\Delta c^{(1,1)}$:

$$\Delta c^{(0,1)} = p^2 \frac{\pi^{\frac{1}{2}} (d - 2) \Gamma\left(\frac{d-1}{2}\right)}{2^{d+1} \Gamma\left(\frac{d}{2}\right)}, \quad (3.80)$$

$$\Delta c^{(1,1)} = -p^2(1 + p^2) \frac{3(d - 1)(d - 2) \Gamma\left(d - \frac{1}{2}\right) \Gamma\left(\frac{d+1}{2}\right)}{4(d + 1) \Gamma\left(\frac{3d}{2}\right)}. \quad (3.81)$$

Looking at these results (3.78), (3.79), (3.80), (3.81) and comparing them with the signs of (3.47),(3.48),(3.49)and (3.50), we again see that whenever Δs at some order is positive (negative) definite, Δc is negative (positive) definite. Therefore, for both the uncharged

black hole (pure stress tensor perturbation) and the charged black hole (mixed stress tensor and current perturbation), we observe that the change in HEE and HSC at some particular order come with opposite sign. We add that this relative minus sign between the change in HEE and HSC also holds for the leading-order result in the case of a perturbation due to a scalar of conformal dimension Δ [74, 87].

3.4 Entanglement Thermodynamics:

The field theories dual to the uncharged and charged AdS black holes are correspondingly charged and uncharged perfect fluids with stress tensor taking the form

$$T_{\mu\nu} = (\mathcal{E} + P)u_\mu u_\nu + P\eta_{\mu\nu}, \quad (3.82)$$

where \mathcal{E} is the energy density, P is the pressure, and u_μ is the fluid velocity. In addition, the fact that the dual field theory is actually a CFT implies that

$$P = \frac{\mathcal{E}}{d-1}. \quad (3.83)$$

Matching this with the boundary metric for the case of the uncharged black hole gives the standard AdS/CFT dictionary relationship between the boundary energy density and bulk geometric data,

$$\mathcal{E} = \frac{d-1}{2} \left(\frac{L}{\ell_P} \right)^{d-1} \frac{1}{z_h^d}.$$

Both the uncharged and charged AdS black holes correspond to perfect fluids at rest, with a fluid velocity is given by $u^\mu = \delta_0^\mu$. The stress tensor for the charged case is $(1 + q^2 z_h^2)$ times the stress tensor for the uncharged case in which the uncharged horizon radius is replaced with the charged one. Both cases have a constant energy density and therefore the energy

contained in the ball entangling region of radius R scales as R^{d-1} for both cases. To be precise, for the uncharged black hole,

$$\Delta E = \int T_{00} d\Omega_{d-2} r^{d-2} dr = \frac{1}{2} \Omega_{d-2} \left(\frac{L}{\ell_P} \right)^{d-1} \frac{R^{d-1}}{z_h^d}, \quad (3.84)$$

and the charged case is the same result multiplied by $(1 + q^2 z_h^2)$. In other words, ΔE is proportional to λ in the uncharged case and η^d in the charged case. This is not just a perturbative result but is an exact one. Meanwhile, for the uncharged black hole, we expand out the entanglement entropy as

$$\Delta S_E = \Delta S_E^{(1)} + \Delta S_E^{(2)} + \dots, \quad (3.85)$$

where $\Delta S_E^{(n)}$ is a term in ΔS_E which is of order λ^n .⁶ We now place the explicit subscript “ E ” to remind the reader that we are dealing with entanglement entropy and not the usual thermodynamic entropy here. Nevertheless, the central idea of entanglement thermodynamics in [8] is to make an analogy with thermodynamics and to define the **entanglement temperature** in such a way that

$$\Delta E = T_E \Delta S_E^{(1)}. \quad (3.86)$$

Let us make the following two observations regarding this relation:

1. This is a perturbative relation that holds only at leading order;
2. To extend this relationship beyond leading order, one must introduce new terms because ΔE is exactly first-order while ΔS_E contains higher-order corrections. Indeed,

⁶Note that $\Delta S^{(n)}$ does not contain explicit powers of λ since that is factored out when we write (3.37). However, our convention here is that $\Delta S_E^{(n)}$ does contain an explicit factor of λ^n .

the new term would serve to cancel $T_E \Delta S_E^{(2)}$ at second order.

On the other hand, as we pass to the non-perturbative regime, in which the sub-region covers more and more of the entire boundary CFT, the entanglement entropy approaches the thermodynamic one, which does satisfy the laws of black hole thermodynamics. We are motivated, therefore, to try to extend the above relation at least to second order. In analogy with the usual first law, we write

$$\Delta E = T_E \Delta S_E + W_E, \tag{3.87}$$

where W_E is some **entanglement work** analogous to thermodynamic work and encompasses the new terms mentioned in point 2 above to make the relation hold to a higher order. It is important to point out that it is ΔE that appears in this relation and not $T_E \Delta \langle H \rangle$, where H is the modular Hamiltonian. Firstly, the modular Hamiltonian is in general a very non-local quantity whose connection to energy is unclear. Only in the case of spherical sub-regions in CFTs in a vacuum do we find such a direct relationship between the modular Hamiltonian and energy. Of course, that happens to be the case in the study in this work, but the first law of entanglement thermodynamics ought to be more widely applicable than that. Secondly, if we were to base the first law around the modular Hamiltonian, then W_E would be equivalent to $T_E S_{\text{rel}}$, where S_{rel} is the relative entropy, which is always non-negative, regardless of the initial and final state. Furthermore, for the first law to have any actual content, the work term must have an entirely distinct ontology from energy and entanglement. Otherwise, W_E could simply be **defined** as $\Delta E - T_E \Delta S_E$. What could this work term be?

We do not know the answer to this question. However, we would like to point out that we are not really the first to pose the question in the first place. The question turns

out to be essentially equivalent to the problem studied in [87] based off of [4]. In fact, the authors of [87] propose an answer to this question: the entanglement work contains a term proportional to the change in sub-region complexity. To be very careful, [87] does not actually propose this directly. Instead, they propose that the Fisher information is proportional to the second-order change in the volume of the RT surface. In the context of our perturbative analysis around pure AdS, the Fisher information is just

$$\mathcal{F} = \frac{d^2}{d\lambda^2} (\Delta \langle H \rangle - \Delta S_E) \Big|_{\lambda=0} = -\frac{2}{\lambda^2} \Delta S_E^{(2)} = \frac{\pi^{3/2}}{2^{d+2}} \frac{(d-1)\Gamma(d+1)}{(d+1)\Gamma(d+\frac{3}{2})} \Omega_{d-2} \left(\frac{L}{\ell_P}\right)^{d-1}. \quad (3.88)$$

On the other hand, the change in RT volume is related to the change in sub-region complexity:

$$\Delta V^{(2)} = \frac{\Omega_{d-2}}{d-1} L^d \Delta c^{(2)} = \frac{\sqrt{\pi}}{2^{d+2}(d-1)(d+1)} \frac{\Gamma(\frac{d+1}{2})}{\Gamma(\frac{d}{2}-1)} \Omega_{d-1} L^d. \quad (3.89)$$

Therefore, the proportionality constant C_d defined in [87] via $\mathcal{F} = C_d \Delta V^{(2)}$ is given by

$$C_d = \frac{\pi(d-1)^2 \Gamma(d+1) \Gamma(\frac{d}{2}-1)}{\lambda^2 L \ell_P^{d-1} \Gamma(d+\frac{3}{2}) \Gamma(\frac{d+1}{2})}. \quad (3.90)$$

Note that this is the first time that this coefficient has actually been computed explicitly since the expression in [87] contains a function of d that was unknown until now. There is an ambiguity in the small parameter λ and thus an ambiguity in the definition of \mathcal{F} . In [75], the derivative is taken with respect to a parameter μ , which is related to our parameter m by $m = 2\mu$. Therefore, our \mathcal{F} in (3.88) is related to the Lashkari-van Raamsdonk expression by $\mathcal{F} = 4R^{2d} \mathcal{F}^{\text{LvR}}$. Note that they also set $L = 1$ and $G_N = \frac{1}{8\pi} \ell_P^{d-1} = 1$. Therefore, one finds $\mathcal{F}^{\text{LvR}} = \frac{\sqrt{\pi}}{2^{d+3}} \frac{(d-1)\Gamma(d+1)}{(d+1)\Gamma(d+\frac{3}{2})} \Omega_{d-2} R^{2d}$, which is indeed $\frac{R^4}{45}$ for AdS₃, as stated in [75].

Therefore, taken at face value, the suggestion in [87] is that $\Delta S_E^{(2)}$ is proportional to

$\Delta V^{(2)}$, where V is the volume of the RT surface. Therefore, though this was not its express intention, [87] suggests identifying the entanglement work with the change in the volume of the RT surface:

$$\Delta E = T_E \Delta S_E + P \Delta V, \quad (3.91)$$

where P is a concomitant pressure⁷, which is related to the coefficient C_d introduced in [87] and computed in (3.90) via

$$P = T_E \frac{\lambda^2}{2} C_d = \frac{d+1}{4\pi R} \left(\frac{R}{z_h} \right)^2 C_d. \quad (3.92)$$

The relationship between volume and complexity then says that we can equally well express the entanglement work in terms of the change in HSC,

$$\Delta E = T_E \Delta S_E + B \Delta C, \quad (3.93)$$

where $B = L \ell_p^{d-1} P$.

In this picture, the change in HEE is morally playing the role of heat and the change in HSC is playing the role of work. In fact, the definition of complexity naturally contains within it connotations of work. It is usually defined roughly as the minimum number of unitary transformations from some prescribed collection of such transformations required to transform some particular reference state into the desired target state. It is sometimes intuitively described as the amount of “computational power” or “resources” needed to perform these operations. It is certainly not a stretch to associate this intuitive idea with some concept of work. Indeed, once a concrete and practicable definition of complexity in field theory is given, and assuming some relation like (3.93) exists, then one could presumably

⁷This pressure is unrelated to what is called **entanglement pressure** in [8].

exploit the relation to run information-theoretic periodic cycles (a.k.a. engines).

The apparent pattern that ΔC and ΔS are of opposite sign at each order is further indication that such a relation (3.93) might hold. However, this cannot be the whole picture. This relation holds up to the second-order but does not hold in the third order. Of course, we should have known that this cannot be the whole picture since it would have implied that ΔS and ΔC are not independent for the case in study. On the other hand, there is a sense in which ΔC carries more, or at least different, information than ΔS , since ΔC requires more information about the embedding function than does ΔS . As we have shown in Section 3.2.3, the n -th order ΔS is determined by the embedding function up to at most half that order. On the other hand, ΔC to n -th order depends on the embedding function up to that same order n . Thus, while there does appear to be a flow of information from being in the form of entanglement to sub-region complexity, this transfer is not complete. From the perspective of a speculative theoretical engine, part of the work in a cycle can arise as changes in complexity, and part of it can arise as something else, just as it can arise as changes in volume as well as particle number in more familiar thermodynamic cases. What other information-theoretic quantities might contribute to W_E is a question worth investigating. There are a number of important works deriving Einstein's equations from entanglement, to first order (e.g., in [93]) and then to second order (e.g., [94]; see also [95]). These relate the variations of the relative entropy to bulk integrals in a formalism developed in [96]. This approach claims an exact first law of entanglement entropy from the start and it is plausible that we are rediscovering this same result perturbatively.

ENTANGLEMENT THERMODYNAMICS
AND FISHER INFORMATION METRIC FOR
NON-SUSY BLACK D3 BRANE

In this chapter, we discuss our results from [6] and [7].

We discuss entanglement and sub-region complexity in a class of non-supersymmetric black solutions that are asymptotically AdS. Non-supersymmetric solutions are an important case study given the QCD theory doesn't enjoy the supersymmetries. Therefore, if a holographic gravity dual of a QCD theory exists, that is also expected to be non-supersymmetric. Firstly, we discuss very briefly about D branes and how $AdS_5 \times S^5$ comes out from the throat of supersymmetric theories. In this context, it is important to mention that the best-studied version of the duality, where the gravity side is $AdS_5 \times S^5$, can be derived from the decoupling limit of the supersymmetric D3 brane solutions of type II B string theory (linearized weak gravity version, SUGRA). Dp branes are extended objects

in p spatial dimensions as solutions of string theory. These branes are objects where open strings end. They can be obtained by quantizing the string with Dirichlet boundary conditions. They can also be realized as objects charged under the antisymmetric tensor fields $A_{\mu_1 \dots \mu_{p+1}}$. They are dynamic objects and follow the action

$$S = -T_{Dp} \int d^{p+1}x [\dots] \quad (4.1)$$

Tension $T_{Dp} = \frac{1}{(2\pi)^p g_s (l_s)^{p+1}}$. Here inverse proportionality with g_s confirms the non-perturbative nature and dependence on l_s is computed from the dimension analysis.

Now we discuss few concepts of Dp branes briefly.

- Dp branes have two kinds of excitations. The d.o.f corresponding to rigid motions can be parametrized by $(9-p)$ coordinates transverse to $(p+1)$ dimensional volume in the 10d target space. These are scalar fields.
- Dp branes also have internal excitations. Here we recall that endpoint of a string is a charge. This charge corresponds to an Abelian gauge field living in the world volume of Dp branes.
- Dirac-Born-Infeld Action takes into account both the excitations

$$S_{DBI} = -T_{Dp} \int d^{p+1}x \sqrt{(g_{\mu\nu} + 2\pi l_s^2 F_{\mu\nu})} \quad (4.2)$$

$g_{\mu\nu}$ is the induced metric on the worldvolume and $F_{\mu\nu}$ is the strength of the Abelian gauge field.

- In flat space the induced metric takes the form

$$g_{\mu\nu} = \eta_{\mu\nu} + (2\pi l_s^2)^2 \partial_\mu \phi^i \partial_\nu \phi^i \quad (4.3)$$

- The Dirac-Born-Infeld action is expanded then up to quadratic terms and we get

$$S_{DBI}^{(2)} = -\frac{1}{g_{YM}^2} \left(\frac{1}{4} F_{\mu\nu} F^{\mu\nu} + \frac{1}{2} \partial_\mu \phi^i \partial^\mu \phi^i + \dots \right) \quad (4.4)$$

which is the ordinary action of gauge field and (9-p) scalar fields with Yang-Mills coupling. $g_{Y-M} = 2(2\pi)^{p-2} (l_s)^{p-3} g_s$.

- In the case of D3 branes in 10 d target space, the world volume is $3 + 1 = 4$ dimensional and we have 6 scalar fields. The corresponding 4 dimensional SU(N) gauge theory can be identified with the super Yang-Mills theory with 4 supersymmetries which is an exact CFT and a major example of the duality. in this case $g_{Y-M}^2 = 4\pi g_s$ (dimensionless).

4.1 D Branes and Relation to Gravity:

In string theory, all kinds of matter distort spacetime. This can be measured by solving Einstein's equation and the action takes the form

$$S = \frac{1}{16\pi G} \int d^{10}x (\sqrt{-g}) R + \dots \quad (4.5)$$

and the 10 d Newton's constant is related to g_s and l_s as

$$16\pi G = (2\pi)^7 (g_s)^2 (l_s)^8 \quad (4.6)$$

Dp branes are solutions to Einstein's equations. If we consider these solutions at the level of linearized weak gravity, the metric for a point-like particle in D dimensions look like

$$ds^2 \approx -(1 + 2\varphi)dt^2 + (1 - \frac{2}{D-3}\varphi)(dx_1^2 + \dots dx_{D-1}^2) \quad (4.7)$$

φ parametrizes the deviation of the metric from D dimensional Minkowski metric. In 4d, φ can be thought of as Newtonian potential and generalizing this idea in D dimensions,

$$\varphi \approx \frac{GM}{r^{D-3}} \quad (4.8)$$

(M is the mass of the particle and $r = \sqrt{(x_1^2 + \dots x_{D-1}^2)}$ is the radial distance in space). φ is a solution of Poisson's equation in D-1 dimensions and the no. of transverse directions of the object is $d_T = D - 1 \Rightarrow D - 3 = d_T - 2$. For an extended along p spatial dimensions $d_T = D - p - 1$ and $\varphi \approx \frac{GM}{r^{D-p-3}}$. Then the metric takes the form

$$ds^2 = (1 + 2\varphi)[-dt^2 + dx_1^2 + \dots + dx_p^2] + (1 - \frac{2(p+1)}{D-p-3}\varphi)[dx_{p+1}^2 + \dots dx_{D-1}^2] \quad (4.9)$$

From 10d supergravity solution, the exact metric for D3 brane takes the form

$$ds^2 = H^{-\frac{1}{2}}(-dt^2 + dx_1^2 + dx_2^2 + dx_3^2) + H^{\frac{1}{2}}(dr^2 + r^2 d\Omega_5^2) \quad (4.10)$$

where $H = 1 + \frac{L^4}{r^4}$ is the warp factor and $L^4 = 4\pi N g_s l_s^4$.

In linearized level this makes $\varphi \approx -\frac{1}{4}\frac{L^4}{r^4}$. and thus from our previous form $GM \approx L^4$. The geometry of this solution is asymptotically a 10d Minkowski spacetime with a throat of infinite size. If we take $r \ll 1$ in the throat, then $H = \frac{L^4}{r^4}$. Then the metric becomes

$$ds^2 = \frac{r^2}{L^2}(-dt^2 + dx_1^2 + dx_2^2 + dx_3^2) + \frac{L^2}{r^2}dr^2 + L^2 d\Omega_5^2 \quad (4.11)$$

Just changing the variable r as $r = \frac{L^2}{z}$ we get

$$ds^2 = \frac{L^2}{z^2}(-dt^2 + dx_1^2 + dx_2^2 + dx_3^2 + dz^2) + L^2 d\Omega_5^2 \quad (4.12)$$

which is nothing but the metric of $\text{AdS}_5 \times S^5$. In the following section, we briefly discuss the origin of the non-supersymmetric D branes we study and their decoupling limit. In this limit, again a strong-weak version of duality is expected to hold but the strongly coupled field theory, in this case, is supposed to be a non-supersymmetric deformation of CFT.

4.2 Non-supersymmetric ‘black’ D3 branes and decoupling

limit:

To derive the non-Susy Dp branes, we start from the following action

$$S = \frac{1}{16\pi G} \int d^{10}x \sqrt{-g} \left[e^{-2\phi} (R + 4\partial_\mu \phi \partial^\mu \phi) - \frac{1}{2 \cdot (8-p)!} F_{[8-p]}^2 \right], \quad (4.13)$$

where G is 10d Newton’s constant, ϕ is the dilaton, g is the determinant of the 10d string frame metric, R is the Ricci scalar and $F_{[8-p]}$ is $(8-p)$ Ramond-Ramond form field. The standard procedure afterward is to solve the equations of motion from this action by choosing an appropriate form-field and a static, spherically symmetric p brane metric ansatz. The metric ansatz should satisfy the expected isometries of the action, which is $ISO(p, 1) \times SO(9-p)$. But the difference from the supersymmetric solution is that while solving the equations of motion of the metric, one needs to relax the supersymmetry condi-

tion by introducing a nonzero term in the right-hand side of the equation of motion, which otherwise would have been zero. By introducing this explicitly and not respecting the supersymmetry condition, one can get the non-Susy Dp brane solutions. We will not write the zero temperature solutions explicitly here. But it can be found in [97]. In the following, we discuss the black non-Susy solution from which one can easily get the zero temperature result back by taking the appropriate limit of parameters.

The ‘black’ non-susy D3 brane solution of type IIB string theory has been discussed in detail in [98]. The black version is constructed by introducing anisotropy in t as well as one of the brane directions. The purpose for our discussion here is to fix the notation and convention for the computation of HEE and HSC in the next sections. The solution in the Einstein frame takes the form,

$$\begin{aligned}
ds^2 &= F_1(\rho)^{-\frac{1}{2}} G(\rho)^{-\frac{\delta_2}{8}} \left[-G(\rho)^{\frac{\delta_2}{2}} dt^2 + \sum_{i=1}^3 (dx^i)^2 \right] + F_1(\rho)^{\frac{1}{2}} G(\rho)^{\frac{1}{4}} \left[\frac{d\rho^2}{G(\rho)} + \rho^2 d\Omega_5^2 \right] \\
e^{2\phi} &= G(\rho)^{-\frac{3\delta_2}{2} + \frac{7\delta_1}{4}}, \quad F_{[5]} = \frac{1}{\sqrt{2}} (1 + *) Q \text{Vol}(\Omega_5).
\end{aligned} \tag{4.14}$$

where the functions $G(\rho)$ and $F(\rho)$ are defined as,¹

$$G(\rho) = 1 + \frac{\rho_0^4}{\rho^4}, \quad F_1(\rho) = G(\rho)^{\frac{\alpha_1}{2}} \cosh^2 \theta - G(\rho)^{-\frac{\beta_1}{2}} \sinh^2 \theta \tag{4.15}$$

Here $\delta_1, \delta_2, \alpha_1, \beta_1, \theta, \rho_0, Q$ are the parameters characterizing the solution. Now to compare this solution with that given in eq.(6) of [98], we note that we have replaced δ by δ_2 here and also, the function $F(\rho)$ there is related to $F_1(\rho)$ by the relation $F_1(\rho) = G(\rho)^{3\delta_1/8} F(\rho)$.

¹To be precise, $G(\rho)$ is the function the logarithm of which is introduced in the R.H.S of the equation of motion to relax the supersymmetry condition. Therefore had the function be simply 1, the solution of equation of motion would give us the standard D3 branes.

The parameters α and β there are related to α_1 and β_1 by the relations $\alpha_1 = \alpha + 3\delta_1/4$ and $\beta_1 = \beta - 3\delta_1/4$. We point out that the parameters are not all independent but they satisfy the following relations

$$\begin{aligned}\alpha_1 - \beta_1 &= \alpha - \beta + 3\delta_1/2 = 0 \\ \alpha_1 + \beta_1 &= \alpha + \beta = \sqrt{10 - \frac{21}{2}\delta_2^2 - \frac{49}{2}\delta_1^2 + 21\delta_2\delta_1} \\ Q &= (\alpha_1 + \beta_1)\rho_0^4 \sinh 2\theta\end{aligned}\tag{4.16}$$

Note that the solution has a curvature singularity at $\rho = 0$ and also the metric does not have the full Poincare symmetry $ISO(1, 3)$ in the brane world-volume directions, rather, it is broken to $R \times ISO(3)$ and this is the reason we call it ‘black’ non-Susy D3 brane solution. However, we put black in an inverted comma because this solution does not have a regular horizon as in ordinary black brane but, has a singular horizon. The standard zero temperature non-Susy D3 brane solution given in eq. (1) of [97] can be recovered from (4.14) by simply putting $\delta_2 = 0$ and identifying $7\delta_1/4$ as δ there. We remark that despite the solution (4.14) has a singular horizon we can still define a temperature as argued in [99] and by comparing the expression for the temperature there we can obtain the temperature of the ‘black’ non-Susy D3 brane as,

$$T_{\text{nonSusy}} = \left(\frac{-2\delta_2}{(\alpha_1 + \beta_1)^2} \right)^{\frac{1}{4}} \frac{1}{\pi\rho_0 \cosh \theta}\tag{4.17}$$

From the above expression, it is clear that for the reality of the temperature the parameter δ_2 must be less or equal to zero. It is straightforward to check that when $\delta_2 = -2$ and $\delta_1 = -12/7$ (which implies $\alpha_1 = \beta_1 = 1$ and $\alpha_1 + \beta_1 = 2$), the above solution (4.14) reduces precisely to the ordinary black D3 brane solution and the temperature (4.17) also

reduces to the Hawking temperature of the ordinary black D3 brane.

From now on we will put $\alpha_1 + \beta_1 = 2$ for simplicity. Therefore, from the first relation in (4.16), we have $\alpha_1 = 1$ and $\beta_1 = 1$. In this case, the parameters δ_1 and δ_2 will be related (see the second equation in (4.16)) by

$$42\delta_2^2 + 49\delta_1^2 - 84\delta_1\delta_2 = 24 \quad (4.18)$$

The function $F_1(\rho)$ given in (4.15) then reduces to

$$F_1(\rho) = G(\rho)^{-\frac{1}{2}}H(\rho), \quad \text{where,} \quad H(\rho) = 1 + \frac{\rho_0^4 \cosh^2 \theta}{\rho^4} \equiv 1 + \frac{R_1^4}{\rho^4} \quad (4.19)$$

Therefore the Einstein frame metric in (4.14) reduces to

$$ds^2 = H(\rho)^{-\frac{1}{2}}G(\rho)^{\frac{1}{4}-\frac{\delta_2}{8}} \left[-G(\rho)^{\frac{\delta_2}{2}} dt^2 + \sum_{i=1}^3 (dx^i)^2 \right] + H(\rho)^{\frac{1}{2}} \left[\frac{d\rho^2}{G(\rho)} + \rho^2 d\Omega_5^2 \right] \quad (4.20)$$

where $H(\rho)$ is given in (4.19). The decoupled geometry can be obtained by zooming into the region

$$\rho \sim \rho_0 \ll \rho_0 \cosh^{\frac{1}{2}} \theta \quad (4.21)$$

Note that in this limit $\theta \rightarrow \infty$ and the function $H(\rho)$ can be approximated as $H(\rho) \approx R_1^4/\rho^4$, but $G(\rho)$ remains unchanged. The metric (4.20) then reduces to,

$$ds^2 = \frac{\rho^2}{R_1^2} G(\rho)^{\frac{1}{4}-\frac{\delta_2}{8}} \left[-G(\rho)^{\frac{\delta_2}{2}} dt^2 + \sum_{i=1}^3 (dx^i)^2 \right] + \frac{R_1^2}{\rho^2} \frac{d\rho^2}{G(\rho)} + R_1^2 d\Omega_5^2 \quad (4.22)$$

where $R_1 = \rho_0 \cosh^{\frac{1}{2}} \theta$ is the radius of the transverse 5-sphere which decouples from the five dimensional asymptotically AdS₅ geometry. As the 5-sphere decouples, we will work

with the rest of the five dimensional geometry to compute the HEE in the next section.

This geometry is the gravity dual of a non-supersymmetric, non-conformal QFT in (3+1) dimensions at a finite temperature which is also confining and has a running coupling constant very much like QCD. As we saw the geometry is asymptotically AdS₅ which means that it can be thought of as some non-supersymmetric and non-conformal deformation of the CFT which is $\mathcal{N} = 4$, $D = 4$ SU(N) super Yang-Mills theory at large N . We compute the EE, complexity, and Fisher information metric holographically in this background. The goal of this study would be to gain a better understanding of the various phases of QCD-like theories and the transitions among them since it is believed that the EE and the complexity are possibly related to some universal properties like order parameter or some renormalization group flow [26]. However, this will be clearer once we have a better picture of the holographic complexity in the (strongly coupled) interacting field theories. In thermodynamics, the entropy of a system can be increased by injecting energy into the system, where the proportionality constant is given by the inverse of temperature. This leads to an energy conservation relation $\Delta E = T\Delta S$, the first law of thermodynamics. An analogous problem was addressed in [81] for the EE, i.e., to see how the EE of a certain region grows with the increase in energy. Here the EE is computed using AdS/CFT. The excited state of a CFT is given by the deformation of AdS whose EE can be computed using the RT proposal. This is then compared with the time component of the boundary stress tensor T_{tt} or the energy density. For a small subsystem A , the total energy is found to be proportional to the increase in EE and the proportionality constant is c/ℓ , where c is a universal constant and ℓ is the size of the subsystem. This has been identified with the entanglement temperature in analogy with the first law of thermodynamics [81] and we discussed this in chapter 3 as well. However, in [8], it has been noted that this is not the complete story. Since the first law contains more terms here also ΔE can have a term analogous to $P\Delta V$

term. Indeed, by calculating the other components of the boundary stress tensor it has been found that ΔE contains a term $d/(d+2)V_d\Delta P_x$ for asymptotically AdS_{d+2} space, where ΔP_x is the pressure normal to the entangling surface and V_d is the volume. Therefore the analogous entanglement thermodynamical relation takes the form [8],

$$\Delta E = T_E\Delta S_E + \frac{d}{d+2}V_d\Delta P_x \quad (4.23)$$

However, in the study of 3 based on [5], we already absorbed this $V\Delta P$ term in the $T\Delta S$ term. In this chapter we consider the non-Susy D3 brane or, to be precise, a finite temperature version of that solution in type IIB string theory [98]. We use this gravity dual to compute the EE of the associated QFT from the Ryu-Takayanagi prescription. Since the non-Susy D3 brane in the decoupling limit has an asymptotically AdS_5 geometry, the HEE can be written as a pure AdS_5 part and the additional part which can be thought of as the EE associated with an excited state. We use Fefferman-Graham coordinates to compute the HEE and this helps us to identify the boundary stress tensor quite easily [100, 101]. Having identified the boundary stress tensor we then check that the additional EE of the excited state indeed satisfies the first law like thermodynamical relation we just mentioned in (4.23) for a small subsystem. We have identified the entanglement temperature in this case which is inversely related to the size of the entangling region by a universal constant and also an entanglement pressure normal to the entangling surface. We also checked that at higher temperatures the HEE makes a cross-over to the thermal entropy of standard black D3 brane.

The rest of the chapter is organized as follows. Firstly, we discuss the EE computations, entanglement thermodynamics of the non-Susy black brane, and its crossover with the thermal entropy of standard black brane in high-temperature limit in section 4.3. These

calculations are done for a strip sub-region choice since it gives us an easier way to choose the high-temperature limit whereas, for the spherical sub-region, the perturbative treatment doesn't work well for the high-temperature limit and one necessarily has to use numerics, which is too hard to practically perform in that case. Then for the latter part of the chapter, we study the HEE, HSC, and Fisher information for the non-Susy case with the spherical entangling region in section 4.4.

4.3 Entanglement and Thermal Entropy cross over with Strip Sub-region:

4.3.1 Holographic entanglement entropy in FG coordinates:

In this subsection we first rewrite our asymptotically AdS₅ metric (leaving out the 5-sphere part) given by

$$ds^2 = \frac{\rho^2}{R_1^2} G(\rho)^{\frac{1}{4} - \frac{\delta_2}{8}} \left[-G(\rho)^{\frac{\delta_2}{2}} dt^2 + \sum_{i=1}^3 (dx^i)^2 \right] + \frac{R_1^2}{\rho^2} \frac{d\rho^2}{G(\rho)} \quad (4.24)$$

in the Fefferman-Graham form and then compute the HEE from this geometry. Note that as $\rho \rightarrow \infty$, $G(\rho) \rightarrow 1$ and the metric reduces to AdS₅ form. The $(d + 2)$ -dimensional asymptotically AdS space can be written in Fefferman-Graham coordinates as,

$$ds_{d+2}^2 = \frac{R_1^2}{r^2} dr^2 + \frac{r^2}{R_1^2} g_{\mu\nu}(x, r) dx^\mu dx^\nu \quad (4.25)$$

where $g_{\mu\nu} = \eta_{\mu\nu} + h_{\mu\nu}(x, r)$ with

$$h_{\mu\nu}(x, r) = h_{\mu\nu}^{(0)}(x) + \frac{1}{r^2} h_{\mu\nu}^{(2)}(x) + \dots + \frac{1}{r^{d+1}} h_{\mu\nu}^{(d+1)}(x) + \dots \quad (4.26)$$

and for $d = \text{odd}$, the $(d + 3)/2$ -th term can contain an additional $\log r$ piece, however, for our solution (4.24) this does not appear. Now in order to express (4.24) in the form of (4.25), we must change the radial coordinate ρ to r . By inspecting (4.24) and (4.25) (for $d = 3$), we get the relation,

$$\rho^2 + \sqrt{\rho^4 + \rho_0^4} = r^2 \quad (4.27)$$

and inverting this relation we get,

$$\rho^2 = \frac{r^2}{2} - \frac{\rho_0^4}{2r^2} \quad (4.28)$$

By scaling $r \rightarrow \sqrt{2}r$, the above relation reduces to

$$\rho^2 = r^2 \left(1 - \frac{\rho_0^4}{4r^4} \right) \quad (4.29)$$

Using (4.29) the metric (4.24) takes the form,

$$ds^2 = \frac{r^2}{R_1^2} \left[- \left(1 + \frac{3\delta_2 \rho_0^4}{8 r^4} \right) dt^2 + \left(1 - \frac{\delta_2 \rho_0^4}{8 r^4} \right) \sum_{i=1}^3 (dx^i)^2 \right] + \frac{R_1^2}{r^2} dr^2 \quad (4.30)$$

Since here we are considering only weakly excited states, our geometry will be near the boundary and that is the reason as a first order approximation we have replaced $(1 - \rho_0^4/r^4)^a$ by $(1 - a\rho_0^4/r^4)$ for any real number a in writing the metric (4.30). This choice is also needed so that we can apply Ryu-Takayanagi prescription for the calculation of EE [3]. To compute HEE, we choose another coordinate z by the relation $z = R_1^2/r$ and rewrite the metric in the following form,

$$ds^2 = \frac{R_1^2}{z^2} \left[- \left(1 + \frac{3\delta_2 z^4}{8 z_0^4} \right) dt^2 + \left(1 - \frac{\delta_2 z^4}{8 z_0^4} \right) \sum_{i=1}^3 (dx^i)^2 + dz^2 \right] \quad (4.31)$$

where $z_0^4 = R_1^8/\rho_0^4$. This is the form of the metric in Fefferman-Graham coordinates.

Now to compute the holographic entanglement entropy, we have to first calculate the minimal area of the surface embedded in the time slice of the background (4.31) bounded by the edge of A , i.e., ∂A which is a strip given by $-\ell/2 \leq x_1 \leq \ell/2$ and $0 \leq x_{2,3} \leq L$. We parameterize the surface γ_A by $x_1 = x_1(z)$, then the area of the embedded surface would be given as,

$$\text{Area}(\gamma_A) = \int dx_1 dx_2 dx_3 \sqrt{g} \quad (4.32)$$

where g is the determinant of the metric induced on γ_A . For the strip and for the parameterization mentioned above, the area reduces to

$$\text{Area}(\gamma_A) = R_1^3 \int dx_2 dx_3 dz \frac{\sqrt{\left[1 + \left(1 - \frac{\delta_2 z^4}{8 z_0^4}\right) x_1'^2\right] \left(1 - \frac{\delta_2 z^4}{4 z_0^4}\right)}}{z^3} \quad (4.33)$$

Here ‘prime’ denotes the derivative with respect to z . Now since x_1 is a cyclic coordinate in the above integral (4.33), we get a constant of motion as follows,

$$\left(\frac{R_1}{z}\right)^3 \frac{\left(1 - \frac{\delta_2 z^4}{4 z_0^4}\right) x_1'}{\sqrt{\left[1 + \left(1 - \frac{\delta_2 z^4}{8 z_0^4}\right) x_1'^2\right]}} = k = \text{constant} \quad (4.34)$$

Solving this we get x_1' to be

$$x_1' = \frac{k}{\sqrt{\left(1 - \frac{\delta_2 z^4}{8 z_0^4}\right) \left[\left(1 - \frac{3\delta_2 z^4}{8 z_0^4}\right) \left(\frac{R_1}{z}\right)^6 - k^2\right]}} \quad (4.35)$$

Actually here we are considering the hanging string configuration given by (4.35) in which the two end points of the string is at the boundary $z = 0$ and has a turning point at z_* where

dz/dx vanishes. This determines the constant of motion k in terms of z_* as,

$$k^2 = \left(1 - \frac{3\delta_2 z_*^4}{8 z_0^4}\right) \left(\frac{R_1}{z_*}\right)^6 \quad (4.36)$$

Substituting this value of k in (4.35) and integrating we find the size of the entangling region in terms of z_* as,

$$\ell = 2 \int_0^{z_*} dz \frac{\left(1 - \frac{3\delta_2 z_*^4}{16 z_0^4}\right)}{\sqrt{\left(1 - \frac{\delta_2 z_*^4}{8 z_0^4}\right) \left[\frac{z_*^6}{z^6} - 1 - \frac{3\delta_2 z_*^4}{8 z_0^4} \left(\frac{z_*^2}{z^2} - 1\right)\right]}} \quad (4.37)$$

We will assume that the subsystem is very small such that $\ell \ll z_0$ which amounts to the condition that γ_A is close to the asymptotically AdS₅ boundary. We note from the above that when the parameter δ_2 related to the temperature of the non-susy D3 brane (see eq.(4.17)) is put to zero, the metric in (4.31) reduces to that of AdS₅ and the constant of motion (4.36), i.e., the turning point z_* as well as the size of the entangling region in terms of z_* (4.37), take the same forms as those of AdS₅ case. Therefore, $\delta_2 \neq 0$ solutions are the deformations of AdS₅ and represent excited states in the boundary theory. The above relation (4.37) can be simplified (as $z, z_* \ll z_0$) as,

$$\begin{aligned} \ell &= 2 \int_0^{z_*} dz \frac{z^3/z_*^3}{\sqrt{1 - \frac{z^6}{z_*^6}}} \left[1 - \frac{3\delta_2 z_*^4}{16 z_0^4} + \frac{\delta_2 z^4}{16 z_0^4} + \frac{3\delta_2 z^4}{16 z_0^4} \frac{1}{\left(1 + \frac{z^2}{z_*^2} + \frac{z^4}{z_*^4}\right)} + \dots \right] \\ &= \frac{2\sqrt{\pi}\Gamma\left(\frac{2}{3}\right)}{\Gamma\left(\frac{1}{6}\right)} z_{*(AdS_5)} + \delta z_* \end{aligned} \quad (4.38)$$

where $z_{*(AdS_5)}$ is the turning point for AdS₅ and δz_* is the deviation from that value. It has been shown earlier that there is no change of EE upto the first order due to this change of the turning point from AdS₅. So, in evaluating EE we will use the turning point corresponding

to AdS₅ only and omit the subscript ‘AdS₅’ for brevity. To compute EE, we use the value of k from (4.36) in (4.35) and substitute it in (4.33) to first obtain the minimized area as,

$$\text{Area}(\gamma_A^{\min}) = 2 \int_0^L dx_2 \int_0^L dx_3 \int_\epsilon^{z_*} dz \left(\frac{R_1}{z} \right)^6 \sqrt{\frac{\left(1 - \frac{5\delta_2 z^4}{8 z_0^4}\right)}{\left(1 - \frac{3\delta_2 z^4}{8 z_0^4}\right) \left(\frac{R_1}{z}\right)^6 - \left(1 - \frac{3\delta_2 z_*^4}{8 z_0^4}\right) \left(\frac{R_1}{z_*}\right)^6}} \quad (4.39)$$

where ϵ is an IR cut-off and then use equation (2.21) to obtain the EE upto first order in z^4/z_0^4 as,

$$S_E = S_{E(0)} + \frac{R_1^3 L^2}{4G_{(5)}} \int_0^{z_*} dz \left[\frac{\frac{(-3\delta_2)z^4}{8z_0^4}}{z^3 \sqrt{1 - \frac{z^6}{z_*^6}}} + \frac{\frac{\delta_2 z^4}{8z_0^4} \sqrt{1 - \frac{z^6}{z_*^6}}}{z^3} \right] \quad (4.40)$$

In the above

$$S_{E(0)} = \frac{2R_1^3 L^2}{4G_{(5)}} \int_\epsilon^{z_*} \frac{dz}{z^3 \sqrt{1 - \left(\frac{z}{z_*}\right)^6}} \quad (4.41)$$

is the EE of the pure AdS₅ background. Note that $S_{E(0)}$ is divergent and that is the reason we put an IR cutoff at ϵ to make it finite, but the additional term in (4.40) is divergence free and we can evaluate the integrals to get the change in EE as,

$$\begin{aligned} \Delta S_E &= \frac{R_1^3 L^2}{4G_{(5)}} z_*^2 \left[\frac{(-3\delta_2) \sqrt{\pi} \Gamma\left(\frac{1}{3}\right)}{48 z_0^4 \Gamma\left(\frac{5}{6}\right)} + \frac{\delta_2 \sqrt{\pi} \Gamma\left(\frac{1}{3}\right)}{80 z_0^4 \Gamma\left(\frac{5}{6}\right)} \right] \\ &= \frac{R_1^3 L^2}{4G_{(5)}} z_*^2 \frac{(-\delta_2) \sqrt{\pi} \Gamma\left(\frac{1}{3}\right)}{20 z_0^4 \Gamma\left(\frac{5}{6}\right)} \end{aligned} \quad (4.42)$$

Here z_* is the value of the turning point for pure AdS₅ background given by

$$z_* = \frac{\ell \Gamma\left(\frac{1}{6}\right)}{2\sqrt{\pi} \Gamma\left(\frac{2}{3}\right)} \quad (4.43)$$

Using this in (4.42) we get,

$$\Delta S_E = \frac{(-\delta_2) R_1^3 L^2 \ell^2 \Gamma^2\left(\frac{1}{6}\right) \Gamma\left(\frac{1}{3}\right)}{320 \sqrt{\pi} G_{(5)} z_0^4 \Gamma^2\left(\frac{2}{3}\right) \Gamma\left(\frac{5}{6}\right)} \quad (4.44)$$

This is the change in the EE of the decoupled theory associated with the ‘black’ non-Susy D3 brane from the pure AdS₅ solution. We remark that as $\delta_2 = 0$ implies from (4.17) that the temperature of the non-Susy D3-brane vanishes, ΔS_E given in (4.44) also vanishes. This means that the zero-temperature non-Susy D3 brane also has vanishing ΔS_E , similar to the case of ordinary black D3 brane, where it vanishes when the temperature goes to zero.

As we have already mentioned in section 2, the non-susy D3 brane solution can be reduced to standard black D3 brane solution when the parameters take the values $\delta_2 = -2$ and $\delta_1 = -12/7$. Simply taking this limit in (4.44), we find that the change in EE takes the form,

$$\Delta S_E = \frac{R_1^3 L^2 \ell^2 \Gamma^2\left(\frac{1}{6}\right) \Gamma\left(\frac{1}{3}\right)}{160 \sqrt{\pi} G_{(5)} z_0^4 \Gamma^2\left(\frac{2}{3}\right) \Gamma\left(\frac{5}{6}\right)} \quad (4.45)$$

This result can be compared with that given in [81] and we find that they indeed match once we identify $1/z_0^4 = m$ and $d = 4$.

4.3.2 Entanglement thermodynamics:

As we mentioned in the previous subsection, the asymptotically AdS space in $(d + 2)$ dimensions can be expressed in Fefferman-Graham coordinates and it is given in (4.25). In this coordinate one can extract the form of boundary stress tensor as follows [100, 101],

$$\langle T_{\mu\nu}^{(d+1)} \rangle = \frac{(d+1) R_1^d}{16\pi G_{(d+2)}} h_{\mu\nu}^{(d+1)} \quad (4.46)$$

The decoupled ‘black’ non-Susy D3 brane geometry (leaving out the S^5 part) in Fefferman-Graham coordinate is given in (4.31). So, using this general formula (4.46) for (4.31), we can write down the form of the stress tensor for the boundary theory of ‘black’ non-susy D3 brane as,

$$\langle T_{tt} \rangle = \frac{-3R_1^3 \delta_2}{32\pi G_{(5)}}, \quad \langle T_{x_i x_j} \rangle = \frac{-R_1^3 \delta_2}{32\pi G_{(5)}} \delta_{ij}, \quad \text{where } i, j = 1, 2, 3. \quad (4.47)$$

As we mentioned before, since the parameter $\delta_2 \leq 0$, both temporal as well as spatial components of the stress tensor are positive semi-definite. Also since here we are considering AdS_5 , we have put $d = 3$ in (4.46). Now using these values (4.47) we can rewrite the change in EE given by the first expression in (4.42) as,

$$\Delta S_E = \frac{L^2 z_*^2 \pi^{\frac{3}{2}} \Gamma\left(\frac{1}{3}\right)}{6 \Gamma\left(\frac{5}{6}\right)} \left[\langle T_{tt} \rangle - \frac{3}{5} \langle T_{x_1 x_1} \rangle \right] \quad (4.48)$$

Putting the value of z_* from (4.43) we get,

$$\Delta S_E = \frac{L^2 \ell^2 \sqrt{\pi} \Gamma^2\left(\frac{1}{6}\right) \Gamma\left(\frac{1}{3}\right)}{24 \Gamma^2\left(\frac{2}{3}\right) \Gamma\left(\frac{5}{6}\right)} \left[\langle T_{tt} \rangle - \frac{3}{5} \langle T_{x_1 x_1} \rangle \right] \quad (4.49)$$

In terms of the stress tensors the change in total energy and the pressure are defined as,

$$\Delta E = L^2 \ell \langle T_{tt} \rangle, \quad \Delta P_{x_1 x_1} = \langle T_{x_1 x_1} \rangle \quad (4.50)$$

Using this in (4.49) we get the change in EE as,

$$\Delta S_E = \ell \frac{\sqrt{\pi} \Gamma^2\left(\frac{1}{6}\right) \Gamma\left(\frac{1}{3}\right)}{24 \Gamma^2\left(\frac{2}{3}\right) \Gamma\left(\frac{5}{6}\right)} \left[\Delta E - \frac{3}{5} \Delta P_{x_1 x_1} V_3 \right] \quad (4.51)$$

where $V_3 = L^2\ell$ is the volume of the subspace. Comparing this with the first law of thermodynamics we identify the entanglement temperature to be

$$T_E = \frac{24\Gamma\left(\frac{5}{6}\right)\Gamma^2\left(\frac{2}{3}\right)}{\ell\sqrt{\pi}\Gamma\left(\frac{1}{3}\right)\Gamma^2\left(\frac{1}{6}\right)} \quad (4.52)$$

We note that the entanglement temperature is inversely proportional to the size ℓ of the entangling region with a universal proportionality constant [81]. Thus from here, we conclude that the decoupled theory of ‘black’ non-susy D3 brane satisfies the first law of entanglement thermodynamics

$$\Delta E = T_E\Delta S_E + \frac{3}{5}\Delta P_{x_1x_1}V_3 \quad (4.53)$$

This is indeed the relation we mentioned in (4.23) for $d = 3$ [8].

4.3.3 Cross-over to thermal entropy:

In this subsection we will show how the total HEE of the decoupled theory of ‘black’ non-susy D3 brane we calculated in (4.40) reduces to thermal entropy of that of standard black D3 brane. For this purpose we first look at the expression for the size of the entangling region in (4.37). By defining z/z_* as x , the integral can be written as,

$$\begin{aligned} \frac{\ell}{2} &= z_* \int_0^1 dx \frac{x^3 \left(1 - \frac{3\delta_2 z_*^4}{16 z_0^4}\right)}{\sqrt{\left(1 - \frac{\delta_2 z_*^4}{8 z_0^4} x^4\right) \left[1 - x^6 - \frac{3\delta_2 z_*^4}{8 z_0^4} x^4 (1 - x^2)\right]}} \\ &= z_* \mathcal{I} \left(\frac{z_*}{z_0}\right) \end{aligned} \quad (4.54)$$

On the other hand the total area integral given in (4.39) can be written as,

$$\begin{aligned}
\text{Area}(\gamma_A^{\min}) &= \frac{2R_1^3 L^2}{z_*^2} \int_0^1 dx \frac{1}{x^3} \sqrt{\frac{\left(1 - \frac{5\delta_2}{8} \frac{z_*^4}{z_0^4} x^4\right)}{\left(1 - \frac{3\delta_2}{8} \frac{z_*^4}{z_0^4} x^4\right) - \left(1 - \frac{3\delta_2}{8} \frac{z_*^4}{z_0^4}\right) x^6}} \\
&= \frac{2R_1^3 L^2}{z_*^2} \tilde{\mathcal{I}}\left(\frac{z_*}{z_0}\right)
\end{aligned} \tag{4.55}$$

In the high temperature limit $z_* \rightarrow z_0$ and both the integrals \mathcal{I} and $\tilde{\mathcal{I}}$ are dominated by the pole at $x = 1$ and therefore have the same values, i.e., in this limit

$$\mathcal{I}\left(\frac{z_*}{z_0}\right) \approx \tilde{\mathcal{I}}\left(\frac{z_*}{z_0}\right) \tag{4.56}$$

From the second expression of (4.54) we, therefore, have

$$\mathcal{I}\left(\frac{z_*}{z_0}\right) = \frac{\ell}{2z_*} \approx \tilde{\mathcal{I}}\left(\frac{z_*}{z_0}\right) \tag{4.57}$$

Using this in the second expression of (4.55) and then dividing by $4G_{(5)}$, we get the EE at high temperature as,

$$S_E = \frac{\text{Area}(\gamma_A^{\min})}{4G_{(5)}} = \frac{R_1^3 L^2 \ell}{4G_{(5)} z_*^3} = \frac{\pi^3 R_1^3 V_3}{4G_{(5)} (\pi z_0)^3} \tag{4.58}$$

Now using the five dimensional Newton's constant $G_{(5)} = (\pi R_1^3)/(2N^2)$, where N is the number of branes and $1/(\pi z_0) = T$, where T , is the temperature of the standard black D3 brane, we get from (4.58)

$$\frac{S_E}{V_3} = \frac{\pi^2}{2} N^2 T^3 \tag{4.59}$$

the thermal entropy of a standard black D3 brane. This clearly shows that at high temperature the entanglement entropy of a non-susy D3 brane makes a cross-over [102] to the thermal entropy of a black D3 brane.

4.4 EE and complexity for (decoupled) ‘black’ non-susy D3 brane in case of spherical subsystem:

The decoupled geometry of ‘black’ non-susy D3 brane is given in eq.(4.22). To compare our results with those of the previous section we will not directly use this geometry, but instead try to recast the solution in a form very similar to the AdS₅ black hole geometry. For this purpose we first make a coordinate transformation $\tilde{\rho}^4 = \rho^4 + \rho_0^4$. Then we make another coordinate transformation by taking $\tilde{\rho} = \frac{R_1^2}{z}$. With these transformations the decoupled geometry of non-susy ‘black’ D3 brane (4.22) takes the form

$$ds^2 = \frac{R_1^2}{z^2} \left[-(1 - mz^4)^{\frac{1}{4} - \frac{3\delta_2}{8}} dt^2 + (1 - mz^4)^{\frac{1}{4} + \frac{\delta_2}{8}} \sum_{i=1}^3 (dx_i)^2 + \frac{dz^2}{(1 - mz^4)} \right] \quad (4.60)$$

where $m = \frac{1}{z_0^4}$ and $z_0 = \frac{R_1^2}{\rho_0}$. To compute the entanglement entropy, the complexity and the associated Fisher information metric for the decoupled geometry of ‘black’ non-Susy D3 brane we will use the metric given in (4.60) with the choice of a spherical subsystem. We remark that as the Ryu-Takayanagi area or the volume formula uses the Einstein-frame metric, we also use the Einstein frame metric for the decoupled ‘black’ non-Susy D3 brane geometry. This, in turn, takes into account that we have a non-trivial dilaton in the background. The area integral, after taking the embedding $r = r(z)$, in this case takes the form,

$$A_{nsD3} = 4\pi R_1^3 \int dz \frac{r(z)^2 (1 - mz^4)^{\frac{\delta_2}{8} - \frac{1}{4}}}{z^3} \left[1 + (1 - mz^4)^{\frac{5}{4} + \frac{\delta_2}{8}} r'(z)^2 \right]^{\frac{1}{2}} \quad (4.61)$$

Again, as before, we are assuming the small subsystem and consider up to the second-order change in the metric. To minimize this area, we use the Euler-Lagrange equation of motion once we consider the area as an action integral. The equation of motion is a bit long and so we do not write it explicitly here. We just give its solution. As mentioned earlier, we know that by taking $m = 0$, we can get back the pure AdS₅ case. Thus we take our solution as a perturbation over pure AdS₅ and work with the ansatz

$$r(z) = \sqrt{L^2 - z^2} + mr_1(z) + m^2r_2(z). \quad (4.62)$$

Now solving the equation of motion with this ansatz, and with proper boundary conditions and regularity conditions, we get $r_1(z)$ and $r_2(z)$ to be of the form

$$\begin{aligned} r_1(z) &= \frac{1}{80}\sqrt{L^2 - z^2} [(10 - 3\delta_2)L^4 + (10 - 3\delta_2)L^2z^2 + (\delta_2 + 10)z^4], \\ r_2(z) &= \frac{1}{806400}\sqrt{L^2 - z^2} [(\delta_2(5207\delta_2 - 18900) + 30460)L^8 \\ &\quad + 80(\delta_2(58\delta_2 - 189) + 302)L^6z^2 + 3(\delta_2(683\delta_2 - 2100) + 7660)L^4z^4 \\ &\quad + 8(\delta_2(263\delta_2 - 1260) + 4300)L^2z^6 + 175(\delta_2 + 10)(\delta_2 + 26)z^8] \end{aligned} \quad (4.63)$$

We can now use this form of $r(z)$ to get the relation between ℓ and L , but, what we need is the inverse of that. This comes out as,

$$L = \ell + \frac{1}{80}m\ell^5(3\delta_2 - 10) + m^2\ell^9 \frac{(463\delta_2^2 - 18900\delta_2 + 32540)}{806400} \quad (4.64)$$

Using the form of $r(z)$ along with (4.63) in the area integral (4.61) and then expanding the integral in the second order in m in the way we mentioned before, we perform the integrals up to order m^2 .

After performing the integral (as done before) and replacing L by (4.64), we get the first and second order change of EE with respect to m as,

$$\Delta S_{EE(nsD3)}^{(1)} = -\frac{\pi\delta_2 R_1^3}{20G_5} m\ell^4 \quad (4.65)$$

$$\Delta S_{EE(nsD3)}^{(2)} = \frac{(\delta_2^2 - 10)\pi R_1^3}{3150G_5} m^2\ell^8 \quad (4.66)$$

Note that both of these matches precisely with the change in EE we obtained for AdS₅ black hole once we put $\delta_2 = -2$ and provides a consistency check of our result (4.65) and (4.66).

Now to compute the complexity we have to find the RT volume from the geometry given in (4.60). The volume integral has the form,

$$V_{nsD3} = \frac{4\pi R_1^4}{3} \int_{\epsilon}^L \frac{dz}{z^4} r(z)^3 \left(1 - \frac{\delta_2}{8} m z^4\right)^{\left(\frac{\delta_2}{16} - \frac{1}{8}\right)} \quad (4.67)$$

Putting the functional form of $r(z)$ and expanding up to second order in m , we get the integrals upto second order.

Evaluating these integrals and taking $\epsilon \rightarrow 0$ limit, we find that the change of complexity upto first order in m is zero similar to the case of AdS₅ black hole. On the other hand, the change of complexity in the second order in m is

$$\Delta C_{V(nsD3)}^{(2)} = \left(\frac{4\pi R_1^3}{24\pi G_5}\right) \left[\frac{\pi(60 - 9\delta_2^2)}{10240}\right] (m\ell^4)^2 = \frac{\Delta V_{(nsD3)}^{(2)}}{8\pi R_1 G_5} \quad (4.68)$$

This can be seen to match with the change in AdS₅ black hole complexity once we take $\delta_2 = -2$. Now using the $\langle T_{tt} \rangle$ calculated in the previous section (4.47), the change in

energy for the non-susy geometry can be obtained as

$$\langle T_{tt} \rangle = \frac{-3R_1^3 \delta_2}{32\pi G_5}, \quad \Delta E = \frac{4\pi \ell^3}{3} \langle T_{tt} \rangle = -\frac{\delta_2 R_1^3 m \ell^3}{8G_5}. \quad (4.69)$$

Thus we see that again we can write the change in EE in the form $\Delta S_{EE(nsD3)}^{(1)} = \frac{\Delta E}{T_{ent(nsD3)}}$, where $T_{ent(nsD3)} = \frac{5}{2\pi\ell}$. Note that the entanglement temperature remains the same as for the AdS₅ black hole. Similarly, we can express the change in complexity (4.68) as,

$$\Delta C_{V(nsD3)}^{(2)} = \frac{5(60 - 9\delta_2^2) G_5}{256\pi \delta_2^2 R_1^3} \left(\frac{\Delta E}{T_{ent(nsD3)}} \right)^2 \quad (4.70)$$

We also compute the fidelity and Fisher information metric for the non-Susy geometry. Comparing this with the general expression of a change of volume (3.90), we identify the d -dependent constant C_4 and fidelity in this case as

$$C_4 = \frac{\pi(60 - 9\delta_2^2)}{10240}, \quad \mathcal{F}_{nsD3} = \frac{\pi}{525G_5} R_1^3 m^2 \ell^8 \quad (4.71)$$

The corresponding Fisher information metric has the form

$$\mathcal{G}_{\mathcal{F}_{nsD3}, \lambda} = \partial_\lambda^2 \mathcal{F}_{nsD3} = \frac{2\pi}{525G_5} R_1^3 \quad (4.72)$$

Interestingly, here we observe that both the fidelity and the Fisher information metric do not depend on the non-Susy parameter δ_2 and by comparison we see that they have the same value as those of the AdS₅ black hole. But this is due to the choice of the d -dependent constant C_d in the denominator of the fidelity used in [87]. Next, we consider the direct way of calculating the Fisher information metric as discussed in the previous chapter by taking the second-order change of the relative entropy. Using the definition given in (3.88)

and also the relation for $\Delta V_{(nsD3)}^{(2)}$ in (4.68) we get,

$$\begin{aligned}
G_{\mathcal{F}_{nsD3},\lambda} &= -\frac{2}{\lambda^2} \Delta S_{EE(nsD3)}^{(2)} \\
&= \frac{512(10 - \delta_2^2)}{105\pi(60 - 9\delta_2^2)\pi R_1 \lambda^2 G_5} \Delta V_{(nsD3)}^{(2)} \\
&= \frac{(10 - \delta_2^2)\pi R_1^3}{1575G_5}.
\end{aligned} \tag{4.73}$$

Here we find that the Fisher information metric indeed depends on the non-supersymmetric parameter δ_2 which at $\delta_2 = -2$ gives back the AdS black hole result $G_{\mathcal{F}_{BH},\lambda}$.

It is, therefore, clear that the definition of fidelity, used in [87] which contains the d -dependent constant C_d needed to get the correct AdS black hole result for Fisher information metric, does not produce the correct result for the non-supersymmetric background. This calculation gives the Fisher information metric which is independent of the non-supersymmetric parameter δ_2 and has precisely the same value as that of the AdS₅ black hole. However, a direct way of calculating the Fisher information metric given in [74], yields a different result and in this case, it depends on the non-supersymmetric parameter δ_2 as expected and for $\delta_2 = -2$, it gives the correct AdS₅ black hole result. We observe from (4.73) that the decoupled ‘black’ non-Susy D3 brane geometry stores more quantum Fisher information than its AdS₅ black hole counterpart. For $\delta_2 = 0$ which corresponds to the zero temperature non-Susy solution, in fact, stores the most quantum Fisher information, whereas for $\delta_2 = -2$, which corresponds to the AdS₅ black hole stores the least.

PAGE CURVE AND COMPLEXITY OF
ISLANDS IN MULTIBOUNDARY
WORMHOLE MODELS OF BLACK HOLE
EVAPORATION

This chapter is based on the two papers [9] and [10].

Since the advent of the RT formula, it has gone through many changes. Corrections of the RT formula (equation (2.21)) due to quantum effects of bulk fields were first discussed in [21] and later explored in [22, 103] which introduced the idea of a QES. Of late, the quantum extremal surface program has been very successfully utilized to reproduce the Page curve for an evaporating black hole [104] from semi-classical constructions [105–109]. The difficulty in this program was that a systematic description of fine-grained (entanglement) entropy was missing which can be applied both to the black hole and the radiation.

Hence, the understanding of the Page curve remained incomplete and kept running into elusive contradictions. Using the QES, the authors of [105–109] were able to show that indeed one can systematically start from a pure state black hole for which, in the process of evaporation, a natural definition for consistent fine-grained entropy arises. The curve displayed by this fine-grained entropy is the ever-expected Page curve, fully devoid of any contradictions involving fine-grained-to-coarse-grained shift during the process. In describing such a process successfully, it was found that a bulk region is added to the QES after the Page time and aids in the appearance of the Page curve. These bulk regions are typically known as *islands*. It is also noteworthy that the Page curves are different for the evaporating and the eternal black holes and so are the islands. For the evaporating situation, the degrees of freedom of the BH keep decreasing with time and therefore, the Page curve starts coming down after Page time and comes down to zero when the BH is fully evaporated. In the case of eternal BH however, the Page curve saturates at the Page time and the entanglement between the radiation and the BH remains constant after Page time.

Since the islands came into the picture, they have been greatly investigated, and grasping the origin of islands from a more physical perspective is a subject of current research. In this vein, a few classical models have been introduced [110–112], where the picture is purely classical-gravitational and one gets away by working only with HRT surfaces instead of QES. Ideally, in such a situation, we obtain an analog of an island and a Page curve is also realized. Strictly speaking, however, due to the absence of bulk entanglement entropy, this picture is a purely coarse-grained approach. Nevertheless, these models have played an important role in understanding the origin of the islands from various perspectives and also realizing the analogs of Page curve for other quantum information-theoretic measures e.g; reflected entropy [68], the entanglement of purification [44, 63] etc.

These models rely on multi-boundary wormholes in AdS_3 , which are very special ob-

jects since they can be constructed as quotients of empty AdS_3 by its isometries. Once the fundamental domain is known and one avoids the fixed points to have well-defined curvatures at each point of the fundamental domain, the problems become a lot easier to deal with. As the very name suggests, multi-boundary solutions have multiple boundaries where independent CFTs live. We will call these boundaries as exits throughout this chapter. Now, within the multi-boundary wormhole models of the island, the radiation quanta themselves are typically modeled as multi-partite (at least bipartite, i.e. three-boundary wormhole) systems where they are represented by smaller exits of the multi-boundary wormhole. To begin with, the actual black hole is modeled by a bigger exit and if evaporating, it keeps shrinking with time whereas more and more quanta are accumulated in the smaller exits. In these models, the minimal throat horizons at different times play the role of the HRT surface measuring the entanglement between the black hole and the combination of the Hawking quanta. Since the situation is dynamic, at some critical point, the choice of minimal surface changes and an island is included. There have been a few such models in which the difference is how one stores the emitted quanta in different exits. Different entanglement measures have also been computed within the scope of these models. One among them is the reflected entropy [21, 111] . It measures the entanglement between different parts of a mixed state. For example, one can compute how entangled the different emitted quanta are with each other individually or with the black hole. The Page curve for the reflected entropy differs as well from its entanglement entropy counterpart.

On the other hand as reviewed in subsection 2.4.2, the authors of [63] have conjectured bulk counterparts of a more general information-theoretic quantity called the entanglement of purification. This has been studied both in gravitational setups as well as in free field theories [44, 45, 113, 114]. In the gravitational ones, the holographic EoP is conjectured to be related to the entanglement wedge cross-section. Such results include the study of pure

AdS, BTZ black holes as well as time-dependent scenarios. A study of few other quantum information-theoretic quantities e.g; multipartite entanglement of purification [64,67,115–117], reflected entropy [68,118–122] have been motivated by the EoP computations.

In this chapter, we primarily discuss the possible connections between the multi-boundary wormhole model of BH evaporation and the holographic entanglement of purification in the case of AdS_3 . We use the concepts of the holographic dual of multipartite entanglement of purification for states in the boundary of pure AdS_3 . We use these concepts in the toy model of evaporating black hole [110].

We would try to get an understanding of the islands from the perspective of multipartite EoP. We would also comment upon the analog of the island from the point of view of quantum error correction [123–125], but by taking a detour through the entanglement of purification. This is not very surprising since both of the programs are heavily dependent on the ideas of entanglement wedge reconstruction and nesting. Our study relates the body of a multi-boundary wormhole to a geometric pure state construction. We further figure out how in such a model, there are two sides to the whole story. The classical picture gives us an intuitive understanding of the islands and helps to reproduce the Page curve. But the quantum version of the extremal surface again gives back the familiar paradox addressed by Hawking. Finally, we give resolutions through which one can understand how to deal with the problem both in the toy model as well as in the entanglement of purification case.

Another interesting question that this line of study hopes to answer in the long run is the computational complexity associated with the decoding of the information stored within the evaporating black hole and radiation state. The complexity being in general different from entanglement and by definition, it captures different Physics than the entanglement entropy. Due to the Harlow-Hayden protocol [126] and later works by Susskind and collaborators [127], there is a general idea in the literature that this kind of state de-

coding is an exponentially hard task. By exponentially hard task, one means here that the minimum number of gates equals the minimum number of time steps required to go from one quantum state to another which is exponential in time steps in this case. Hence, the complexity of the evolving black hole state is expected to grow exponentially in time. This is supported by proposals about a state-of-the-art geometric structure known as Python's lunch [127, 128] that shows some signs of why this is supposed to be such a complicated task. Nevertheless, the gravitational proposals of complexity [11, 23, 24] have not yet been able to find a situation that agrees with this particular suggestion.

In this chapter, motivated by these studies, we also study the volumes dual to the throat horizons in the multi-boundary wormhole models sketched above. Primarily put forward by Alishahiha [4] and reviewed in details in chapter 2 and 3, the volumes $V(\mathcal{S})$ subtended by HRT surfaces \mathcal{S} are conjectured to represent the so-called *subregion complexity*,

$$\mathcal{C}_{HSC} = \frac{V(\mathcal{S})}{8\pi L G}, \quad (5.1)$$

where G is Newton's constant and L is the AdS radius. Subregion complexity is argued to measure the difficulty of an algorithm to construct a mixed density matrix. In AdS_3 , this has been studied in detail and is understood as a compression algorithm constructed using tensors [71]. In the tensor network picture, the number of bonds associated with some cost successfully mimics the behavior of subregion complexity. Kinematic space provides yet another way of understanding these volumes [72]. Usually kinematic space yields a description in which the bulk curves are understood roughly as the number of boundary anchored bulk geodesics crossing that curve [129] and the volumes as to the number of such geodesics along with the chord lengths that each of them contribute to the volume. All of these are mostly understood within $\text{AdS}_3/\text{CFT}_2$. Since the multi-boundary wormholes are

also best understood in three spacetime dimensions, we use the machinery built in [71, 72] to study the Page curve analog of subregion complexity in these models.

The remainder of the chapter is structured as follows. In section 5.1, we review the basic ideas that have been instrumental in the derivation of the Page curve for the Black holes and the Hawking radiation. In section 5.2, we discuss the construction of the multi-boundary wormholes in AdS_3 . Then we briefly explain the two multi-boundary models that we worked on in [9] and [10]. In section 5.3, we then discuss the connections, contradictions and resolutions between the $n + 1$ boundary wormhole model and the entanglement of purification found in [9]. Finally, in section 5.4, we discuss volume computations in these models and the main findings of [10].

5.1 A Note on recent developments regarding Page curve:

This is a very brief review of the recent program [105, 107, 110, 130, 131] that has been instrumental in describing the time evolution of a black hole to be a unitary process by considering the combination of an evaporating black hole and the Hawking radiation to form a pure state. It has then been shown that using particular techniques, one can show that separately both system's entanglement entropy follows the same curve which is not ever-growing, but indeed comes down after Page time. This is a path-breaking result since it is the very first time that some program has been able to arguably solve the longstanding information paradox. Although it was always argued since the discovery of AdS/CFT that it can solve the information paradox, this is the very first concrete example where people have been able to show it in a somewhat convincing manner.

The technique through which this program was successful to achieve such a task is though yet to be made complete sense of. It involves the introduction of certain bulk regions called islands, which is essential to derive a Page curve for the emitted Hawking

radiation along with new but familiar concepts of the quantum extremal surface.

5.1.1 Information Paradox and Resolutions (Islands) :

Information is ideally considered to be a sacred thing, which one should always keep track of. If there is a flow of information between two parts of the system, then the information missing in one part should necessarily show up in the other part. But, in the case of the black hole, it has been a longstanding problem in such a scenario. In the case of black holes, the way one typically compares information inside and outside is by specifying the entanglement between the two systems. The paradox appearing in this computation had been a peculiar one since the information found in the radiation outside the black hole seemed to be more than what the black hole could store. If we talk in terms of entanglement entropy, which is a standard information measure between two entangled states, the entanglement entropy of the radiation outside the black hole was found to be growing over for a very long time, whereas the black hole's entropy seemed to become less and less over time. They crossed each other much before the radiation entropy saturates. But, since the evaporating black hole and the radiation states should form a combination that is a pure state, the entanglement between them for all times should be the same. This is one of many ways in which the information paradox can be realized. Let us explain a bit more concretely.

Let us assume that the radiation state is considered just combinations of the Hawking quanta radiated by an evaporating black hole. For all such Hawking quanta, there is one partner-quanta each behind the black hole horizon, which is entangled to its outside partner. Let us schematically write the radiation quanta and their partner modes as a combination, which is a pure state,

$$|\psi\rangle_{rad} \equiv \sum_{\omega, n} e^{-\frac{\omega n}{2}} |n\rangle_{in} |n\rangle_{out} \quad (5.2)$$

at any point of time t , where the time is kept track of the frequencies ω (summed over) and n counts entangled pair of Hawking quanta emitted till that time.

Now, tracing over $|n\rangle_{in}$ states, one can find out the reduced density matrix of the out-state ($\rho_{rad,out}$), which in this case comes out to be in form of a thermal density matrix,

$$\rho_{rad,out} \equiv \sum_{\omega, n} e^{-\omega n} |n\rangle_{out} \langle n|_{out}. \quad (5.3)$$

This leads to the paradox since once the entanglement entropy is calculated for this reduced density matrix following the usual formula of von Neumann entropy, it keeps growing until the black hole evaporates (number of n increases). On the other hand, the Bekenstein Hawking entropy, which is supposed to be representative of black hole entropy keeps decreasing as the black hole evaporates and the area decreases. After some time (known as the Page time),

$$S(\rho_{rad,out}) > \frac{A_{BH}}{4G}. \quad (5.4)$$

The situation then complicates as the bipartite entangled state between the radiation outside and the black hole becomes oversaturating what the black hole can entangle with. In another way, the black hole is entitled to more entanglement than it has microstates available.

There have been several attempts and effort in solving this paradox and deriving a formula which follows the well-known Page evolution (grows initially, then comes down to zero after Page time). But, until very recently, there has not been a convincing way in

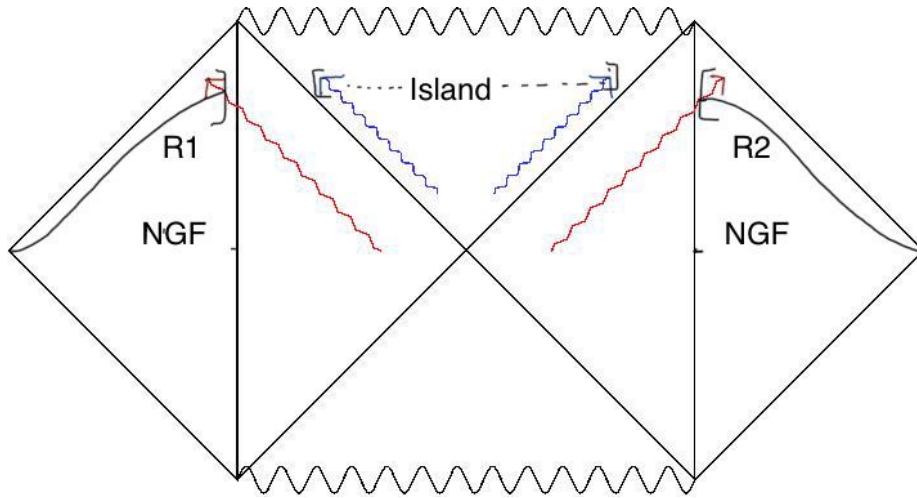


Figure 5.1: Penrose diagram of two sided Black Hole with nontrivial island included (red and blue lines represent Hawking partner modes outside and inside the black hole horizon respectively.)

which people have been able to do it. In this recent set of papers [105, 107, 110, 130, 131], the resolution is brought in by introducing certain regions, termed as islands, which are null before Page time but are non-null region (behind the black hole horizon) after the Page time. This also has to be considered for computing the entanglement entropy of the radiation states. Given such a situation, one has to also work with the idea of quantum extremal surfaces since while computing the entanglement associated with the nontrivial regions behind the horizon, Ryu-Takayanagi also contributes in a nontrivial way to the entanglement entropy of the radiation states.

Let us now look at Figure 5.1 to get a better understanding. We consider a two-sided BH in AdS_3 . The extreme left and extreme right regions represent non-gravitational flat space (NGF) coupled with the asymptotic AdS boundaries. These are needed as we are considering evaporating black holes and these coupled NGFs provide us a way to introduce absorbing boundary conditions in the shared boundary through which outside Hawking quanta can escape (unlike eternal BH case, where the outside quanta are reflected from

the AdS boundary to feed the black hole back). Using this, we compute the entanglement entropy of the outside quanta in the NGFs. It is like stacking up the quanta escaping AdS in the NGFs. But simply doing these would again lead to the usual paradox. Say we compute entanglement entropy at an anchored time-slice t for a region from infinity (in the NGF) to very near the AdS boundary on both sides of AdS. Let us call these two regions $R1$ and $R2$ and their union ($R1 \cup R2 =$) R . $S_{out}[R]$ would again grow for a very large time and lead to the information loss.

The introduction of the islands comes to the rescue here along with the consideration of quantum extremal surfaces. In the picture, where islands are included (shaded region behind the horizon, after the Page time), the new notion of entanglement entropy for the outside quanta looks like,

$$S_{out}[R](new) = \min_I \left[\text{ext}_I \left\{ \frac{A(\partial I)}{4G} + S_{usual}[R \cup I] \right\} \right], \quad (5.5)$$

where ∂I is the boundary of the region enclosed by the islands. S_{usual} is the entanglement between quantum fields in the region $[R \cup I]$ and its complement. This is sometimes also known as bulk entanglement entropy in the standard literature. This is marked as usual here because, before the new development regarding the islands, this is all one used to apply (for region R , I regions were not included) and found the ever-growing curve leading to the usual Hawking's version of the information paradox.

For a given timescale, firstly one has to take all choices of I (any interval in AdS_3 , inside or outside the horizon can be a candidate for I). Then the sum of the two things in the curly bracket has to be extremized. The notion would be that in general, there exists more than one choice of I for which the sum is extremized. One has to choose the one which minimizes the sum at any given time. This solves the paradox since one finds that

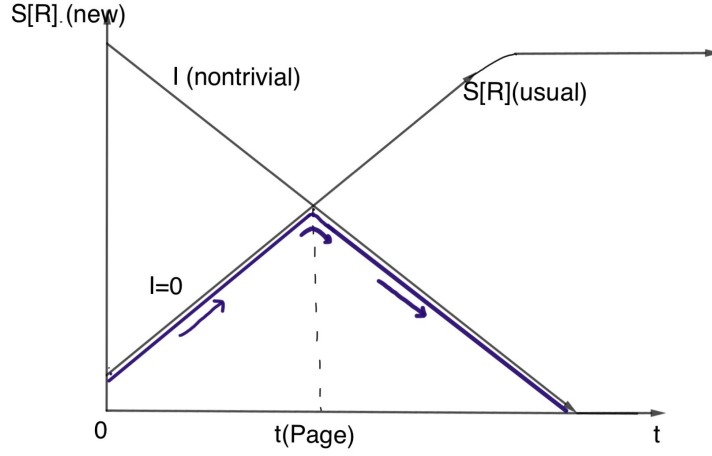


Figure 5.2: Choice of islands before and after Page time and Page Curve

before Page time, minimal choice of island is the null (trivial) one, and therefore up to that time, the new entropy is the same as the usual one which grows. In this case, $\frac{A(\partial I)}{4G}$ is zero whereas $S_{new} = S_{usual}$. But after the Page time, the choice of the island which minimizes the sum among other choices of extremas is the one just behind the horizon. In that case, $\frac{A(\partial I)}{4G}$ becomes the dominant contributor, as in the other part, both the entangled Hawking quanta (inside and outside black hole) are included. In that case, this piece contributes much less as the Hawking quanta are purified. This is an important point we would come back to while making connections to the multi-partite entanglement of purification. But, the dominant contributor ($\frac{A(\partial I)}{4G}$) decreases over time which helps in the production of a Page curve (see Figure 5.2).

5.2 Multiboundary Wormholes and the toy models:

In this section, we briefly discuss multi-boundary wormholes (MbW) in AdS_3 and then we discuss the toy model introduced in [110, 111], where the authors have shown that classical RT surfaces can also reproduce a Page curve in some situations and the aspects of

the newly introduced islands can be given an intuitive understanding from the perspective of quantum error correction [123–125].

Multiboundary wormholes are situations where many boundary CFTs are connected by a wormhole. All these different boundaries are independent of each other. The construction of multi-boundary wormholes in AdS_3 is a well-discussed topic, but an active area of research in itself. In usual understanding, multi-boundary wormholes can be thought of as multiple exits created by quotienting AdS_3 and by removing semicircles from a timeslice of pure AdS_3 by orientation reversing isometries in the upper half-plane. This defines the fundamental domain. Since in three spacetime dimensions, true dynamical degrees of freedom is lacking, only global topological data and boundary dynamics classify a classical saddle implying that for smooth asymptotically AdS_3 , all geometries locally belong to the same universal class and are distinguished only by global features.

In AdS/CFT, this is related to the study of n fold tensor product of CFT states in different boundaries. For $n = 2$, the resulting geometry is of a BTZ which is dual to a TFD (thermofield double) state. [132] is a recent paper that discusses these things in detail. Figure 5.3 is the way one creates two boundaries by removing two semicircles from pure AdS_3 slice at $t = 0$ through a killing vector that generates dilatation. The standard way of addressing dynamical questions in CFTs is the formalism known as Schwinger-Keldysh, which in the context of holography is translated as considering multi-boundary geometries in Euclidean and Lorentzian signature and gluing across a surface of zero extrinsic curvature (boundary anchored geodesics). As a spacelike slice of AdS_3 always maps onto the Poincare disk by stereographic projection, we start with a Poincare disk and take a quotient by a single hyperbolic isometry producing a Riemannian surface with constant -ve curvature everywhere. This manifold is the one that one gets if one cuts a strip bounded by geodesics anchored on the boundary out of the disk and glues it shut. This produces a time-

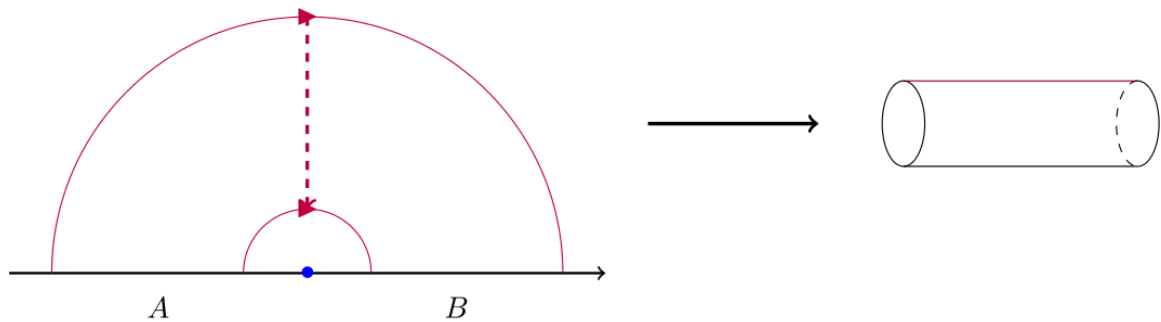


Figure 5.3: Two boundary case and Horizon length, equivalent to EWCS for bipartite system.

symmetric slice at $t = 0$ of a two-sided BTZ. Let us give a surprise at this point. Figure 5.3 is the fundamental domain of a 2 sided BTZ, defined by removing two semicircles that are related through a dilatation. This in Poincare disk representation would simply look like Figure 2.4 of bipartite entanglement of purification, where A and B (bipartitions of the mixed state $A \cup B$) in Figure 2.4 have to be associated with the two boundaries where two CFTs live. We will discuss these connections in detail in the next section.

Nevertheless, one can introduce more and more exits by removing more and more semicircles in an orientation reversing way on one side of the smaller semicircle of Figure 5.3. These removals simply correspond to quotienting by more and more number of isometries. Removing semicircles from the other side would mean introducing handles.¹

A multi-boundary wormhole can be understood as a diagram that resembles a pant with leg space of more than two (typically known as pair of pant geometries in the mathematical community). In such a construction, all the different horizon lengths can be tuned or changed independently in terms of the parameter in the timeslice of AdS_3 through which the semicircles are removed. But for a two-boundary case, there is only one horizon, which both the CFT sees and there is only one parameter involved which is the ratio of the radius

¹The introduction of a handle involves removing two semicircles from two sides of the lower semicircle of Figure 5.3, but it also reduces the number of exits/horizons by one.

of the semicircles in figure 5.3. Starting from $n > 2$, an n -boundary wormhole would have parameters such that all the horizons can be made big or small independently using a non-overlapping set of parameters. A more mathematically sound description of this construction can be found in Section 2 of [10].

5.2.1 Multiboundary Wormhole Models of Black Hole Evaporation:

Having constructed multi-boundary wormholes in hyperbolic geometry, let us discuss the precise models we are interested in. We concentrate on two models which effectively capture some of the central ideas associated with the island program. In both models, we start from a three-boundary wormhole. One of its exits is much larger than the other two, which have a coinciding size. The bigger exit is the analog of the evaporating black hole whereas the smaller ones model the radiation quanta being emitted from the BH. The two models we consider are distinguished by the way the geometry changes with time as more and more quanta get stored in the radiation geometry whereas the BH keeps getting smaller.

a) Three Boundary Model: In the first model, we evolve the exit sizes of a three-boundary wormhole as the system moves forward in time. Therefore, in this model the size of the bigger exit (BH) decreases with time while the smaller exits increase. We insist that the sizes of the smaller exits remain the same as time evolves. Hence, both the smaller exits increase at the same rate. We track the minimal throat horizon lengths corresponding to the union of smaller exits (Hawking quanta) with time. There is a shift in the choice of minimal geodesic at certain timescale, the Page time, after which the connected minimal throat horizon (corresponding to the bigger exit) is the favored choice as opposed to

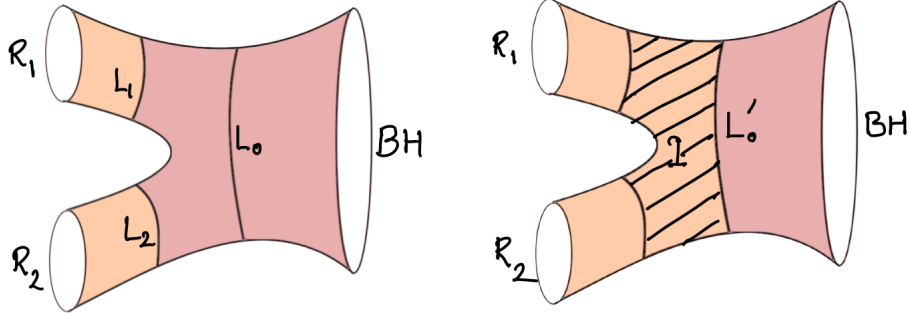


Figure 5.4: Change of preferred HRT in 3 boundary model. Left: Before the Page time the HRT surface separates the R_i from the remainder of the pair of pants. Right: After the Page time L_0 has shrunk to L'_0 and the HRT surface has jumped to include the island I .

the disconnected unions (throat horizons of the smaller exits)². This change of preference gives rise to the Page curve in this model. The situation is shown through the pair of pants geometry in figure 5.4. After the Page transition, the region I is added to the entanglement wedge of the Hawking quanta. This is the representative island in this model. The corresponding Page curve is shown on the left-hand side of figure 5.6. Note that the topology of this model never changes; it remains a three-boundary wormhole at all times.

b) $n + 1$ -Boundary Model: In the second model, instead of increasing the size of the smaller exits, we increase the *number* of smaller exits. Hence, in this model, the topology changes with each time step, and the no. of exits n represents this time. Although it is hard to realize dynamically from Einstein's equations, it is perfectly reasonable as discrete snapshots at different times during the radiation. All the different topologies are time reflection symmetric. The bigger exit, similar to the three-boundary model, keeps decreasing, and again a transition of HRT surface corresponding to the union of the Hawking quanta

²It is to be noted that both these choices are homologous to the BH as well as the union of Hawking quanta for all times. Hence they are the candidate HRT surfaces.

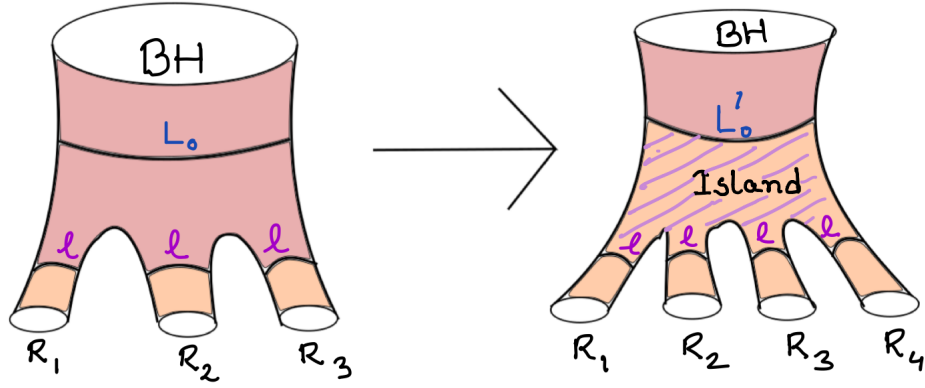


Figure 5.5: Change of preferred HRT in $n + 1$ -boundary model.

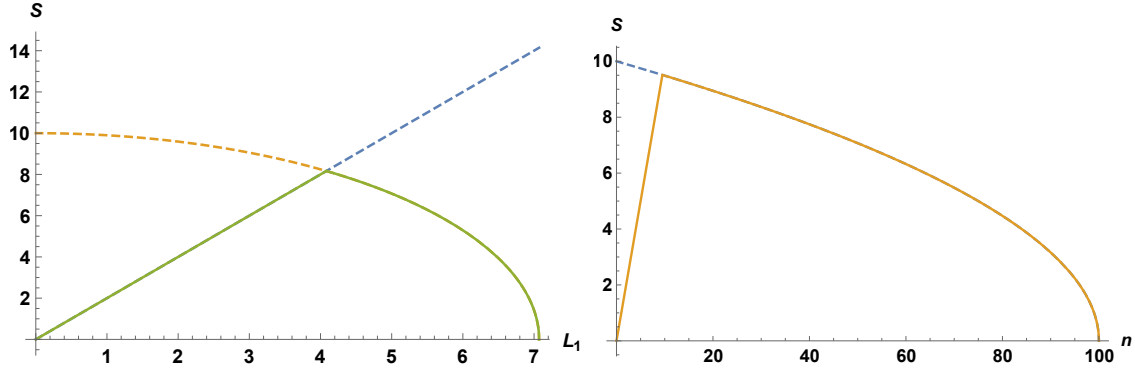


Figure 5.6: Page curves corresponding to the left: three and right: n boundary models.

(union of the n smaller exits in this case) takes place at a certain point of time (n_{page}), this is shown in figure 5.5. The corresponding Page curve is shown on the right-hand side of figure 5.6.

An important assumption made in these models is that the ADM energy is conserved during the evaporation process. The relation between entropy and ADM energy in AdS_3 is the following

$$S = 2\pi\sqrt{\frac{cE}{3}}. \quad (5.6)$$

Now, in three bulk spacetime dimensions, the area of the HRT surface is simply propor-

tional to the length. Let us consider the initial length of the horizon of the evaporating black hole is L_0 which decreases over time as it emits more and several smaller black holes with horizon lengths ℓ . Using the relation between length (entanglement entropy) and ADM energy, one can show that at any point of time, where n (two) smaller black holes have been emitted for the $n + 1$ (3) boundary model, the horizon length of the bigger black hole decreases in the following way,

$$L_{BH} = \sqrt{L_0^2 - n\ell^2} \text{ (} n + 1 \text{ boundary model), } L_{BH} = \sqrt{L_0^2 - 2\ell(t)^2} \text{ (3 boundary model),} \quad (5.7)$$

where the $\ell(t)$ is the time-evolving HRT length for the three boundary model. The union of the length of the horizons of the smaller horizons scales like $L(HQ) = n\ell(2\ell(t))$ for 3 boundary model³. For smaller values of n (for the $n + 1$ boundary model) and t (for the three boundary model), L_{HQ} is the minimal choice, which grows over time as n increases. The L_{BH} decreases as time moves forward. At certain timescale $n \sim \frac{L_0}{\ell}$, L_{BH} and L_{HQ} become comparable and after that L_{BH} becomes the minimal HRT choice.

This region between the chosen HRTs at different times (here the number of exits, n , is considered to be the analog of time), has also similarities with the shared interior that appears in a study of quantum error correction through bulk reconstruction picture. Through this similarity, the authors in [110] provided a possible understanding of the islands, which is due to the full and restricted set of observables that can be reconstructed depending upon which surface is chosen. According to them, as the shared interior is not dual to any single boundary subregion, it appears as a quantum error-correcting region in the computation of entanglement entropy. Now, in the next section, we discuss few connections between the $n + 1$ boundary model and the multipartite entanglement of purification (holographic) with

³ L_{HQ} corresponds to the length of the horizons of the smaller black holes that are analogs of Hawking quanta in the radiation

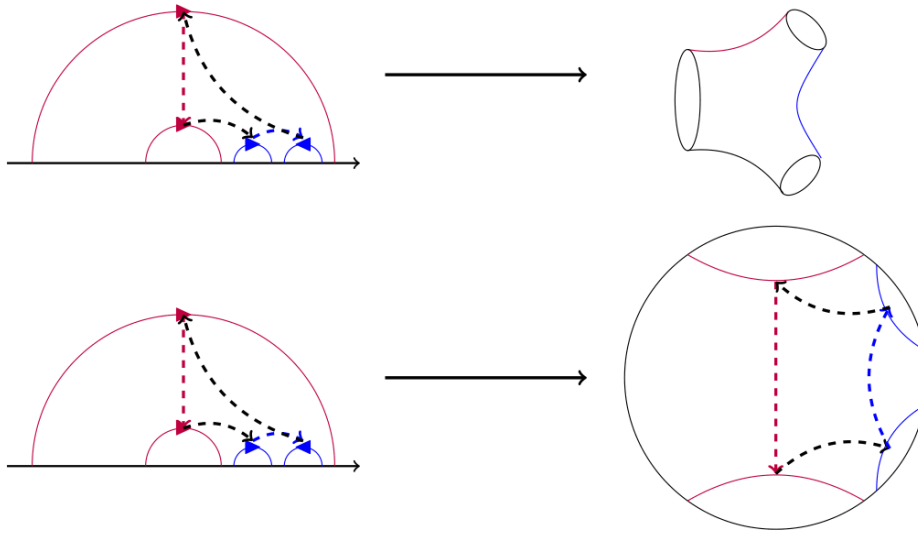


Figure 5.7: The three-boundary Riemann surface as quotients of the two-boundary Riemann surface. The three-boundary surface is obtained by pinching one of the boundaries into two. The island is marked by the closed region spotted by the dotted purple, black, blue, and blackline respectively.

the hope to get a better understanding of what the toy model implies and how can it be connected to the study of multipartite entanglement.

5.3 Connections between EoP and MbW Toy Model:

5.3.1 Connections to be drawn:

The two topics discussed in the two previous sections have striking similarities which are yet to be pointed out. The following observations can be made to help us understand the connections and also give a few important lessons that should be kept in mind while comparing the two scenarios.

1. As we have already pointed out once in the previous section, the pictures of bipartite entanglement of purification where the bipartition made by choosing two disjoint, but substantially larger subregions of a timeslice of pure AdS_3 is very similar to

the construction of a wormhole connecting two boundaries, where the boundaries exactly correspond to subregions A and B of the bipartite system.

To be more exact, in the case of two boundaries, one takes two boundary anchored geodesics in Poincare disk, the fundamental domain (corresponding to the HRT surfaces of the region $A \cup B$ not sharing any endpoints) and uses a unique isometry (dilatation to be precise) that defines a bijective map from points on one of the geodesics to the closest points on the other. This map is the part where one identifies points on the two geodesics periodically and glues them. This isometry doesn't involve any fixed points in the strip between the two geodesics. ⁴

2. Another striking similarity is the entanglement wedge cross-section for a bipartite state is the only possible horizon length that one can compute in a two boundary case. After the identification and gluing procedure is done among the two boundary anchored geodesics in the Poincare disk, all one needs to specify the two-sided BTZ is not two, but a single geodesic specifying the horizon length.

Now, we can also simply go on to pictures including more exits and compare the two cases in one of which, we increase the number of exits in the MbW picture, and in the other picture, we introduce more number of disjoint subregions in one of the subregions A and B . ⁵ But there is one subtlety involved that one should keep in mind while doing so. For $n \geq 3$, one needs to remove two semicircles for introducing each new exit. Thus after $n = 2$, in the partitioning of the boundary, we have to introduce two disjoint subregions at each step in the purification picture, a

⁴Multiboundary wormhole constructions can involve isometries including pathologies like fixed points and closed timelike curves in general. But both can be avoided by making suitable choices as mentioned in [132].

⁵If we introduce more subregions on both sides, that would mean introducing handles in the MbW picture. We avoid such scenarios for the time being.

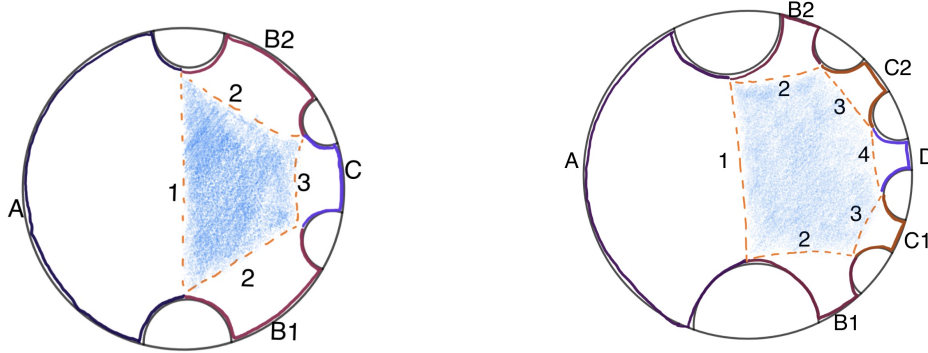


Figure 5.8: Three and Four Boundary cases : Semicircles to be removed are marked. Blue-shaded regions represent the shared interiors. These are the choices that minimize the boundary of the shared interior with respect to the corresponding geometric pure state.

combination of which will be equivalent to the newly constructed boundary.

In doing so, in each step, we should also keep decreasing the size of the other subsystem A very slowly so that our picture goes well with the previously introduced toy model. We also introduce new subsystems in such a way that their contributions in multipartite EoP are much smaller initially w.r.t the contribution of the bigger subregion A .

We can define our newly defined subsystems in the following way so that it again goes well with the boundaries that are defined in the MbW case. We take two disjoint boundary intervals connected to A on two different sides and call them $B1$ and $B2$. We call their union to be a partition B . Similarly, for more exits, we keep taking unions of intervals connected to $B1$ and $B2$ on two sides and define them as a new partition. (as shown in figure 5.8)

3. Now, by looking at the two pictures, one can easily point out that the dotted lines in

Figures 5.5 and 5.7 are equivalent to each other. But, in multipartite EoP, we take the sum of all of them, whereas, in the MbW toy model, they are treated as two different sets that naturally provide one with a way to choose one of them as the HRT surface. If we look at the figures more carefully, it is not hard to find out that the codimension 1 region enclosed by the multipartite entanglement wedge cross-section is the shared interior (/island) in the MbW picture. It is then obvious to define the multipartite entanglement wedge cross-section as the boundary of the nontrivial island. We thus get an understanding of the boundary of the nontrivial island after the Page time in terms of entanglement of purification between the evaporating black holes and the radiation quanta (union of all other boundary subregions except A).

4. An important fact while talking about the connections between the two scenarios is to realize the correspondence between a geometric pure state and the multi-boundary wormholes connecting the bigger and the smaller black holes. In the case of multipartite entanglement of purification, we consider the bulk HRT surfaces for the subsystems of the pure AdS along with the boundary subregions as a geometric pure state,⁶ The multi-boundary wormhole connecting CFTs at different exits acts as a machine to make the whole multipartite state (/combination of multiple exits) a pure state. Making this connection helps us to understand the multi-boundary wormhole along with the exits as a geometric pure state for which we consider the HRT surfaces to compute the entanglement entropy.

⁶To be precise, the HRT surfaces of the multi-boundary cases do not form a closed region by themselves. The shared interior is understood as the union of HRTs along with certain regions of the wormholes connecting different exits. But since while considering a geometric pure state in the dual EoP picture, we make the choices of $\Gamma_{\tilde{A}\tilde{B}}$, $\Gamma_{\tilde{B}\tilde{C}}$ and $\Gamma_{\tilde{A}\tilde{C}}$ in such a way that the combination of them forms a minimally closed curve (See Figure 2.5) among all other choices. This choice is always the minimal choice of choosing the boundary of the analog of the islands.

5.3.2 Realization of over-counting:

The previously mentioned comparisons and connections indeed support the connection between the islands and quantum error connection since multipartite EoP has well-discussed connections to quantum error corrections as well as discussed in [133]. But as mentioned in the formula of quantum extremal surface, if one computes the area (length in case of AdS_3) of the boundary of the island, it doesn't behave as per our expectation. This is because the $A(\partial I) = \Delta_W$ and it consists of both the union of smaller horizons as well as the bigger horizon. It also means that the length of the boundary of the nontrivial island would follow the properties followed by multipartite EoP, which we have already listed in section 2.2.

$$A(\partial I) = \Delta_W = \sqrt{L_0^2 - n\ell^2} + n\ell. \quad (5.8)$$

Now although the length of the bigger horizon keeps decreasing over time, the length of the combination of the smaller ones keeps increasing. The sum of them still grows (see figure 5.9) until the black hole evaporates (in this case, this corresponds to the case where subregion A becomes so small that the entanglement wedge [123] of the partitions simply become the union of the causal wedge of each of them).

Therefore if one strictly assumes the shared interior to be the analog of the nontrivial island, its boundary area is evergrowing even after the Page time. (shown in figure 5.9). Nevertheless, we prescribe the following resolution to the paradox. Our prescription is that this is again the same paradox that this whole program began to deal with. In the toy model, the authors try to realize the notion of the islands just through the classical HRT surfaces neglecting the bulk entropy part (second term in QES equation) assuming that the length of the smaller horizons individually is enough to keep track of the bulk entanglement entropy

associated to the smaller black holes.

The argument is not so unsatisfying once we take into account that the analogs of the Hawking quanta are small black holes in the MbW picture, which are classical geometric objects. But from the point of entanglement of purification, when we consider the whole multipartite EWCS, we include both the bigger black hole horizon as well as the smaller ones. This, if translated to the statements made in [110], effectively means that we double count the bulk entropy of Hawking quanta in multi-partite EWCS. Hence, once the island is included, in our calculations, the entanglement between the partner modes of the emitted quanta also contributes to the multipartite EoP. But, in fact, as the new HRT includes both the partners, they are purified. Multipartite EoP is insensitive to this purification and overcounts this to make the entanglement of purification larger than it should be.

The final resolution on the choice of multipartite entanglement wedge cross-section can be drawn from [134] in which again multipartite entanglement has been studied in detail. Drawing connections from that paper, we can resolve the problem in the following way. As one of the black holes is considered to be much much bigger than the other ones, primarily all other horizon lengths can be considered as $\ell \rightarrow 0$. The reverse limit would be taking the smaller horizons ℓ to be finite whereas $L_{BH} \rightarrow \infty$. In both of these limits, the combined state behaves like a bipartite state [134] between the bigger BH and the union of the smaller ones. In that situation, the multipartite case boils down to a simplified bipartite case where the entanglement of purification reduces to usual entanglement entropy. Therefore, one can simply choose either the union of the horizons of smaller black holes or the horizon of the bigger black hole as the HRT surface depending on whichever is minimal at that time. But even in that scenario, if the newly entered shared interior is considered to be the analog of the nontrivial island, the growth of the length of the boundary of the island is paradoxical. The reason why this paradox arises only in the toy model is that in this case, the analog of

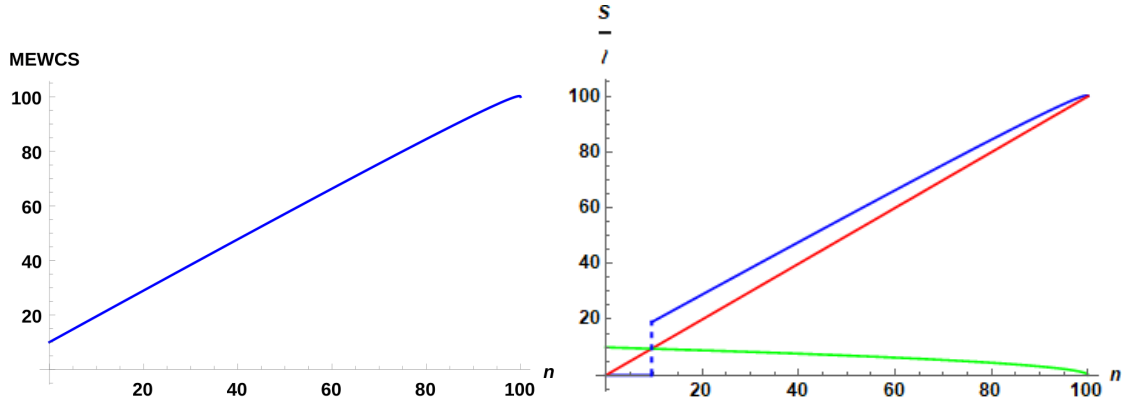


Figure 5.9: (left) Growth of the multipartite EWCS (for the minimal choice). (right) Comparison between primary (red) and later (green) choice of HRT with the minimal island (blue) growth at different times.

islands is connected to the earlier null island. On the other hand, in the case of the actual case, the island is behind the black hole horizon and is disconnected from the trivial island choice before the Page time.

If we treat different smaller black holes differently, we would have to necessarily consider multipartite entanglement of purification. Say we consider the bigger black hole as subsystem A, whereas \$n\$ smaller black holes as \$B_1, B_2, \dots\$, and \$B_n\$, then Multipartite EoP should be

$$\Delta_P(A : B_1 : \dots : B_n) = \frac{1}{n} \min_{|\psi\rangle_{Pure}} \sum_{i=1}^n (S_{AA'} + S_{B_i B'_i}). \quad (5.9)$$

In this scenario, where all the smaller black holes are treated as a combination, and along with the bigger black hole, they form a pure state, we can take \$A' = B'_i = \emptyset\$ and therefore,

$$\Delta_{(n+1)P}(A : B_1 : \dots : B_n) = \Delta_{(2)P}(A : B) = \frac{1}{2}(S_A + S_B). \quad (5.10)$$

Note that it is necessary to consider the full state as a bipartite pure state. A multipartite pure state would not solve the problem. For example, if we considered that the

combination of the big black hole and n smaller black holes to be an $(n + 1)$ -partite pure state, we would have to still apply property 2 of the multipartite EoP.

$$\Delta_P(A : B_1 : \dots : B_n) = \sum_{i=1}^n (S_A + S_{B_i}) = \sqrt{L_0^2 - n\ell^2} + n\ell, \quad (5.11)$$

where for each small black hole, even after the Page time, ℓ would be the HRT surface for individual smaller black holes instead of L_{BH} . Thus the multipartite EoP would still give us the ever-growing entanglement. Thus the resolution appears only when in the limit of a very large number of very small black holes, we take the union of the smaller black holes to be a single mixed state, which along with the large black hole state forms a bipartite pure state.

5.4 Sub-region Complexity in AdS₃ and multi-boundary models:

In this section, we describe the computations of volume in AdS₃ and the multi-boundary wormhole exits, which have mostly to do with the topology of the bulk region. This is crucial for our study of complexity in [10].

5.4.1 Volumes in AdS₃:

In this chapter, we content ourselves with constant time slices of AdS₃ space-time. The HRT formula [2, 3, 19] suggests that the entanglement entropy of any region A on the boundary of AdS₃ is equivalent to the length of the bulk geodesic $\gamma_{RT}(A)$ anchored at ψA ; one also needs to introduce a cutoff surface γ_ϵ near the boundary for regularization. Our primary interest is in the volume of the co-dimension-1 surface Σ with boundary $\partial\Sigma = \gamma_{RT}(A) \cup A_\epsilon$, where A_ϵ is the segment of the cutoff surface γ_ϵ , which hovers over A . This volume appears in the original definition of holographic complexity in (5.1). In this work,

we employ, however, an alternate definition of subregion complexity put forward in [71].

Definition 1. *Let $\Sigma \subset \mathbb{H}^2$ be a hyperbolic surface with boundary $\partial\Sigma = \gamma_{RT}(A) \cup A_\epsilon$ for boundary interval A . Its topological subregion complexity is defined through*

$$\mathcal{C}_{HSC}(A) \equiv -\frac{1}{2} \int_{\Sigma} R d\sigma, \quad (5.12)$$

where R is the scalar curvature of the bulk space-time.

In the cases of interest in this chapter, R is a constant so that the topological subregion complexity (5.12) and the original proposal (5.1) differ only in normalization. One benefit of using topological complexity is that it is naturally dimensionless as desired for complexities. However, the main advantage of (5.12) lies in the fact that it determines the complexity completely by topological data through the use of the Gauss-Bonnet theorem

Theorem 1. *Let Σ be an orientable, compact, two-dimensional Riemannian manifold with piecewise smooth boundary $\partial\Sigma$ and scalar curvature R . Denote by k_g the geodesic curvature of the curve carved out by $\partial\Sigma$. Then*

$$-\frac{1}{2} \int_{\Sigma} R d\sigma = \int_{\partial\Sigma} k_g ds + \sum_{i=1}^r \alpha_i - 2\pi\chi(\Sigma), \quad (5.13)$$

where $\chi(\Sigma)$ is the Euler characteristic of Σ . r is the number of corners in $\partial\Sigma$ and α_i are the corner angles at which the piecewise smooth segments of $\partial\Sigma$ intersect.

The geodesic curvature k_g measures how much $\partial\Sigma$, or any other curve under scrutiny, deviates from a geodesic. If we anchor Σ at a boundary interval A , then the left hand side is of course the topological complexity $\mathcal{C}_{HSC}(A)$. Moreover, in this case, the corner angles α_i are always $\pi/2$ [35] since geodesics γ_{RT} intersect the cutoff surface perpendicularly.

Let us illustrate the formula with standard examples. In the simplest case the subsystem A is a single connected interval $A \in [x_1, x_2]$. The boundary has two corners, those at which γ_{RT} and A_ϵ intersect, each of which contributes $\pi/2$, yielding

$$\int_{\partial\Sigma} k_g ds + \sum_{i=1}^2 \alpha_i = \frac{x_2 - x_1}{\epsilon} + 2 \times \frac{\pi}{2}. \quad (5.14)$$

The Euler characteristic of Σ is 1 as it is topologically equivalent to a disk, thus we obtain

$$\mathcal{C}_{HSC}(A) = \frac{x_2 - x_1}{\epsilon} - \pi. \quad (5.15)$$

As another example let us consider two disjoint sub-regions $A = A_1 \cup A_2$, where $A_1 = [x_1, x_2]$ and $A_2 = [x_3, x_4]$, ($x_1 < x_2 < x_3 < x_4$). There are two candidate HRT surfaces for this configuration. In phase I the complexity is simply the sum of that for each subregion, i.e.

$$\mathcal{C}_I = \frac{x_2 - x_1}{\epsilon} + \frac{x_4 - x_3}{\epsilon} - 2\pi \quad (5.16)$$

In phase II where Σ is a connected surface, only $\chi(\Sigma)$ is different and hence

$$\mathcal{C}_{II} = \frac{x_2 - x_1}{\epsilon} + \frac{x_4 - x_3}{\epsilon} + 4 \times \frac{\pi}{2} - 2\pi = \frac{x_2 - x_1}{\epsilon} + \frac{x_4 - x_3}{\epsilon} \quad (5.17)$$

Thus subregion complexity exhibits a discontinuous jump at the transition. It is easy to generalize this result for an arbitrary number of intervals and has been shown in [71], which also considers non-zero temperature.

Volumes in Multiboundary Wormholes:

Let us now consider the multi-boundary wormhole model. We are interested in the evolution of subregion complexity associated with the Hawking radiation during evapora-

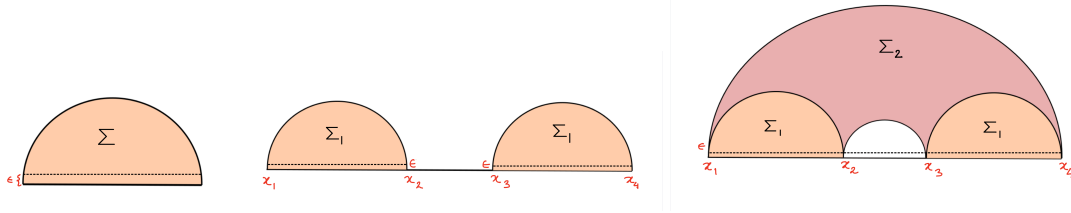


Figure 5.10: HRT surfaces and entanglement wedges in AdS_3 for one (left) and two intervals. The latter has two phases, (middle) Phase I and (right) Phase II.

tion. In the toy model of [110] the evaporation is described by an initial large black hole regurgitating smaller black holes, which represent the Hawking quanta. For simplicity, all such black holes are considered to be placed in their own separate asymptotically-AdS space-time. As the evaporation proceeds, the asymptotically-AdS regions are connected by a wormhole with an increasing number of exits. The subregion we are concerned with is the union of all the smaller exits at one instant of time.

As described in [110] and 5.2.1 above, there are two competing HRT surfaces for the sub-region of our choice, viz. $\cup_{j=2}^n \ell_j$ and L_0 . The corresponding entanglement wedges have been illustrated in figure 5.5. At the Page transition, the entanglement wedge changes which results in a constant shift of complexity.

a) Three boundary model: As explained before, we fix the two smaller boundaries by identifying the pair of geodesics that are not concentric. We assume these two semicircles to be of the same radius in our consideration, as shown in 5.11. In addition, we also assume that the corresponding throat horizons are of the same length. This assumption constrains the choice of parameters in the fundamental domain in a particular way as mentioned in [111, 112]. The relation is between the center of the non-concentric semicircles. Among these two, let the center of the semicircle near $x = 0$ be c_1 and the other one is c_2 . Note that these are the semicircles removed to create a three-boundary wormhole from the two-boundary case. Recall that for the latter, one has to identify two concentric semicircles in

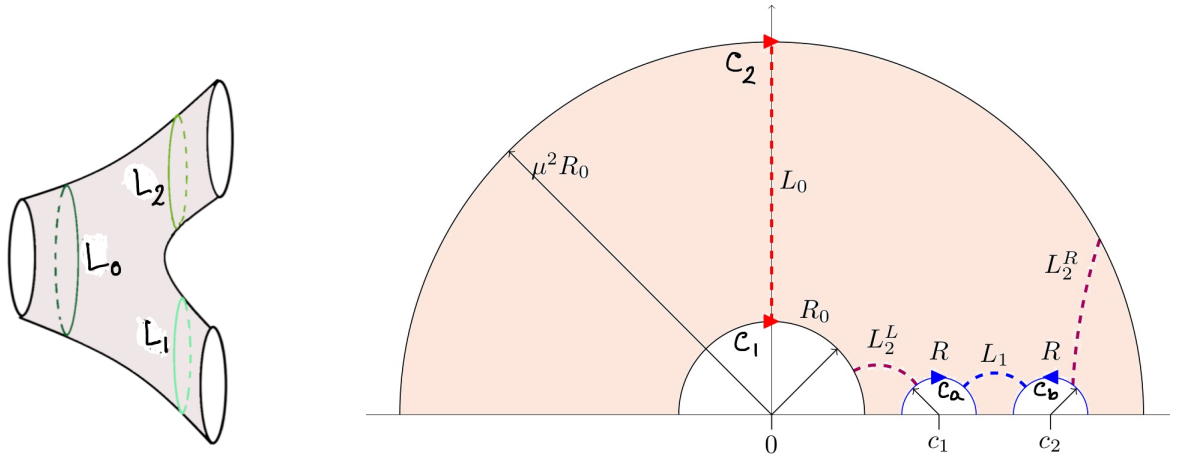


Figure 5.11: Pair of Pants and Polygonal Representation. In the figure, concentric geodesic edges are denoted by C_1 and C_2 , whereas C_a and C_b stand for geodesics that are not concentric. c_1 and c_2 denote the centres of the non-concentric geodesics on the horizontal plane.

the UHP. These two concentric semicircles have their center at $x = 0$ and their radii R_0 and $\mu^2 R_0$ respectively, where $\mu > 1$. For the three-boundary evaporating model, we have $\mu \geq 1$, which saturates at the end of the evaporation process. The relation constrained by the fact that the two throat horizons are of equal length is $c_2 = \mu c_1$. Let us label the radii of these two semicircles as R_1 and R_2 . In this chapter, we work with the particular choice $R_1 = R_2 = R$.⁷ We also make the following choice for c_1 , and thus also for c_2 , motivated by [111],

$$c_1 = \frac{\mu + 1}{2} R_0, \quad c_2 = \mu c_1. \quad (5.18)$$

Our parameter choices secure the positivity of the volumes of the smaller exits for all times, as desired. We should nevertheless keep in mind that among these two equal throat horizons, one is connected whereas the other is disconnected according to the construction, see figure 5.11. Let us call the connected one L_1 and the disconnected one $L_2 = L_2^L + L_2^R =$

⁷In [111], the authors assumed $R_2 = \mu R_1$. But in that case, one ends up with negative volumes for the smaller exits, which is unsatisfying physically.

L_1 , where the superscripts stand for left and right. It is easy to see that once R_0 is specified and we assume that with time L_1 and L_2 increase, while the primarily bigger vertical throat horizon L_0 keeps decreasing via $L'_0 = \sqrt{L_0^2 - 2L_1^2}$, the only time dependence left to be solved for a consistent construction is the time dependence of R . In this case, we replace time by the increasing length L_1 (or equivalently L_2) and plot the volumes with increasing L_1 . There are two solutions of $R = R(L_1)$. Ideally, R should also depend upon μ . But since L'_0 can be written either simply in terms of L_1 or equivalently in terms of μ , there is a relation between these two, $\mu = e^{\frac{\sqrt{L_0^2 - 2L_1^2}}{2}}$, with L_0 chosen to be a constant (the starting length of the vertical throat horizon).

The expressions for L_1 and L_2 are the following once the equality constraint, hyperbolicity condition, and the equation (5.18) are used

$$L_1 = \log \left[\cot \left[\frac{1}{2} \text{Arcsec} \left(\frac{\mu^2 - 1}{\sqrt{(\mu^2 - 1)^2 - 16R^2}} \right) \right] \right] - \log \left[\tan \left[\frac{1}{2} \text{Arcsec} \left(\frac{\mu^2 - 1}{\sqrt{(\mu^2 - 1)^2 - 16R^2}} \right) \right] \right] \quad (5.19)$$

$$L_2 = \log \left[\cot \left[\frac{1}{2} \text{Arcsec} \left(\frac{\mu(\mu^2 - 1) \sqrt{\mu^2 ((\mu^2 - 1)^2 - 16R^2)}}{\mu^6 - 2\mu^4 + \mu^2 - 8(\mu^2 + 1)R^2} \right) \right] \right] - \log \left[\tan \left[\frac{1}{2} \arccos \left(\frac{\mu^5 + \mu - 2\mu^3(4R^2 + 1) - 8\mu R^2}{(\mu^2 - 1) \sqrt{\mu^2 ((\mu^2 - 1)^2 - 16R^2)}} \right) \right] \right] \quad (5.20)$$

Given the above expressions of L_1 and L_2 , we solve for R asking for the linear growth of L_1 so that we can use it as an analog of time.⁸ There are two solutions, both of which

⁸It is important to note that solving this R for given parameter choices is just for exactness and calculation

feature positive volumes for any instance of time, as required by consistency, in particular of the fundamental domain. It is also easy to check that for both of the solutions, L_1 and L_2 are indeed equal to each other.

Just to be precise, let us mention the volumes of the smaller exits at any particular instant in terms of the parameters of the fundamental domain.

$$V_1 = \frac{(c_1 - R - R_0) + (\mu^2 R_0 - c_2 - R)}{\epsilon}, \quad (5.21)$$

and

$$V_2 = \frac{(c_2 - c_1 - 2R)}{\epsilon} \quad (5.22)$$

where ϵ is again a UV cutoff. The total volume is simply $V = V_1 + V_2$. At the Page time, when the minimal surface corresponding to the union of the smaller exits changes from $L_1 + L_2$ to (the decreased) L'_0 , a volume is added to the previous volume V . We will come back to this point in the next subsection and where we present plots of the volumes corresponding to the two solutions of $R = R(L_1)$.

b) $n + 1$ -boundary model: This is a good time to explain how we wish to perceive black hole evaporation á la [110] from the quotient perspective with more details about the explicit construction. Recall figure 5.4. We start with three exits and at each time-step include two more geodesics with opposite orientations, which upon identification provide a new boundary. For simplicity, we consider all semicircles to have the same radius at any moment. The radius is thus a function of the number of exits, which is an analog of discretized time.

The moduli space of an $n + 1$ -boundary wormhole contains $n + 1$ physical parame-

of volume. In general, for any constant or functional dependence of R , L_1 and L_2 , although they look different, scale in the exact similar way with μ .

ters that characterize the system. These are the periodic geodesics between two identified semicircles in our quotient picture. Consider the 3-boundary construction in figure 5.11. The dashed lines denote the geodesics which after performing proper identification become closed and the metric outside the causal development of these closed curves is the BTZ metric [135]. Thus the periodic geodesics can be identified as black hole horizons and in fact, constitute the candidate HRT surfaces in the evaporation model. In figure 5.11 we have denoted the identification of each geodesic with the corresponding BH horizon for the 3-boundary wormhole.

The sub-region complexity is essentially determined by the volume under the horizons. Before Page time, it is the volume under $\cup_{j=2}^n \ell_j$ while after Page time it is that under L'_0 as marked in figure 5.5. The explicit formulae for the volumes are given below. Here we only point out that they depend on the radii of the semicircles and the length of the horizons. The horizon lengths are in general difficult to compute, the authors of [132] provide two of the three lengths for the 3-boundary wormhole

$$L_0 = L \log(\mu^2), \quad (5.23)$$

$$L_1 = 2L \operatorname{arcsinh} \left[\sqrt{\left(\frac{d}{R}\right)^2 - 1} \right], \quad (5.24)$$

but an analytic answer for $L_2 = L_2^L \cup L_2^R$ remains elusive. Here L is the AdS radius and d is the distance between the centers of the orientation reversed semicircles, other parameters are explained in figure 5.11. After identification, L_0 becomes the horizon of the parent black hole. Throughout the calculation, we shall follow the footsteps of [110] and assume all smaller horizons have equal length L_1 .

In our model, we demand that all smaller semicircles have identical radii, R , at any

moment in time. Since we accommodate an increasing number of semicircles, hence also boundaries, in the same region as time progresses, R cannot remain constant. Also, starting from the three-boundary wormhole, as we increase the number of boundaries, the distance (say d_1) between the centers of the semicircles are managed in a way to make sure that all the other disconnected throat horizons, except for the one that is attached to the concentric semicircles, have the same length as the connected one between the first set of orientation reversed semicircles. Therefore, in our model, we make sure that out of the $(n - 1)$ smaller exits, $(n - 2)$ have the same horizon length and only the remaining one is assumed to have constrained equality. There is no way to fix the time dependence of R explicitly. We can however assert that it must satisfy the constraint

$$R(n) < \frac{(\mu^2(n) - 1)}{4(n - 1)} R_0, \quad (5.25)$$

where n denotes the number of smaller exits. This constraint makes sure that the adequate number of semicircles are accommodated within the interval $(\mu^2(n) - 1) R_0$.

Choosing a good function, one that satisfies (5.25), we can determine the volume and complexity through the help of (5.23). As we will see, it exhibits a finite discontinuity at the Page transition. The source of this discontinuity is purely topological, which we explain in section 5.4.1. Thereafter we give explicit formulae for the volumes and show complete evolution of complexity during the entire evaporation process.

Gauss-Bonnet & hyperbolic polygons

As explained in subsection 5.4.1, the Gauss-Bonnet theorem plays a central role in the calculations of volumes in AdS_3 . Here, we discuss another consequence of the Gauss-Bonnet theorem (5.13), which regards the computation of the area of hyperbolic triangles.

Corollary 2. *Consider a $2d$ hyperbolic surface. Let it be tessellated by triangles with*

angles $(\alpha, \beta, \gamma) = \left(\frac{2\pi}{p}, \frac{2\pi}{q}, \frac{2\pi}{r}\right)$. Then the Gauss-Bonnet theorem along with the triangle group imply the following relation

$$\frac{\pi}{p} + \frac{\pi}{q} + \frac{\pi}{r} < \pi. \quad (5.26)$$

The area of the hyperbolic triangle, therefore, becomes $|(\pi - \alpha - \beta - \gamma)|L^2$, where L stands for an intrinsic length scale, which is the AdS radius.

We choose $L = 1$ for the remainder of this section. Next, we aim for the computation of the volumes⁹ of the different kinds of causal shadow regions that crossed our way when contemplating multi-boundary wormholes. As explained previously, these regions correspond to the analog of islands in our models. In the following, we describe a simple way to compute such volumes in two-dimensional hyperbolic space. In the following, we will only make use of the above-mentioned area of a hyperbolic triangle to compute the area of any hyperbolic polygon in two-dimensional hyperbolic space.

A general look into causal shadows: Let us first point out to the reader that the causal shadow volumes that are added to the entanglement wedge of the radiation subsystem after the Page time, both in the case of the three-boundary as well as the $n + 1$ -boundary model, are hyperbolic polygons in general.

For the three-boundary case, the region is a hyperbolic octagon, whereas, for the n -boundary scenario, the region is a hyperbolic $4n_{Page}$ -gon. n_{Page} stands for the n -value at which the Page transition, or in case of volume, the wheel-eyeglass phase transition [136], occurs.

Therefore, the first thing to understand is that in the case of the $n + 1$ -boundary model,

⁹Strictly speaking, our volumes are of course areas, but we stick with conventional terminology of higher-dimensional geometries.

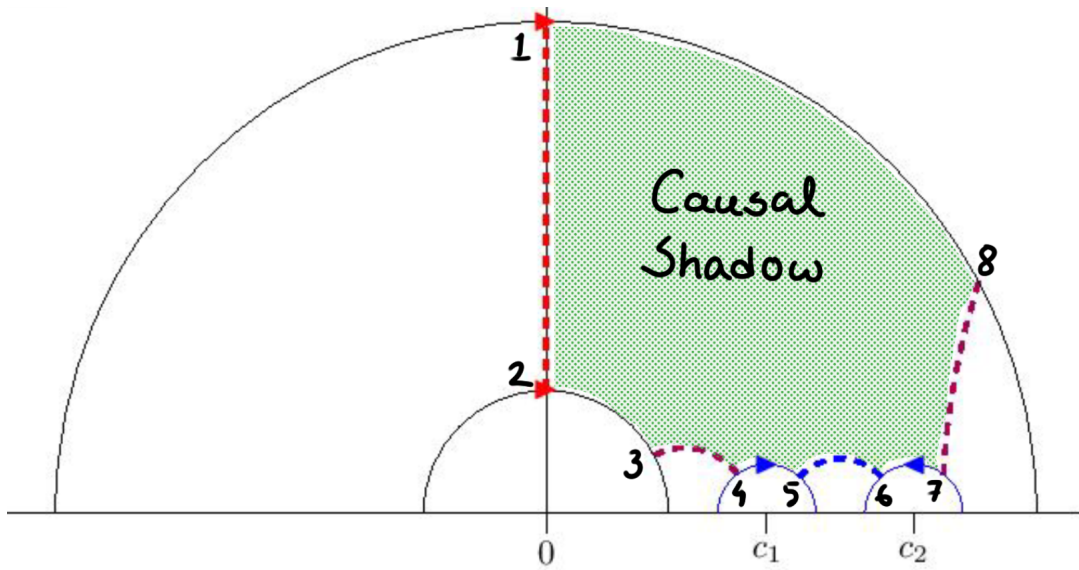


Figure 5.12: Hyperbolic octagon and Causal Shadow in three-boundary wormhole model.

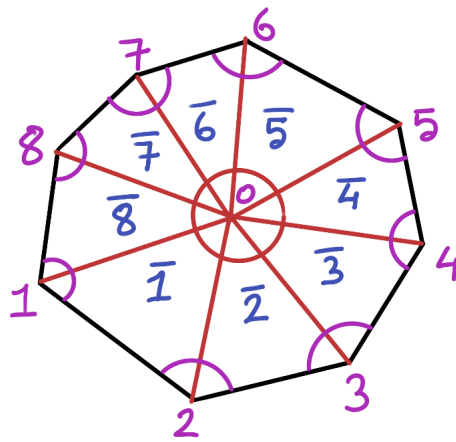


Figure 5.13: Hyperbolic octagon through hyperbolic triangles.

the structure of the causal shadow depends upon the Page time. Now, let us understand the volumes of general hyperbolic polygons in terms of hyperbolic triangles. Firstly, we discuss the three-boundary causal shadow and then generalize it to a general number of boundaries.

Hyperbolic octagon: First, we discuss the three-boundary case. In this case, as mentioned in 5.4.1, the minimal surface change gives an additional contribution to the volume of the radiation subsystem. Now, from the Figure 5.12, we can see that this is the causal shadow region. For the three-boundary case, as has been marked in the figure, eight vertices are constructing a hyperbolic polygon. In general, it can have any volume depending on the nature of the edges of the polygon. However, in our case, we easily see that at each vertex at least one of its edges is always a geodesic (throat horizon) in the fundamental domain of the three-boundary wormhole. Now, any bulk curve or geodesic in the fundamental domain is bound to hit the boundary of the domain with a corner angle $\frac{\pi}{2}$.¹⁰

Knowing the corner angles, we can use the formula for the area of the hyperbolic triangle in computing the area of the hyperbolic octagon by dividing it into eight triangles as shown in Figure 5.13.

The vertices of the octagon are marked by the numbers $i = 1, 2, \dots, 8$ and the eight triangles that we divide this octagon into have a common vertex 0. The sum of all angles joined at the center 0, we call these $\angle i0j$ with $i, j = 1, 2, \dots, 8$, is of course 2π . This allows for a simple derivation of the octagon's volume,

$$\begin{aligned} \text{Area of the octagon}(\Delta V_{(3)}) &= \sum_{i,j(i \neq j)} \Delta(i0j) = \sum_{\bar{I}} \Delta(\bar{I}) , (\bar{I} = 1, 2, \dots, 8) \\ &= 8\pi - \sum_{i,j(i \neq j)} \angle i0j - \sum \text{Corner angles} = 8\pi - 2\pi - (8 \times \frac{\pi}{2}) = 2\pi. \quad (5.27) \end{aligned}$$

Hence, the area of the hyperbolic octagon is constant in our case and the volume experiences a jump of 2π at the Page transition (wheel-eyeglass phase transition). In Figure

¹⁰Another way of understanding these bulk geodesics and the corner angles is as entanglement wedge cross-sections as pointed out in [9, 70] and as proved in [137] using Klein coordinates.

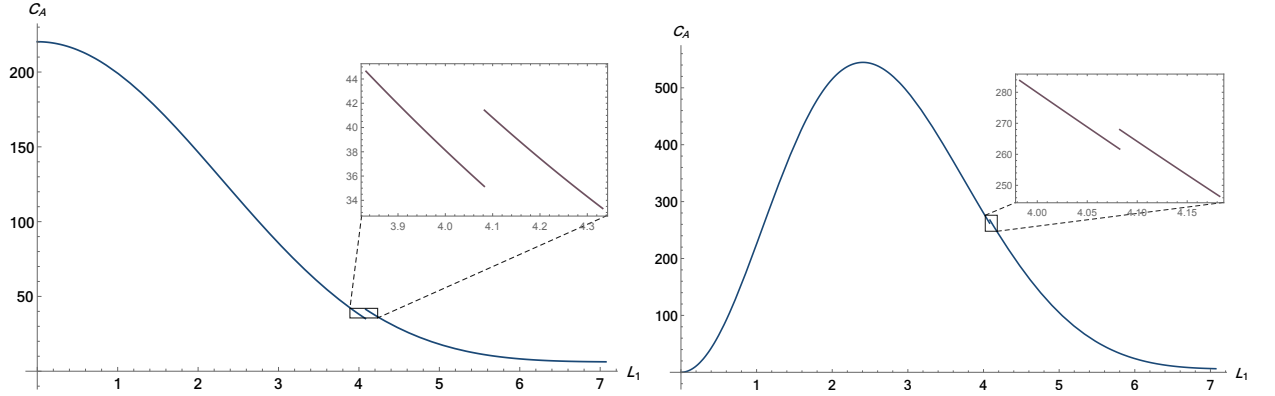


Figure 5.14: Complexity plots of 3 boundary island model for two solutions of R

5.14, we have shown the volume vs time plots for the two solutions of R (time-dependent radius of the non-concentric pair of semicircles) as mentioned in 5.4.1.

Hyperbolic m -gon: Now we generalize our previous computation for any general m -gon of the given kind, i.e; the corner angles being $\frac{\pi}{2}$. In this case as it turns out again, we can divide it into m hyperbolic triangles and the area simply becomes,

$$\text{Area of } m\text{-gon} = m\pi - 2\pi - m\frac{\pi}{2} = \pi\left(\frac{m}{2} - 2\right). \quad (5.28)$$

Now for a given $n + 1$ -boundary wormhole, we find that the value of m becomes $m = 4n$. Therefore, for the $n + 1$ -boundary wormhole, the volume that is added at the Page transition becomes,

$$\text{Jump in volume: } \Delta V_{(n)} = [2(n_{Page} - 1) - 2]\pi = (2n_{Page} - 4)\pi. \quad (5.29)$$

Hence, we find that for the $n + 1$ -boundary model, the jump in volume depends on the Page time whereas, for the three-boundary model, it does not. For the three-boundary case, there is no topology change in the process of evaporation and therefore, the previous result,

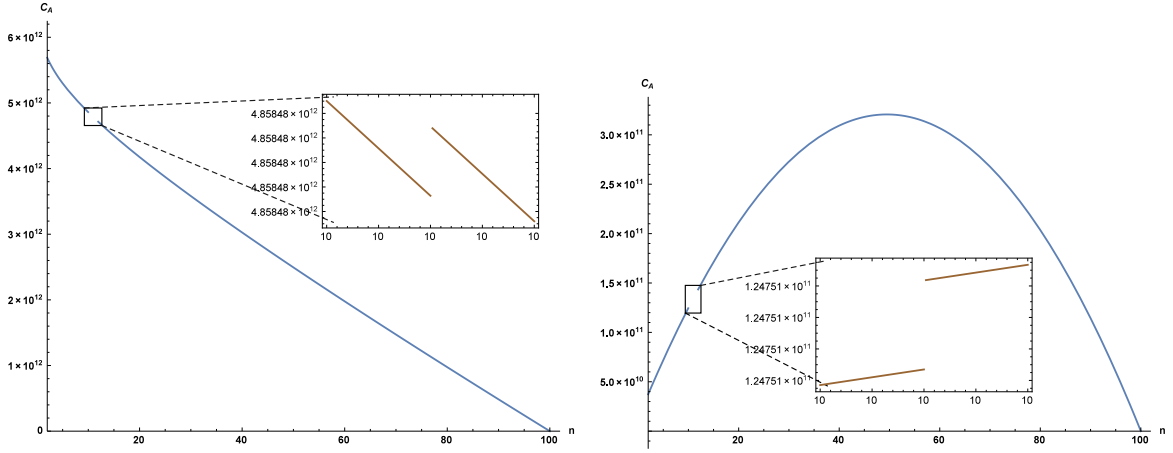


Figure 5.15: Complexity plots of $n + 1$ boundary island model for two choices of R .

2π , is recovered by setting $n_{Page} = 3$.

The full evolution of holographic complexity during the evaporation is illustrated in figure 5.15 for two different choices of $R(n)$, both of which obey (5.25). While there exists a large pool of choices for $R(n)$ producing distinct plots, we emphasize that all of them have similar qualitative features as either of our two choices for $R(n)$,

$$\begin{aligned}
 R_a(n) &= \frac{100 - n}{(2n + 2)^{1.05}} \\
 R_b(n) &= (100 - n) \times 10^{-3}
 \end{aligned}
 \tag{5.30}$$

Indeed, our choices seem to have been conjured out of the blue. They are not completely ad-hoc, though. While certainly not unique; these are two of the many choices which ensure that at any moment all circles can be sufficiently accommodated in the fundamental domain as well as generate physically meaningful plots of the volume. In absence of any true analytical time-dependence of R , these are our best guides to fix a meaningful evolution of complexity. Further, we assumed that the disconnected throat horizons were equally divided into two halves with each of them having length $\frac{L_1}{2}$, where L_1 is the length

of the solely connected horizon and we have already assumed all horizons to have the same length. Under these assumptions and with the help of equations (5.23) and (5.24), we can express the volume associated with each smaller horizon as

$$V_{initial} = \frac{4(n-1) \left(\cosh\left(\frac{\ell}{4}\right) - 1 \right) R(n)}{\epsilon} + \frac{2 \left(\cosh\left(\frac{\ell}{2}\right) - 1 \right) R(n)}{\epsilon} \quad (5.31)$$

This is the volume that goes into the complexity before Page time, after the Page transition there's a constant addition (5.29) to the volume. The figures clearly display these required features.

5.5 Results

In this chapter, we have discussed the details of the recent progress concerning the black hole information paradox and Page curve. Then we have discussed the MbW models that mimic the evaporating BH vs radiation scenario. We have drawn connections between the $(n+1)$ boundary model and the multipartite EoP building on [9]. The boundary of the analog islands is seen to be dual to the multipartite EoP after Page time. However, applying the island formula naively lands one into the paradox once more where the multipartite entanglement keeps growing. Therefore, it is instructive to take proper limits at which bipartite entanglement dominates, and then we get the correct Page curve.

For the volumes, which are supposed to represent the sub-region complexity of the radiation state [10], we get two candidate curves for both the three and $(n+1)$ boundary models. In this case, there is a jump at Page time for both the candidate curves and the jump is argued to be dual to the complexity of purification (CoP). The idea is that due to the purification of Hawking quanta at Page time, there are extra gates needed to radiation state at Page time. Same jump was found to be multi-partite CoP in the studies [138, 139].

We discuss these implications in a more detailed fashion in the next chapter.

DETAILS OF EMBEDDING FUNCTIONS
FOR CHARGED AND UNCHARGED ADS
BH

A.1 Uncharged BH Embedding

The second-order embedding functions $y_2(x)$ in dimensions 3 to 7 are

$$y_2^{\text{AdS}_3}(x) = \frac{\sqrt{1-x^2}}{360} (48 - 32x^2 + 3x^4), \quad (\text{A.1})$$

$$y_2^{\text{AdS}_4}(x) = \frac{\sqrt{1-x^2}}{4480} (513 - 771x^2 + 346x^4 - 40x^6) + \frac{3}{140} \left(\frac{\ln(1 + \sqrt{1-x^2})}{\sqrt{1-x^2}} - 1 \right), \quad (\text{A.2})$$

$$y_2^{\text{AdS}_5}(x) = \frac{(1-x^2)^{3/2}}{4200} (376 - 592x^2 + 267x^4 - 35x^6), \quad (\text{A.3})$$

$$y_2^{\text{AdS}_6}(x) = \frac{\sqrt{1-x^2}}{66528x^2} (320 - 4935x^2 + 18045x^4 - 24469x^6 + 15607x^8 - 4592x^{10} + 504x^{12}) + \frac{10}{2079} \left(\frac{1}{x^2} + 2 - \frac{3 \ln(1 + \sqrt{1-x^2})}{\sqrt{1-x^2}} \right), \quad (\text{A.4})$$

$$y_2^{\text{AdS}_7}(x) = \frac{(1-x^2)^{5/2}}{168168} (11140 - 28356x^2 + 25227x^4 - 9006x^6 + 1155x^8). \quad (\text{A.5})$$

The inverse relations require us to define the variable $u = y/y(0)$:

$$x_2^{\text{AdS}_3}(u) = \frac{\sqrt{1-u^2}}{40} (3u^4 + 4u^2 + 8), \quad (\text{A.6})$$

$$x_2^{\text{AdS}_4}(u) = \frac{\sqrt{1-u^2}}{4480(1+u)^2} (240u^8 + 480u^7 + 639u^6 + 798u^5 + 634u^4 + 890u^3 + 1122u^2 + 1310u + 703) + \frac{3}{140\sqrt{1-u^2}} \ln\left(\frac{1+u}{2}\right), \quad (\text{A.7})$$

$$x_2^{\text{AdS}_5}(u) = \frac{\sqrt{1-u^2}}{4200} (175u^8 + 328u^6 + 228u^4 + 380u^2 + 464), \quad (\text{A.8})$$

$$\begin{aligned}
x_2^{\text{AdS}_6}(u) &= \frac{\sqrt{1-u^2}}{66528(1+u)^2} (2268u^{12} + 4536u^{11} + 6853u^{10} + 9170u^9 + 8046u^8 + 6922u^7 \\
&\quad + 5838u^6 + 7526u^5 + 9294u^4 + 10138u^3 + 11222u^2 + 11666u + 5353) \\
&\quad - \frac{10}{693\sqrt{1-u^2}} \ln\left(\frac{1+u}{2}\right), \tag{A.9}
\end{aligned}$$

$$\begin{aligned}
x_2^{\text{AdS}_7}(u) &= \frac{\sqrt{1-u^2}}{168168} (4851u^{12} + 10332u^{10} + 8196u^8 + 6180u^6 + 9452u^4 \\
&\quad + 11168u^2 + 12884). \tag{A.10}
\end{aligned}$$

Note that $y(0)$ is the turning point of the RT surface in the bulk. The point of defining u is to impose the boundary condition $x(u = 1) = 0$. Now, we present the third-order embedding functions only in the $y(x)$ parametrization:

$$y_3^{\text{AdS}_3}(x) = \frac{\sqrt{1-x^2}}{15120} (3x^6 - 46x^4 + 584x^2 - 816), \tag{A.11}$$

$$\begin{aligned}
y_3^{\text{AdS}_4}(x) &= \frac{3}{280} (1-x^2)^{3/2} + \frac{(1-x^2)}{2508800} (1400x^8 - 13055x^6 + 89470x^4 - 204924x^2 + 128544) \\
&\quad + \frac{3}{560} (3x^2 - 4) \ln(1 + \sqrt{1-x^2}) - \frac{3}{280} \left(\frac{\ln(1 + \sqrt{1-x^2})}{\sqrt{1-x^2}} - 1 \right), \tag{A.12}
\end{aligned}$$

$$\begin{aligned}
y_3^{\text{AdS}_5}(x) &= \frac{(1-x^2)^{3/2}}{30030000} (21175x^{10} - 193940x^8 + 1106251x^6 - 2993238x^4 \\
&\quad + 3441368x^2 - 1405296), \tag{A.13}
\end{aligned}$$

$$\begin{aligned}
y_3^{\text{AdS}_6}(x) &= \frac{1-x^2}{684972288x^2} (513513x^{16} - 5481333x^{14} + 32079432x^{12} - 109571268x^{10} \\
&\quad + 211009892x^8 - 225264756x^6 + 128106720x^4 - 37981640x^2 + 2196480) \\
&\quad - \frac{10\sqrt{1-x^2}}{6237} (3x^6 - 4x^4 - 7x^2 + 2) + \frac{10(1-x^2)}{2079} (3-2x^2) \ln(1+\sqrt{1-x^2}) \\
&\quad + \frac{40}{2079} \left(\frac{\ln(1+\sqrt{1-x^2})}{\sqrt{1-x^2}} - 1 \right), \tag{A.14}
\end{aligned}$$

$$\begin{aligned}
y_3^{\text{AdS}_7}(x) &= \frac{(1-x^2)^{5/2}}{760455696} (569415x^{14} - 5926650x^{12} + 32824206x^{10} - 109100880x^8 \\
&\quad + 208361675x^6 - 222638554x^4 + 124255928x^2 - 28455732). \tag{A.15}
\end{aligned}$$

We are able to give the exact embedding for the AdS₃ BH. This is given by

$$y^{\text{AdS}_3}(x) = \frac{1}{\sqrt{\lambda}} \sqrt{1 - \frac{\cosh^2(x\sqrt{\lambda})}{\cosh^2(\sqrt{\lambda})}}. \tag{A.16}$$

The perturbative expansion of this around $\lambda = 0$ up to third order precisely gives the AdS₃ second- and third-order results given above.

A.2 Charged BH Embedding

The $(2d-2)$ -order embedding functions $y_{(0,1)}(x)$ in dimensions 4 to 7 are

$$y_{(0,1)}^{\text{AdS}_4}(x) = \frac{1}{30} p^2 \left[\sqrt{1-x^2} (3x^4 - 8x^2 + 9) + 8 \left(\frac{\ln(1+\sqrt{1-x^2})}{\sqrt{1-x^2}} - 1 \right) \right], \tag{A.17}$$

$$y_{(0,1)}^{\text{AdS}_5}(x) = \frac{1}{70} p^2 (1-x^2)^{\frac{3}{2}} (5x^4 - 13x^2 + 11), \tag{A.18}$$

$$\begin{aligned}
y_{(0,1)}^{\text{AdS}_6}(x) &= \frac{1}{315}p^2 \left[\frac{\sqrt{1-x^2}}{2x^2} (35x^{10} - 160x^8 + 286x^6 - 240x^4 + 63x^2 - 32) \right. \\
&\quad \left. + 16 \left(\frac{1}{x^2} + 2 - \frac{3 \ln(1 + \sqrt{1-x^2})}{\sqrt{1-x^2}} \right) \right], \tag{A.19}
\end{aligned}$$

$$y_{(0,1)}^{\text{AdS}_7}(x) = -\frac{p^2}{4158} (1-x^2)^{\frac{5}{2}} (189x^6 - 672x^4 + 852x^2 - 409). \tag{A.20}$$

The $(3d-2)$ -order embedding functions $y_{(1,1)}(x)$ in dimensions 4 to 7 are

$$\begin{aligned}
y_{(1,1)}^{\text{AdS}_4}(x) &= \frac{p^2(1+p^2)}{15} \left[2(1-x^2)^{\frac{3}{2}} + \frac{1-x^2}{480} (135x^6 - 990x^4 + 2328x^2 - 1568) \right. \\
&\quad \left. + 2 \left(1 - \frac{\ln(1 + \sqrt{1-x^2})}{\sqrt{1-x^2}} \right) + (3x^2 - 4) \ln(1 + \sqrt{1-x^2}) \right], \tag{A.21}
\end{aligned}$$

$$\begin{aligned}
y_{(1,1)}^{\text{AdS}_5}(x) &= -\frac{p^2(1+p^2)}{23100} (1-x^2)^{\frac{3}{2}} (405x^8 - 3020x^6 + 7833x^4 - 9199x^2 + 4261) \\
&\tag{A.22}
\end{aligned}$$

$$\begin{aligned}
y_{(1,1)}^{\text{AdS}_6}(x) &= \frac{p^2(1+p^2)}{945} \left[-\frac{16\sqrt{1-x^2}}{x^2} (3x^6 - 4x^4 - 7x^2 + 2) \right. \\
&\quad - \frac{1-x^2}{9240} (138600x^{12} - 1258950x^{10} + 4551330x^8 - 8660015x^6 + 9241635x^4 \\
&\quad \quad - 5719176x^2 + 2593616) + 48(1-x^2)(3-2x^2) \ln(1 + \sqrt{1-x^2}) \\
&\quad \left. + 32 \left(\frac{1}{x^2} - 7 + \frac{6 \ln(1 + \sqrt{1-x^2})}{\sqrt{1-x^2}} \right) \right], \tag{A.23}
\end{aligned}$$

$$y_{(1,1)}^{\text{AdS}_7}(x) = -\frac{p^2(1+p^2)}{989604} (1-x^2)^{\frac{5}{2}} \left(14175x^{12} - 125832x^{10} + 447405x^8 - 837755x^6 + 887386x^4 - 510857x^2 + 127526 \right). \quad (\text{A.24})$$

As we can see by looking at these embedding functions, $y_{(0,1)}(x)$ always carries the pre-factor p^2 with it whereas $y_{(1,1)}(x)$, being a mixing of orders d and $(2d-2)$, consistently carries a pre-factor $p^2(1+p^2)$ along with it. In our plots of the embedding functions, we plot the functions of x apart from these pre-factors. If one wishes to get the exact rescaled plots for some particular p , these plots will be rescaled with these respective pre-factors.

We also have the inverse forms of these embedding functions. But we do not present them as they are very big expressions and we do not necessarily need them. The results were reproduced using the inverse embedding functions as well and were unchanged.

A.3 Fourth-Order Change in Entanglement Entropy

The fourth-order change in HEE is given by

$$\begin{aligned} \Delta s^{(4)} &= (s_{0,1111} + s_{1,111} + s_{2,11} + s_{3,1} + s_{4,0}) + (s_{0,22} + s_{0,112} + s_{1,12} + s_{2,2}) \\ &\quad + (s_{0,13} + s_{1,3}) + s_{0,4} \\ &= (s_{0,1111} + s_{1,111} + s_{2,11} + s_{3,1} + s_{4,0}) - s_{0,22}, \end{aligned} \quad (\text{A.25})$$

where the contribution of y_4 and y_3 vanish by virtue of the Euler-Lagrange equations for y_0 and y_1 , respectively. Furthermore, and the contribution of y_2 simplifies significantly by virtue of the Euler-Lagrange equation for y_2 itself. These simplifications are discussed and proven in Section 3.2.3.

Despite the simplifications, this still depends explicitly on y_2 . Since we are unable to perform the requisite integrals using the general form of y_2 as a function of d given in (3.19), we have to infer the general formula for $\Delta S^{(4)}$ from results at specific values of d . In general, this is a difficult task and we cannot yet give a general formula for $\Delta S^{(4)}$. Nevertheless, we give the values of $\Delta S^{(4)}$ for AdS₃ to AdS₇ below.

AdS _{$d+1$}	$\Delta S^{(4)}$ (in units of $2\pi\Omega_{d-2}\left(\frac{L}{\ell_P}\right)^{d-1}m^4R^{4d}$)
AdS ₃	$-\frac{1}{37800}$
AdS ₄	$\frac{643689}{3139136000} - \frac{9\ln 2}{19600}$
AdS ₅	$-\frac{213784}{3350221875}$
AdS ₆	$\frac{5(-824827123+931170240\ln 2)}{33539518244232}$
AdS ₇	$-\frac{54651392}{5471241090315}$

Note that, just like $\Delta S^{(2)}$ and $\Delta S^{(3)}$, we find that $\Delta S^{(4)}$ is also of fixed sign. In this case, $\Delta S^{(4)}$ is negative. This suggests that the change in HEE is of fixed sign at each order and it appears to alternate from positive to negative at odd and even orders, respectively. There may be interesting physics underlying this observation, which we postpone to future investigation.

BIBLIOGRAPHY

- [1] J. M. Maldacena, *The Large N limit of superconformal field theories and supergravity*, *Int. J. Theor. Phys.* **38** (1999) 1113–1133, [hep-th/9711200].
- [2] S. Ryu and T. Takayanagi, *Holographic derivation of entanglement entropy from AdS/CFT*, *Phys. Rev. Lett.* **96** (2006) 181602, [hep-th/0603001].
- [3] S. Ryu and T. Takayanagi, *Aspects of Holographic Entanglement Entropy*, *JHEP* **08** (2006) 045, [hep-th/0605073].
- [4] M. Alishahiha, *Holographic Complexity*, *Phys. Rev. D* **92** (2015) 126009, [1509.06614].
- [5] A. Bhattacharya, K. T. Grosvenor and S. Roy, *Entanglement Entropy and Subregion Complexity in Thermal Perturbations around Pure-AdS Spacetime*, *Phys. Rev. D* **100** (2019) 126004, [1905.02220].
- [6] A. Bhattacharya and S. Roy, *Holographic entanglement entropy and entanglement thermodynamics of ‘black’ non-susy D3 brane*, *Phys. Lett. B* **781** (2018) 232–237, [1712.03740].

- [7] A. Bhattacharya and S. Roy, *Holographic entanglement entropy, subregion complexity and Fisher information metric of ‘black’ non-susy D3 brane*, *Phys. Lett. B* **800** (2020) 135032, [1807.06361].
- [8] D. Allahbakhshi, M. Alishahiha and A. Naseh, *Entanglement Thermodynamics*, *JHEP* **08** (2013) 102, [1305.2728].
- [9] A. Bhattacharya, *Multipartite purification, multiboundary wormholes, and islands in AdS_3/CFT_2* , *Phys. Rev. D* **102** (2020) 046013, [2003.11870].
- [10] A. Bhattacharya, A. Chanda, S. Maulik, C. Northe and S. Roy, *Topological shadows and complexity of islands in multiboundary wormholes*, [2010.04134].
- [11] A. R. Brown, D. A. Roberts, L. Susskind, B. Swingle and Y. Zhao, *Holographic Complexity Equals Bulk Action?*, *Phys. Rev. Lett.* **116** (2016) 191301, [1509.07876].
- [12] E. Witten, *Anti-de Sitter space and holography*, *Adv. Theor. Math. Phys.* **2** (1998) 253–291, [hep-th/9802150].
- [13] A. V. Ramallo, *Introduction to the AdS/CFT correspondence*, *Springer Proc. Phys.* **161** (2015) 411–474, [1310.4319].
- [14] V. E. Hubeny, *The AdS/CFT Correspondence*, *Class. Quant. Grav.* **32** (2015) 124010, [1501.00007].
- [15] N. Kajuri, *Lectures on Bulk Reconstruction*, *SciPost Phys. Lect. Notes* **22** (2021) 1, [2003.00587].

- [16] J. M. Maldacena, *Eternal black holes in anti-de Sitter*, *JHEP* **04** (2003) 021, [hep-th/0106112].
- [17] M. Ammon and J. Erdmenger, *Gauge/gravity duality: Foundations and applications*. Cambridge University Press, Cambridge, 4, 2015.
- [18] J. Erdmenger, *Introduction to Gauge/Gravity Duality*, *PoS TASI2017* (2018) 001, [1807.09872].
- [19] V. E. Hubeny, M. Rangamani and T. Takayanagi, *A Covariant holographic entanglement entropy proposal*, *JHEP* **07** (2007) 062, [0705.0016].
- [20] A. Lewkowycz and J. Maldacena, *Generalized gravitational entropy*, *JHEP* **08** (2013) 090, [1304.4926].
- [21] T. Faulkner, A. Lewkowycz and J. Maldacena, *Quantum corrections to holographic entanglement entropy*, *JHEP* **11** (2013) 074, [1307.2892].
- [22] N. Engelhardt and A. C. Wall, *Quantum Extremal Surfaces: Holographic Entanglement Entropy beyond the Classical Regime*, *JHEP* **01** (2015) 073, [1408.3203].
- [23] L. Susskind, *Computational Complexity and Black Hole Horizons*, *Fortsch. Phys.* **64** (2016) 24–43, [1403.5695].
- [24] A. R. Brown, D. A. Roberts, L. Susskind, B. Swingle and Y. Zhao, *Complexity, action, and black holes*, *Phys. Rev. D* **93** (2016) 086006, [1512.04993].
- [25] M. A. Nielsen, M. R. Dowling, M. Gu and A. C. Doherty, *Quantum Computation as Geometry*, *Science* **311** (Feb, 2006) 1133–1135, [quant-ph/0603161].

- [26] S. Chapman, M. P. Heller, H. Marrochio and F. Pastawski, *Toward a definition of complexity for quantum field theory states*, *Phys. Rev. Lett.* **120** (2018) 121602, [1707.08582].
- [27] R. Jefferson and R. C. Myers, *Circuit complexity in quantum field theory*, *JHEP* **10** (2017) 107, [1707.08570].
- [28] H. A. Camargo, P. Caputa, D. Das, M. P. Heller and R. Jefferson, *Complexity as a novel probe of quantum quenches: universal scalings and purifications*, *Phys. Rev. Lett.* **122** (2019) 081601, [1807.07075].
- [29] A. Bhattacharyya, T. Takayanagi and K. Umemoto, *Universal Local Operator Quenches and Entanglement Entropy*, *JHEP* **11** (2019) 107, [1909.04680].
- [30] T. Ali, A. Bhattacharyya, S. S. Haque, E. H. Kim, N. Moynihan and J. Murugan, *Chaos and Complexity in Quantum Mechanics*, *Phys. Rev. D* **101** (2020) 026021, [1905.13534].
- [31] H. Araki and E. H. Lieb, *Entropy inequalities*, *Communications in Mathematical Physics* **18** (June, 1970) 160–170.
- [32] M. Nielsen and I. Chuang, *Quantum computation and quantum information*. Cambridge University Press, 2010.
- [33] E. H. Lieb and M. B. Ruskai, *A Fundamental Property of Quantum-Mechanical Entropy*, *Phys. Rev. Lett.* **30** (1973) 434–436.
- [34] J. Kiefer, *Optimum experimental designs*, *Journal of the Royal Statistical Society: Series B (Methodological)* **21** 272–304.

- [35] M. Rangamani and T. Takayanagi, *Holographic entanglement entropy*, *Lecture Notes in Physics* (2017) .
- [36] M. Srednicki, *Entropy and area*, *Phys. Rev. Lett.* **71** (1993) 666–669, [hep-th/9303048].
- [37] P. Calabrese and J. L. Cardy, *Entanglement entropy and quantum field theory*, *J. Stat. Mech.* **0406** (2004) P06002, [hep-th/0405152].
- [38] P. Calabrese and J. L. Cardy, *Entanglement entropy and quantum field theory: A non-technical introduction*, *Int. J. Quant. Inf.* **4** (2006) 429, [quant-ph/0505193].
- [39] H. Casini and M. Huerta, *A Finite entanglement entropy and the c-theorem*, *Phys. Lett. B* **600** (2004) 142–150, [hep-th/0405111].
- [40] H. Casini and M. Huerta, *Universal terms for the entanglement entropy in 2+1 dimensions*, *Nucl. Phys. B* **764** (2007) 183–201, [hep-th/0606256].
- [41] M. Cramer, J. Eisert, M. B. Plenio and J. Dreissig, *An Entanglement-area law for general bosonic harmonic lattice systems*, *Phys. Rev. A* **73** (2006) 012309, [quant-ph/0505092].
- [42] M. B. Plenio, J. Eisert, J. Dreissig and M. Cramer, *Entropy, entanglement, and area: analytical results for harmonic lattice systems*, *Phys. Rev. Lett.* **94** (2005) 060503, [quant-ph/0405142].
- [43] M. M. Wilde, *Quantum Information Theory*. Cambridge University Press, USA, 1st ed., 2013.

- [44] A. Bhattacharyya, T. Takayanagi and K. Umemoto, *Entanglement of Purification in Free Scalar Field Theories*, *JHEP* **04** (2018) 132, [1802.09545].
- [45] A. Bhattacharyya, A. Jahn, T. Takayanagi and K. Umemoto, *Entanglement of Purification in Many Body Systems and Symmetry Breaking*, *Phys. Rev. Lett.* **122** (2019) 201601, [1902.02369].
- [46] B. M. Terhal, M. Horodecki, D. W. Leung and D. P. DiVincenzo, *The entanglement of purification*, *Journal of Mathematical Physics* **43** (Sept., 2002) 4286–4298, [quant-ph/0202044].
- [47] S. Bagchi and A. K. Pati, *Monogamy, polygamy, and other properties of entanglement of purification*, **91** (Apr., 2015) 042323, [1502.01272].
- [48] Y. Guo and L. Zhang, *Multipartite entanglement measure and complete monogamy relation*, **101** (Mar., 2020) 032301, [1908.08218].
- [49] R. Horodecki, P. Horodecki, M. Horodecki and K. Horodecki, *Quantum entanglement*, *Reviews of Modern Physics* **81** (Apr., 2009) 865–942, [quant-ph/0702225].
- [50] D. Yang, K. Horodecki, M. Horodecki, P. Horodecki, J. Oppenheim and W. Song, *Squashed entanglement for multipartite states and entanglement measures based on the mixed convex roof*, *arXiv e-prints* (Apr., 2007) arXiv:0704.2236, [0704.2236].
- [51] D. Avis, P. Hayden and I. Savov, *Distributed compression and multiparty squashed entanglement*, *Journal of Physics A Mathematical General* **41** (Mar., 2008) 115301, [0707.2792].

- [52] M. R. Dowling and M. A. Nielsen, *The geometry of quantum computation*, *arXiv e-prints* (Dec, 2006) quant-ph/0701004, [quant-ph/0701004].
- [53] M. A. Nielsen, *A geometric approach to quantum circuit lower bounds*, *arXiv preprint quant-ph/0502070* (2005) .
- [54] R. Khan, C. Krishnan and S. Sharma, *Circuit Complexity in Fermionic Field Theory*, *Phys. Rev.* **D98** (2018) 126001, [1801.07620].
- [55] L. Hackl and R. C. Myers, *Circuit complexity for free fermions*, *JHEP* **07** (2018) 139, [1803.10638].
- [56] J. Erdmenger, M. Gerbershagen and A.-L. Weigel, *Complexity measures from geometric actions on Virasoro and Kac-Moody orbits*, *JHEP* **11** (2020) 003, [2004.03619].
- [57] M. Flory and M. P. Heller, *Conformal field theory complexity from Euler-Arnold equations*, *JHEP* **12** (2020) 091, [2007.11555].
- [58] M. Flory and M. P. Heller, *Geometry of Complexity in Conformal Field Theory*, *Phys. Rev. Res.* **2** (2020) 043438, [2005.02415].
- [59] P. Caputa and J. M. Magan, *Quantum Computation as Gravity*, *Phys. Rev. Lett.* **122** (2019) 231302, [1807.04422].
- [60] E. Caceres, S. Chapman, J. D. Couch, J. P. Hernandez, R. C. Myers and S.-M. Ruan, *Complexity of Mixed States in QFT and Holography*, *JHEP* **03** (2020) 012, [1909.10557].

- [61] H. A. Camargo, L. Hackl, M. P. Heller, A. Jahn, T. Takayanagi and B. Windt, *Entanglement and Complexity of Purification in (1+1)-dimensional free Conformal Field Theories*, 2009.11881.
- [62] M. Headrick and T. Takayanagi, *A Holographic proof of the strong subadditivity of entanglement entropy*, *Phys. Rev. D* **76** (2007) 106013, [0704.3719].
- [63] T. Takayanagi and K. Umemoto, *Entanglement of purification through holographic duality*, *Nature Phys.* **14** (2018) 573–577, [1708.09393].
- [64] K. Umemoto and Y. Zhou, *Entanglement of Purification for Multipartite States and its Holographic Dual*, *JHEP* **10** (2018) 152, [1805.02625].
- [65] N. Jokela and A. Pönni, *Notes on entanglement wedge cross sections*, *JHEP* **07** (2019) 087, [1904.09582].
- [66] K. Tamaoka, *Entanglement Wedge Cross Section from the Dual Density Matrix*, *Phys. Rev. Lett.* **122** (2019) 141601, [1809.09109].
- [67] N. Bao and I. F. Halpern, *Conditional and Multipartite Entanglements of Purification and Holography*, *Phys. Rev.* **D99** (2019) 046010, [1805.00476].
- [68] S. Dutta and T. Faulkner, *A canonical purification for the entanglement wedge cross-section*, 1905.00577.
- [69] M. Headrick, *Entanglement Renyi entropies in holographic theories*, *Phys. Rev. D* **82** (2010) 126010, [1006.0047].
- [70] N. Bao, A. Chatwin-Davies and G. N. Remmen, *Entanglement of Purification and Multiboundary Wormhole Geometries*, *JHEP* **02** (2019) 110, [1811.01983].

- [71] R. Abt, J. Erdmenger, H. Hinrichsen, C. M. Melby-Thompson, R. Meyer, C. Northe et al., *Topological Complexity in AdS_3/CFT_2* , *Fortsch. Phys.* **66** (2018) 1800034, [1710.01327].
- [72] R. Abt, J. Erdmenger, M. Gerbershagen, C. M. Melby-Thompson and C. Northe, *Holographic Subregion Complexity from Kinematic Space*, *JHEP* **01** (2019) 012, [1805.10298].
- [73] V. Vedral, *The role of relative entropy in quantum information theory*, *Rev. Mod. Phys.* **74** (Mar, 2002) 197–234.
- [74] D. D. Blanco, H. Casini, L.-Y. Hung and R. C. Myers, *Relative Entropy and Holography*, *JHEP* **08** (2013) 060, [1305.3182].
- [75] N. Lashkari and M. Van Raamsdonk, *Canonical energy is quantum fisher information*, *JHEP* **04** (2016) 153, [1508.00897].
- [76] D. L. Jafferis, A. Lewkowycz, J. Maldacena and S. J. Suh, *Relative entropy equals bulk relative entropy*, *JHEP* **06** (2016) 004, [1512.06431].
- [77] X. Dong and A. Lewkowycz, *Entropy, Extremality, Euclidean Variations, and the Equations of Motion*, *JHEP* **01** (2018) 081, [1705.08453].
- [78] A. Belin, N. Iqbal and S. F. Lokhande, *Bulk entanglement entropy in perturbative excited states*, *SciPost Phys.* **5** (2018) 024, [1805.08782].
- [79] A. Ghosh and R. Mishra, *Inhomogeneous jacobi equation for minimal surfaces and perturbative change in holographic entanglement entropy*, *Phys. Rev.* **D97** (2018) 086012, [1710.02088].

- [80] S. He, J.-R. Sun and H.-Q. Zhang, *On holographic entanglement entropy with second order excitations*, *Nucl. Phys.* **B928** (2018) 160–181, [1411.6213].
- [81] J. Bhattacharya, M. Nozaki, T. Takayanagi and T. Ugajin, *Thermodynamical property of entanglement entropy for excited states*, *Phys. Rev. Lett.* **110** (2013) 091602, [1212.1164].
- [82] A. Uhlmann, *The transition probability for states of *-algebras.*, *Annalen Phys.* **42** (1985) 524.
- [83] M. Hayashi, *Quantum Information: an Introduction*. Springer-Verlag, 2006.
- [84] D. Petz and C. Ghinea, *Introduction to quantum fisher information*, in *Quantum probability and related topics*, vol. 1. World Scientific, 2011. DOI.
- [85] M. Miyaji, T. Numasawa, N. Shiba, T. Takayanagi and K. Watanabe, *Distance between quantum states and gauge-gravity duality*, *Phys. Rev. Lett.* **115** (2015) 261602, [1507.07555].
- [86] M. Alishahiha and A. Faraji Astaneh, *Holographic Fidelity Susceptibility*, *Phys. Rev.* **D96** (2017) 086004, [1705.01834].
- [87] S. Banerjee, J. Erdmenger and D. Sarkar, *Connecting Fisher information to bulk entanglement in holography*, *JHEP* **08** (2018) 001, [1701.02319].
- [88] A. Bernamonti, F. Galli, J. Hernandez, R. C. Myers, S.-M. Ruan and J. Simón, *First Law of Holographic Complexity*, *Phys. Rev. Lett.* **123** (2019) 081601, [1903.04511].
- [89] M. A. Nielsen, M. R. Dowling, M. Gu and A. C. Doherty, *Quantum computation as geometry*, *Science* **311** (2006) 1133–1135.

- [90] M. Taylor and W. Woodhead, *Renormalized entanglement entropy*, *JHEP* **08** (2016) 165, [1604.06808].
- [91] S. Siklos, *The papperitz equation*, MAE207 Applications of Complex Analysis Course Notes, Department of Mathematics and Theoretical Physics, University of Cambridge, <http://www.damtp.cam.ac.uk/user/stcs/courses/fcm/handouts/papperitz.pdf>, 2007.
- [92] O. Ben-Ami and D. Carmi, *On volumes of subregions in holography and complexity*, *JHEP* **11** (2016) 129, [1609.02514].
- [93] E. Oh, I. Y. Park and S.-J. Sin, *Complete Einstein equations from the generalized First Law of Entanglement*, *Phys. Rev.* **D98** (2018) 026020, [1709.05752].
- [94] T. Faulkner, F. M. Haehl, E. Hijano, O. Parrikar, C. Rabideau and M. Van Raamsdonk, *Nonlinear Gravity from Entanglement in Conformal Field Theories*, *JHEP* **08** (2017) 057, [1705.03026].
- [95] T. Jacobson, *Entanglement Equilibrium and the Einstein Equation*, *Phys. Rev. Lett.* **116** (2016) 201101, [1505.04753].
- [96] S. Hollands and R. M. Wald, *Stability of Black Holes and Black Branes*, *Commun. Math. Phys.* **321** (2013) 629–680, [1201.0463].
- [97] K. Nayek and S. Roy, *Decoupling limit and throat geometry of non-susy D3 brane*, *Phys. Lett.* **B766** (2017) 192–195, [1608.05036].
- [98] S. Chakraborty, K. Nayek and S. Roy, *Wilson loop calculation in QGP using non-supersymmetric AdS/CFT*, *Nucl. Phys.* **B937** (2018) 196–213, [1710.08631].

- [99] Y. Kim, B.-H. Lee, C. Park and S.-J. Sin, *Gluon condensation at finite temperature via ads/cft*, *JHEP* **09** (2007) 105, [hep-th/0702131].
- [100] V. Balasubramanian and P. Kraus, *A stress tensor for anti-de sitter gravity*, *Commun. Math. Phys.* **208** (1999) 413–428, [hep-th/9902121].
- [101] S. de Haro, S. N. Solodukhin and K. Skenderis, *Holographic reconstruction of space-time and renormalization in the ads / cft correspondence*, *Commun. Math. Phys.* **217** (2001) 595–622, [hep-th/0002230].
- [102] X. Dong, S. Harrison, S. Kachru, G. Torroba and H. Wang, *Aspects of holography for theories with hyperscaling violation*, *JHEP* **06** (2012) 041, [1201.1905].
- [103] N. Engelhardt and S. Fischetti, *Surface Theory: the Classical, the Quantum, and the Holographic*, *Class. Quant. Grav.* **36** (2019) 205002, [1904.08423].
- [104] D. N. Page, *Information in black hole radiation*, *Phys. Rev. Lett.* **71** (1993) 3743–3746, [hep-th/9306083].
- [105] A. Almheiri, N. Engelhardt, D. Marolf and H. Maxfield, *The entropy of bulk quantum fields and the entanglement wedge of an evaporating black hole*, *JHEP* **12** (2019) 063, [1905.08762].
- [106] G. Penington, *Entanglement Wedge Reconstruction and the Information Paradox*, *JHEP* **09** (2020) 002, [1905.08255].
- [107] A. Almheiri, R. Mahajan, J. Maldacena and Y. Zhao, *The Page curve of Hawking radiation from semiclassical geometry*, *JHEP* **03** (2020) 149, [1908.10996].
- [108] G. Penington, S. H. Shenker, D. Stanford and Z. Yang, *Replica wormholes and the black hole interior*, 1911.11977.

- [109] A. Almheiri, R. Mahajan and J. E. Santos, *Entanglement islands in higher dimensions*, *SciPost Phys.* **9** (2020) 001, [1911.09666].
- [110] C. Akers, N. Engelhardt and D. Harlow, *Simple holographic models of black hole evaporation*, *JHEP* **08** (2020) 032, [1910.00972].
- [111] T. Li, J. Chu and Y. Zhou, *Reflected Entropy for an Evaporating Black Hole*, *JHEP* **11** (2020) 155, [2006.10846].
- [112] V. Balasubramanian, A. Kar, O. Parrikar, G. Sárosi and T. Ugajin, *Geometric secret sharing in a model of Hawking radiation*, *JHEP* **01** (2021) 177, [2003.05448].
- [113] P. Caputa, M. Miyaji, T. Takayanagi and K. Umemoto, *Holographic Entanglement of Purification from Conformal Field Theories*, *Phys. Rev. Lett.* **122** (2019) 111601, [1812.05268].
- [114] C. Akers and P. Rath, *Entanglement Wedge Cross Sections Require Tripartite Entanglement*, *JHEP* **04** (2020) 208, [1911.07852].
- [115] N. Bao and I. F. Halpern, *Holographic Inequalities and Entanglement of Purification*, *JHEP* **03** (2018) 006, [1710.07643].
- [116] Y. Kusuki and K. Tamaoka, *Dynamics of Entanglement Wedge Cross Section from Conformal Field Theories*, *Phys. Lett. B* **814** (2021) 136105, [1907.06646].
- [117] K. Umemoto, *Quantum and Classical Correlations Inside the Entanglement Wedge*, *Phys. Rev.* **D100** (2019) 126021, [1907.12555].
- [118] N. Bao and N. Cheng, *Multipartite Reflected Entropy*, *JHEP* **10** (2019) 102, [1909.03154].

- [119] J. Chu, R. Qi and Y. Zhou, *Generalizations of Reflected Entropy and the Holographic Dual*, *JHEP* **03** (2020) 151, [1909.10456].
- [120] M. Moosa, *Time dependence of reflected entropy in rational and holographic conformal field theories*, *JHEP* **05** (2020) 082, [2001.05969].
- [121] H.-S. Jeong, K.-Y. Kim and M. Nishida, *Reflected Entropy and Entanglement Wedge Cross Section with the First Order Correction*, *JHEP* **12** (2019) 170, [1909.02806].
- [122] Y. Kusuki and K. Tamaoka, *Entanglement Wedge Cross Section from CFT: Dynamics of Local Operator Quench*, *JHEP* **02** (2020) 017, [1909.06790].
- [123] D. Harlow, *TASI Lectures on the Emergence of Bulk Physics in AdS/CFT*, *PoS TASI2017* (2018) 002, [1802.01040].
- [124] F. Pastawski, B. Yoshida, D. Harlow and J. Preskill, *Holographic quantum error-correcting codes: Toy models for the bulk/boundary correspondence*, *JHEP* **06** (2015) 149, [1503.06237].
- [125] X. Dong, D. Harlow and A. C. Wall, *Reconstruction of Bulk Operators within the Entanglement Wedge in Gauge-Gravity Duality*, *Phys. Rev. Lett.* **117** (2016) 021601, [1601.05416].
- [126] D. Harlow and P. Hayden, *Quantum Computation vs. Firewalls*, *JHEP* **06** (2013) 085, [1301.4504].
- [127] A. R. Brown, H. Gharibyan, G. Penington and L. Susskind, *The Python's Lunch: geometric obstructions to decoding Hawking radiation*, *JHEP* **08** (2020) 121, [1912.00228].

- [128] N. Bao, A. Chatwin-Davies and G. N. Remmen, *Warping Wormholes with Dust: a Metric Construction of the Python's Lunch*, *JHEP* **09** (2020) 102, [2006.10762].
- [129] B. Czech, L. Lamprou, S. McCandlish and J. Sully, *Integral Geometry and Holography*, *JHEP* **10** (2015) 175, [1505.05515].
- [130] A. Almheiri, R. Mahajan and J. Maldacena, *Islands outside the horizon*, 1910.11077.
- [131] A. Almheiri, T. Hartman, J. Maldacena, E. Shaghoulian and A. Tajdini, *Replica Wormholes and the Entropy of Hawking Radiation*, *JHEP* **05** (2020) 013, [1911.12333].
- [132] E. Caceres, A. Kundu, A. K. Patra and S. Shashi, *A Killing Vector Treatment of Multiboundary Wormholes*, *JHEP* **02** (2020) 149, [1912.08793].
- [133] J. Kudler-Flam and S. Ryu, *Entanglement negativity and minimal entanglement wedge cross sections in holographic theories*, *Phys. Rev.* **D99** (2019) 106014, [1808.00446].
- [134] V. Balasubramanian, P. Hayden, A. Maloney, D. Marolf and S. F. Ross, *Multiboundary Wormholes and Holographic Entanglement*, *Class. Quant. Grav.* **31** (2014) 185015, [1406.2663].
- [135] K. Skenderis and B. C. van Rees, *Holography and wormholes in 2+1 dimensions*, *Commun. Math. Phys.* **301** (2011) 583–626, [0912.2090].
- [136] A. Peach and S. F. Ross, *Tensor Network Models of Multiboundary Wormholes*, *Class. Quant. Grav.* **34** (2017) 105011, [1702.05984].

- [137] P. Nguyen, T. Devakul, M. G. Halbasch, M. P. Zaletel and B. Swingle, *Entanglement of purification: from spin chains to holography*, *JHEP* **01** (2018) 098, [1709.07424].
- [138] V. Balasubramanian, M. DeCross, A. Kar and O. Parrikar, *Binding Complexity and Multiparty Entanglement*, *JHEP* **02** (2019) 069, [1811.04085].
- [139] E. Cáceres, J. Couch, S. Eccles and W. Fischler, *Holographic Purification Complexity*, *Phys. Rev. D* **99** (2019) 086016, [1811.10650].
- [140] S. F. Lokhande, G. W. J. Oling and J. F. Pedraza, *Linear response of entanglement entropy from holography*, *JHEP* **10** (2017) 104, [1705.10324].
- [141] A. Bhattacharyya, A. Shekar and A. Sinha, *Circuit complexity in interacting QFTs and RG flows*, *JHEP* **10** (2018) 140, [1808.03105].
- [142] T. Ali, A. Bhattacharyya, S. Shajidul Haque, E. H. Kim and N. Moynihan, *Time evolution of complexity: A critique of three methods*, *JHEP* **04** (2019) 087, [1810.02734].
- [143] S. Chapman, J. Eisert, L. Hackl, M. P. Heller, R. Jefferson, H. Marrochio et al., *Complexity and entanglement for thermofield double states*, *SciPost Phys.* **6** (2019) 034, [1810.05151].
- [144] D. Ge and G. Policastro, *Circuit Complexity and 2D Bosonisation*, *JHEP* **10** (2019) 276, [1904.03003].
- [145] P. Caputa, N. Kundu, M. Miyaji, T. Takayanagi and K. Watanabe, *Anti-de sitter space from optimization of path integrals in conformal field theories*, *Phys. Rev. Lett.* **119** (2017) 071602, [1703.00456].

- [146] P. Caputa, N. Kundu, M. Miyaji, T. Takayanagi and K. Watanabe, *Liouville action as path-integral complexity: From continuous tensor networks to ads/cft*, *JHEP* **11** (2017) 097, [1706.07056].
- [147] H. A. Camargo, M. P. Heller, R. Jefferson and J. Knaute, *Path integral optimization as circuit complexity*, *Phys. Rev. Lett.* **123** (2019) 011601, [1904.02713].
- [148] Z. Fu, A. Maloney, D. Marolf, H. Maxfield and Z. Wang, *Holographic complexity is nonlocal*, *JHEP* **02** (2018) 072, [1801.01137].
- [149] J. Hernandez, R. C. Myers and S.-M. Ruan, *Quantum Extremal Islands Made Easy, PartIII: Complexity on the Brane*, 2010.16398.
- [150] A. Dymarsky and A. Shapere, *Solutions of modular bootstrap constraints from quantum codes*, 2009.01236.
- [151] A. Dymarsky and A. Shapere, *Quantum stabilizer codes, lattices, and CFTs*, 2009.01244.
- [152] H. Geng, A. Karch, C. Perez-Pardavila, S. Raju, L. Randall, M. Riojas et al., *Information Transfer with a Gravitating Bath*, 2012.04671.
- [153] A. Bhattacharya, A. Bhattacharyya, P. Nandy and A. K. Patra, *Islands and complexity of eternal black hole and radiation subsystems for a doubly holographic model*, *JHEP* **05** (2021) 135, [2103.15852].